1988

Predicting Contaminant Concentration Values In Environmental Flows

Handson Yip

NOTICE

The quality of this microform is heavily dependent upon the quality of the original thesis submitted for microfilming. Every effort has been made to ensure the highest quality of reproduction possible.

If pages are missing, contact the university which granted the degree.

Some pages may have indistinct print especially if the original pages were typed with a poor typewriter ribbon or if the university sent us an inferior photocopy.

Previously copyrighted materials (journal articles, published tests, etc.) are not filmed.

Reproduction in full or in part of this microform is governed by the Canadian Copyright Act, R.S.C. 1970, c. C-30.

AVIS

La qualité de cette microforme dépend grandement de la qualité de la thèse soumise au microfilmage. Nous avons tout fait pour assurer une qualité supérieure de reproduction.

S'il manque des pages, veuillez communiquer avec l'université qui a conféré le grade.

La qualité d'impression de certaines pages peut laisser à désirer, surtout si les pages originales ont été dactylographiées à l'aide d'un ruban usé ou si l'université nous a fait parvenir une photocopie de qualité inférieure.

Les documents qui font déjà l'objet d'un droit d'auteur (articles de revue, tests publiés, etc.) ne sont pas microfilmés.

La reproduction, même partielle, de cette microforme est soumise à la Loi canadienne sur le droit d'auteur, SRC 1970, c. C-30.

Predicting Contaminant Concentration Values In Environmental Flows

by

Handson Yip

Department of Applied Mathematics

Submitted in partial fulfillment

of the requirements for the degree of

Doctor of Philosophy

Faculty of Graduate Studies

The University of Western Ontario

London, Ontario

April 1988

ISBN 0-315-43281-0

Abstract

A generic, small-time, asymptotic solution for the convective-diffusion equation was expressed as a three-dimensional, Hermite-polynomial expansion. This solution was used in a versatile scheme to describe mean values of concentration of contaminant in environmental flows. An analytical solution and a simple finite difference scheme was used to validate that scheme. The scheme was then used, with empirical information from the flow-field, to describe an elevated line and point source in a region of constant stress within a turbulent boundary-layer where detailed measurements of mean values of concentration of contaminant were used for comparison. The results from that comparison showed the scheme was capable of predicting values of concentration of contaminant in the intermediate region and far-field region of that flow-configuration. Cross-terms in the convective-diffusion equation were shown to be insignificant at large distances from the source. The fluctuating field of concentration was derived, in a simple way, from the mean field of concentration in both the near-source region and far-field region. In the intermediate region, a simple extension of this method was shown to receive support from experimental data. Empirical information extracted from the mean field and mean-squared field were used in a Beta distribution to predict the probability density functions for concentration of contaminant. The results from the Beta distribution were shown to agree with measured probability density functions, except in the near-wall region.

Acknowledgments

I would like to express my sincere gratitude to Professor Paul Sullivan for his guidance and encouragements during the course of this work. My association with him during the last six years has been a valuable learning experience, which I will always cherish.

I am also grateful to Professor R. Migneron and Professor D. Naylor for their influence during the early years of my graduate education. It was certainly my pleasure and good fortune to be associated with them.

Special thanks to Dr. R.W. Derksen for use of his computer software, which facilitated the writing of this thesis.

The work in this thesis was done while I held an N.S.E.R.C. and an Ontario Graduate Scholarship, and I gratefully acknowledge both.

Table of Contents

List of Figures

Nomenclature

a_i	coefficients of the Taylor series for κ_{11}, $i = 0,1,2$
b_i	coefficients of the Taylor series for κ_{22}, $i = 0,1,2$
c_i	coefficients of the Taylor series for κ_{33}, $i = 0,1,2$
ϵ_i	coefficients of the Taylor series for κ_{13} and κ_{31}, $i = 0,1,2$
d_i	coefficients of the Taylor series for the mean, streamwise velocity, $i = 1,2$
$\underline{x}$	position vector in space
x_1, z	variables representing the vertical direction
x_2, y	variables representing the lateral direction
x_3, x	variables representing the horizontal direction
U_i	components of the mean velocity vector
κ_{ij}	diffusivity tensor, $i = 1,2,3$ and $j = 1,2,3$
$C(\underline{x},t)$	mean concentration at a point in space represented by the vector $\underline{x}$, at time t
$C(\underline{x})$	steady-state mean concentration at a point in space represented by the vector $\underline{x}$
$\hat{C}(\underline{x},t)$	non-dimensional mean concentration
C_m, $C(0)$	maximum mean concentration
$\Gamma(\underline{x},t+\Delta t)$	mean concentration for one discrete time-step
D_{ijk}	coefficients of the three-dimensional Hermite-polynomial expansion
H_{ijk}	three-dimensional Hermite polynomials
M_{mnp}	moments of the concentration distribution
$\overline{M}_{mnp}$	non-dimensional moments of the concentration distribution
Q_e	emission rate of source
R	correlation matrix
R^{-1}	inverse of the correlation matrix
$\lvert R \rvert$	determinant of the correlation matrix
r_{ij}	elements of the correlation matrix

σ_i	standard deviation, $i = 1,2,3$
t	dimensional time
τ	non-dimensional time
T	non-dimensional time in exact solution
h	non-dimensional parameter representing the cross-terms in the exact solution
$g(\underline{X})$	quadratic form
$\gamma(\underline{Y})$	reciprocal form
h_1	source height in the Raupach and Legg experiment
$u(z)$	mean streamwise velocity
u_*	Friction velocity
k	von Karman's constant
z_0	roughness parameter
z_1	nominal size of gravel
F	Flux of contaminant through a plane normal to the flow
θ_*	mean temperature scale
H	boundary layer height in Fackrell and Robins (1982) experiment
H_r	boundary layer height in Robins and Fackrell (1978) experiment
H_1	Source height in Smith (1957) solution
Δx, Δz	grid sizes
τ_0	shear stress at the wall
ρ_0	fluid density
$\bar{x}_i$	center of mass of contaminant cloud
$c(\underline{x},t)^2$, c^2	mean-squared concentration values (fluctuations)
$\hat{c}^2$	maximum mean-squared concentration values
$\hat{c}$	maximum root mean-squared concentration values
$p(\theta;\underline{x},t)$	probability density function for contaminant concentration
$\pi(\underline{x},t)$	probability of finding a point denoted by the vector $\underline{x}$, at time t, in marked fluid
θ_0	initial contaminant concentration value
$\dot{\epsilon}_1$, C_0, $\bar{\alpha}$, M_2	constants O(1)

$\hat{\theta}$	local concentration scale
D	molecular diffusion
δ	plume half-width (i.e., the location at where the concentration falls to 1/2 of the maximum value)
κ_0	coefficient in the Smith (1957) diffusivity profile
u_0	coefficient in the Smith (1957) velocity profile

Chapter One

Background

1.1 Introduction

The study of dispersing contaminants in environmental flows is important to the assessment of the hazards that result from pollutants released into atmospheric boundary-layers, lakes, and rivers. Ruptured gas-pipes, toxic spills, stack-gas emissions, and sewage discharges are some common examples of realistic releases of contaminant that occur in many domestic and industrial processes. The kind of hazard assessment employed depends on the nature of the environmental problem. For example, in the case of a ruptured gas-pipe one is interested in evaluating the risk of exceeding a dangerous concentration of toxic gas (Wilson, 1982); in the

planning of industrial plants, attention is on the distribution of airborne contaminants near a heavily populated area (Scorer, 1968); in the study of sewage discharges in rivers, one is interested in minimizing the high levels of effluents downstream (Smith, 1981, 1982a).

The assessment of the potential hazards from an accidental spill of toxic contaminant is seldom simple because of the complex nature of environmental flows. Such flows are characteristically three-dimensional, unsteady, and inhomogeneous. These problematic features of environmental flows are very important because they are likely to play a dominant role during the spread of contaminant. Ideally, when an accidental spill of toxic contaminant occurs in the environment, one would like to find a multi-point probability density function for the concentration of contaminant. This, however, is an unrealistic expectation for these complex, environmental flows. The lowest order moments (i.e., the ensemble-mean and variance) of the single-point probability density function for the concentration of contaminant appear to be sensible and practical objectives for now. The ensemble-mean concentration, alone, does not ensure an adequate evaluation of some environmental hazards. A satisfactory assessment of the environmental hazards from toxic waste should take into account the fluctuating values of concentration (or r.m.s.) because these are often comparable with, or greater than, the ensemble-mean values of concentration (pp.231, Csanady, 1973). There are, however, some practical applications in environmental flows where the distribution of ensemble-mean concentration is useful. For example, the far-field,

ensemble-averaged, near-ground concentrations from stack-gas emissions are of interest. In assessing the hazards from an accidental release of flammable fluid, the mean and the fluctuating values of concentration may be inappropriate. In the context of flammability, a meaningful question to ask is, "what is the risk of exceeding a dangerous level of combustible gas?" Here the use of a probability density function for the concentration of contaminant (more precisely, a cumulative distribution function) is applicable. Thus it is of practical importance to predict at least the first two moments of the probability density function for the concentration of contaminant.

With the overwhelming complexities of environmental flows, one requires a robust and flexible "solution-scheme" to model the mean and fluctuating values of concentration in natural flows.

1.2 The basic model equation describing the ensemble-mean concentration

The Convective-diffusion equation,

$$\frac{\partial C}{\partial t} + U_i \frac{\partial C}{\partial x_i} = \frac{\partial}{\partial x_i}\left(\kappa_y \frac{\partial C}{\partial x_j}\right), \qquad (1.1)$$

with the appropriate boundary conditions and initial conditions, is a common equation used to predict the distributions of ensemble-mean concentration from sources in a region of constant stress (with zero horizontal pressure gradient)

within a turbulent boundary-layer (Smith, 1957; Csanady, 1973; Monin and Yaglom , 1971). The thickness of this region ranges from 10 to 100 metres within the earth's boundary-layer.

Equation (1.1) is a model equation derived from an ad-hoc, mathematical closure-assumption (see pp.30, Hinze, 1975) which is not always a truthful representation of the physical mechanisms. Such a model equation needs to be verified with experimental data. Despite the controversies over the closure-assumption used in the model equation (Sreenivasan, Tavoularis, and Corrsin, 1982), the detailed modeling of the term κ_y is likely to be an insignificant feature relative to the approximations and modeling of the dominant features of environmental flows (Sullivan, 1983). The basic closure-assumption used in equation (1.1) is known as a gradient type model (Sreenivasan et al., 1982), which leads to a mathematical simplification. In order for gradient type models to be valid, the turbulent length-scales of motion for the transport of contaminant must be smaller than the scales of inhomogeneity of $C(\underline{x},t)$ (pp.4, Pasquill, 1974; Sreenivasan et al., 1982). This restriction is thought to be met when the model equation is used to describe, in a fixed frame of reference, a constant release of contaminant in a turbulent boundary-layer (pp.4, Pasquill, 1974), where the vertical length-scales of turbulent motion are never larger than the vertical scale of inhomogeneity of $C(\underline{x},t)$ (except near an elevated source). This is evident from observing a continuous, ground-level plume in a neutral, turbulent boundary-layer (see plate one, Sutton,

1953). For an elevated source, a time-dependent diffusivity is necessary to adequately describe the dispersion process in the near-field region (Sullivan, 1983).

Herein x_1 and z, x_2 and y, and x_3 and x represent the vertical, lateral, and streamwise directions respectively. The model equation (1.1) includes a temporal term and a convective term on the left-hand-side. U_i is the i^{th} component of the mean-velocity vector in the i^{th} direction. $C(\underline{x},t)$ is the mean concentration of contaminant at a point located by the vector $\underline{x}$, at time t. In a statistical sense (perhaps a more natural representation), $C(\underline{x},t)$ is the probability of finding marked fluid at a point located by the vector $\underline{x}$, at time t. Emphasis is on the description of a passive scalar dispersing in a steady, turbulent boundary-layer, where detailed measurements of concentration made in a wind-tunnel are available for experimental verification of the model equation (1.1) (Raupach and Legg, 1983; Fackrell and Robins, 1982).

The model equation (1.1) is here restricted in application to a passive contaminant. Any changes to the original concentration, that can result from chemical reactions between the ambient fluid and the contaminant or buoyant forces, will provide an inaccurate prediction of $C(\underline{x},t)$. Such a restriction is an impediment to the consideration of a chemical reaction, as in the dilution of contaminant emanating from a toxic spill or in the near-field description of ocean out-falls where buoyant forces are dominant. On the other hand, some important

far-field problems do occur where a relatively large volume of sample is used and the time after release is sufficiently long to ensure that the effects of buoyancy are negligible. In such circumstances the model equation (1.1) can be applied. The random field in which a passive scalar spreads is incompressible, and this is consistent with the fact that the majority of environmental flows are incompressible. Figure 1 is a schematic view of a passive contaminant in a shear flow. The frame of reference in figure 1 is fixed, which is convenient because most measurements are made in a fixed frame of reference (i.e., Eulerian coordinates).

The spread of a cloud of contaminant in atmospheric conditions can not be accurately described by a constant diffusivity, and the use of a variable diffusivity is necessary (Saffman, 1962). Hence, κ_y is a function of height. There appears to be no restriction that the diffusivity tensor $\kappa_y(x_1)$ must be diagonal. Matsuoka (1961) was the first to assume that the diffusivity tensor was symmetric. In a subsequent paper, Gee and Davies (1964) pointed out an inconsistency in Matsuoka's assumption of a symmetric diffusivity tensor, and then showed that it is asymmetric. Aside from analytical considerations of the off-diagonal terms in the turbulent diffusivity tensor, there is experimental evidence to support the existence of these terms. Detailed experiments by Tavoularis and Corrsin (1981) indicate that the off-diagonal terms are non-zero and related to the diagonal components in a simple, homogeneous, shear flow. In atmospheric applications where the far-field region is of interest, the effects of these off-diagonal terms are questionable and their importance, in an atmospheric context, needs assessment.

The flow over a flat, solid boundary is a typical flow-configuration which will be used to assess the model equation (1.1). In this flow, there is a region near the wall where the gradients of velocity are large; away from the wall, the gradients of velocity are approximately constant. This results in a region of constant stress where the stresses are approximately equal to the shear stress at the wall designated by $u_* = \sqrt{\tau_0/\rho_0}$, where u_*, τ_0 and ρ_0 represent the friction velocity, shear stress at the wall, and density of the fluid respectively. In this region an expression for the vertical diffusivity is commonly derived using Reynold's analogy (see Smith, 1957; Monin and Yaglom,1971). That is,

$$\kappa_{11}\frac{\partial u}{\partial z} = \text{constant} \qquad (1.2)$$

In chapter four, equation (4.3a) results from (1.2) when the velocity profile represented by equation (4.1) is used.

1.3 Some salient features of environmental flows

It is imperative to outline some of the dominant features of environmental flows that will have significant effects on the spread of contaminant so these may be accounted for in the solution scheme. Two main factors are responsible for making the spread of contaminant complex in an environmental flow: the intrinsic, time-varying properties of the flow-field, and the presence of a solid boundary leading to inhomogeneities in the flow-field.

Although the earth's turbulent boundary-layer (within 100 metres) resembles the inner portion of a two-dimensional boundary-layer over a flat plate when the flow is steady, this steady feature seldom happens in practice. Most natural, turbulent flows over a solid boundary are time-dependent and sheared. These intrinsic features are evident from changing wind speeds during different times of the day, and changing gradients of velocity that occur in the boundary-layer.

Furthermore, there are sudden changes in the velocity's direction, which must be accounted for during the modeling process. Any three-dimensional scheme would be suitable for taking into account these changes. After all, turbulence is three-dimensional (the phenomenon of vortex stretching only occurs in three dimensions). The unsteady feature, which is likely to be the most dominant feature, can complicate the interpretation of experimental data when the sample-time is larger than the time-scale of a typical eddy. Sullivan (1983) provides an effective method for handling the unsteadiness using a diffusivity dependent on the sample-time. There is no doubt that the unsteady feature of an environmental flow is likely to have a significant effect on the spread of contaminant, and must be considered in the modeling process.

The presence of a solid boundary in a turbulent flow is responsible for causing the flow to be inhomogeneous (i.e., most statistical properties of the flow are space dependent). The turbulent length-scales appear to have a functional dependence on the vertical direction. In the region away from the solid wall, the cloud of contaminant grows in size because it is continuously affected by the large

scales of motion. This results in a much faster cloud growth than would be the case without a solid boundary. Near the solid wall, the length-scales of the turbulent motion are very small relative to the length-scales in a region away from the wall. In a flow over a smooth wall, the small turbulent length-scales adjacent to the wall cause a build-up of contaminants near and on the solid boundary (pp.14, Csanady, 1973). For real fluids, the no-slip boundary condition at the wall is likely to compound this build-up.

Many important flows involve a uniform, rough surface; for example, the flow over a grass field. The flow over a rough wall has a structure quite similar to the flow pattern over a smooth wall at heights greater than the characteristic scale of the rough elements, and so it is possible to use most of the standard properties found in smooth-wall flows to study the spread of contaminant in rough-wall flows (pp.139, Townsend, 1976). The thin region adjacent to the wall is a critical region for the evolution of a cloud of contaminant, and requires a solution-scheme that is capable of incorporating semi-empirical information since good theoretical models do not exist for these complex flows. For a flow over a rough wall there will be a circulating region in which the fluid particles are trapped, and for a smooth wall the viscous dominated region adjacent to the wall delays the asymptotic stage of dispersion (Taylor, 1954; Dewey, 1979). The presence of an absorbent boundary can also have a significant effect on the longitudinal dispersion coefficient (Smith, 1983). For a flow of radioactive vapors over a surface covered with grass, the rough surface behaves like a sink (Chamberlain,

1965).

1.4 Some past approaches used to predict the mean and fluctuating concentrations

This section provides a brief review of some past approaches used for predicting the mean and fluctuating values of concentration. The fundamental reasons for the deficiencies of these past approaches provide some of the ideas for the approaches adopted in the subsequent parts of this thesis.

There is minimal effort directed towards developing versatile methods for the prediction of the mean field of concentration, especially methods that consider the significant features of environmental flows. Instead, attention has been focused on models that provide a good comparison with experimental data, but which do not take into account the true physical mechanisms (Hwang et al., 1979; Wilson et al., 1982). A popular approach used to predict the ensemble-mean values of concentration from sources in a turbulent boundary-layer is the application of Gaussian models (Sutton, 1947; Hwang et al., 1979; Wilson et al., 1982), which essentially involve using several numerical constants to provide a good fit to the experimental data. The apparent popularity of Gaussian models stems from the fact that these models are relatively simple and have a good correlation with some experimental data. However, they do not take into account the effects of shear and variable diffusivities, which are important in the modeling process. Large departures of the concentration from the Gaussian distribution take place when the

effects of shear and variable diffusivities are taken into account (Smith, 1957; Sullivan and Yip, 1985). The pioneering work of Lauwerier (1954) and Smith (1957) represents a significant improvement over Gaussian models, but analytical solutions to equation (1.1) are only available for some simple forms of $\kappa_{ij}(\underline{x})$ and $U_i(\underline{x})$.

The concept that particles released in the constant-stress region of a turbulent boundary-layer have similarity properties is another way of describing the gross features of a cloud of marked fluid (Cermak, 1963; Batchelor, 1964). This method provides only the gross features on a cloud of marked fluid if the turbulent boundary-layer is statistically steady, which seldom happens in environmental flows. Furthermore, when a particle is released above the ground (relevant to elevated releases such as a chimney plume), the time it takes for the particle to have its statistical properties independent of the release height is of order h/u_*, where h and u_* are the release height and friction velocity respectively (Batchelor, 1964). However, it is possible that the time it takes the flow-field to change is less than $O(h/u_*)$.

Various fundamental aspects of the fluctuations from a scalar quantity have been examined experimentally by many researchers (La Rue and Libby, 1974; Shaughnessy and Morton, 1977; Warhaft and Lumley, 1978; Tavoularis and Corrsin, 1981). Despite the abundance of experimental evidence available, there

has been minimal progress made towards the development of simple mathematical models that can predict the fluctuating values of concentration of contaminant in environmental flows.

Csanady (pp.233-242, 1973) used K-theory to derive an equation for the variance of concentration, and then calculated a self-similar solution for the variance using a Gaussian distribution for the ensemble-mean field. This method is restricted to finding the distribution of mean-squared concentration when the ensemble-mean field has settled to a Gaussian form, which seldom occurs in the intermediate downstream region of an elevated point-source. The measured profiles of mean concentration provided by Fackrell and Robins (1982) illustrate that feature. Wilson et al. (1982) used a simple Gaussian model to predict the fluctuating values of concentration from a ground-level source in a turbulent boundary-layer. Their model appears to agree with experimental data for that particular case. However, detailed laboratory measurements of radial profiles of concentration from a methane jet of Birch et al. (1978), and vertical (r.m.s.) profiles of temperature from an elevated line-source in a homogeneous, turbulent shear flow (Tavoularis and Corrsin, 1981) indicate that the r.m.s. distribution is not Gaussian. There is also experimental data from natural flows that are consistent with the findings of the aforementioned experiments. Measured profiles of mean-squared concentration (normal to the instantaneous plume axis) from a dye plume released into the surface layer of Lake Huron are shown to be inadequately described by a Gaussian distribution (Chatwin and Sullivan, 1979).

Another approach, more elaborate than the Gaussian models, is a technique called " Second-order modeling". This technique is not new (for historical review of Second-order modeling, see Lumley, 1978), and with the gaining popularity in supercomputers more elaborate second-order models are likely to be explored extensively in the future. Second-order modeling usually involves a set of simultaneous partial differential equations derived from closure-schemes based on physical principles. Sykes, Lewellen and Parker (1984) provide a turbulent transport model, based on second-order closure-schemes, to describe the diffusion of a passive scalar in an inhomogeneous, turbulent, shear flow. Their technique, which uses many closure-assumptions, consists mainly of a set of three partial differential equations representing the ensemble-mean concentration, turbulent flux of concentration, and the variance of concentration. The predicted fluctuations from their turbulent transport model are shown to be in reasonable agreement with the data by Fackrell and Robins (1982) for sources in a turbulent boundary-layer generated by a wind-tunnel. It is questionable, even with the current success of second-order modeling, whether the enormous amounts of computational time (if affordable) required by second-order modeling is justified given the variability in the measured fluctuating values of concentration (Sullivan, 1984; Chatwin, 1984), which are used for assessing the validity of the model.

1.5 Plan of thesis

The main purpose of this thesis is to provide a solution-scheme capable of predicting ensemble-mean values of concentration of contaminant in environmen-

tal flows. The secondary objectives of this thesis include the use of the ensemble-mean values of concentration (which are easily and reliably measured) to predict the fluctuating values of concentration, and prediction of a one-point probability density function for the concentration of contaminant. At the same time, these objectives are supplemented with a computational framework that conveniently allows input of empirical information so that the model equation (1.1), which is derived without recourse to basic physical principles, can be verified with experimental data.

Chapter two focuses on the development of a basic solution-scheme. A general, small-time, asymptotic solution for an instantaneous, point-source release is expressed as a three-dimensional, Hermite-polynomial expansion.

In Chapter three, this generic solution is manipulated by superposition to generate a large-time solution. Solutions from a simple finite-difference scheme and an analytical solution of Smith (1957) are used to compare the results from the superposition procedure. The simulation of a continuous source is described. Special attention is directed towards predicting the ensemble-mean concentration because experimental data for the ensemble-mean are reliable and consistent; thus the validity of the model equation can be tested.

In Chapter four, the scheme is manipulated to simulate an elevated line-source in the constant-stress region within a turbulent boundary-layer. The predicted ensemble-mean values of concentration from the solution-scheme are

compared with the experimental data of Raupach and Legg (1983) for an elevated line-source in a neutral, turbulent boundary-layer generated with a wind-tunnel. The three-dimensional capabilities of the solution-scheme are exploited by modeling an elevated point-source in a turbulent boundary-layer (a flow similar to that of Raupach and Legg, 1983). A practical method is provided for the computation of vertical profiles of ensemble-mean concentration. Results from the simulations are then compared with the experimental data of Fackrell and Robins (1982).

Chapter five addresses the fluctuation problem. It is shown how the ensemble-mean concentration is used to predict the fluctuations. A method simpler and computationally more efficient than second-order modeling is provided. The predicted fluctuations from this simple method are then compared with the measured absolute fluctuations of Fackrell and Robins (1982). Finally, information extracted from the distributions of mean and mean-squared concentration are used in a Beta distribution to predict single-point probability density functions for contaminant concentrations. The results from the Beta distribution are compared with some measured probability density functions from the Fackrell and Robins (1978) experiment.

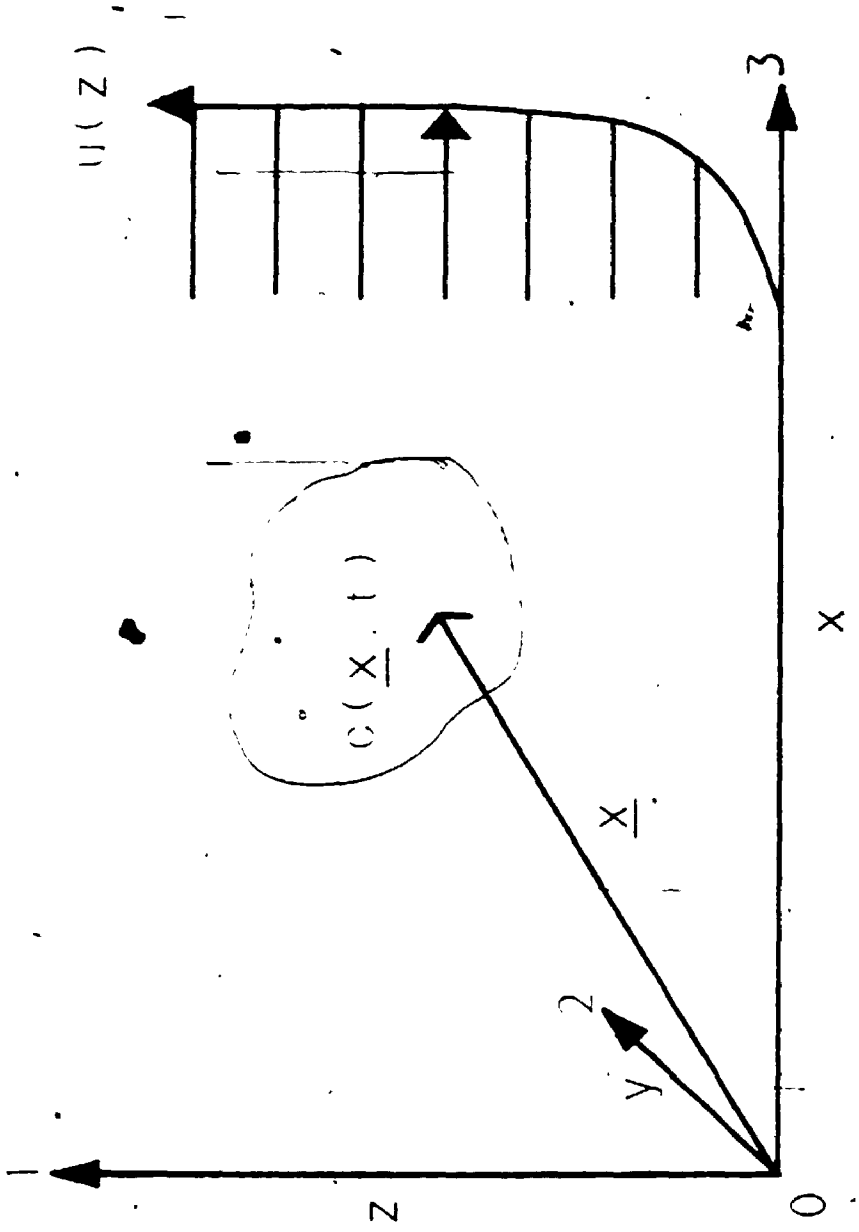

Figure 1
A passive cloud of scalar contaminant in a shear flow

Chapter Two

A Small-time Solution

The main purpose of this chapter is to obtain a general, small-time solution describing an instantaneous point release of contaminant in a shear flow. Such generality is beneficial to the study of the local behavior of a dispersing cloud of contaminant in flows with various diffusivity and velocity profiles. At this stage, it should be emphasized that it is not the sole intention of this thesis to find an elegant solution to equation (1.1), but rather to develop a methodology that can be used in a wide range of turbulent flows in the environment. The general solution from this chapter provides the groundwork for the development of a general framework presented in the following chapter.

2.1 The basic solution-scheme

A local solution for

$$\frac{\partial C}{\partial t}+U_3(x_1)\frac{\partial C}{\partial x_3}=\frac{\partial}{\partial x_1}\left(\kappa_{11}(x_1)\frac{\partial C}{\partial x_1}\right)+\kappa_{22}(x_1)\frac{\partial^2 C}{\partial x_2^2}+\kappa_{33}(x_1)\frac{\partial^2 C}{\partial x_3^2}$$

$$+\kappa_{31}(x_1)\frac{\partial^2 C}{\partial x_3\partial x_1}+\frac{\partial}{\partial x_1}\left(\kappa_{13}(x_1)\frac{\partial C}{\partial x_3}\right), \tag{2.1}$$

when

$$\int_{\substack{\text{all}\\ \text{space}}} C(\underline{x},t)dV(\underline{x})=1 \tag{2.2}$$

and

$$C(\underline{x},0)=\delta(x_1)\delta(x_2)\delta(x_3), \tag{2.3}$$

is expressed as a three-dimensional, Hermite-polynomial expansion. This expansion is

$$C(\underline{x},t)=\frac{\exp(-\frac{1}{2}g(\underline{X}))}{\sigma_1\sigma_2\sigma_3(8\pi^3\mid R\mid)^{1/2}}\left\{\sum_{i+j+k=0}^{\infty}(-1)^{i+j+k}D_{ijk}(t)H_{ijk}(\underline{X})\right\}, \tag{2.4}$$

where

$$X_i=\frac{x_i-\bar{x}_i}{\sigma_i},\qquad i=1,2,3, \tag{2.5}$$

$$g(\underline{X})=\underline{X}^T R^{-1}\underline{X}, \tag{2.6}$$

$$\bar{x}_i=\int_{\substack{\text{all}\\ \text{space}}} x_i C(\underline{x},t)dV(\underline{x}), \tag{2.7}$$

$$r_{ij}=\int_{\substack{\text{all}\\ \text{space}}} X_i X_j C(\underline{x},t)dV(\underline{x}), \tag{2.8}$$

and

$$\sigma_i^2 = \int_{\substack{\text{all}\\ \text{space}}} (x_i - \bar{x}_i)^2 C(\underline{x},t)\,dV(\underline{x}). \tag{2.9}$$

$|R|$, and R^{-1} represent the determinant and inverse of the correlation matrix R, respectively. H_{ijk} are the Hermite polynomials represented by

$$H_{ijk}(\underline{X}) = (-1)^{i+j+k} \exp\left(\frac{1}{2} g(\underline{X})\right) \frac{\partial^{i+j+k}}{\partial X_1^i \partial X_2^j \partial X_3^k} \exp\left(-\frac{1}{2} g(\underline{X})\right). \tag{2.10}$$

With the use of the orthogonal property of the Hermite polynomials, the corresponding coefficients are expressed by

$$D_{ijk}(t) = \frac{(-1)^{i+j+k}}{i!j!k!} \int_{\substack{\text{all}\\ \text{space}}} G_{ijk}(\underline{X}) C(\underline{x},t)\,dV(\underline{x}), \tag{2.11}$$

where the adjoint Hermite polynomial,

$$G_{ijk}(\underline{Y}) = (-1)^{i+j+k} \exp\left(\frac{1}{2}\gamma(\underline{Y})\right) \frac{\partial^{i+j+k}}{\partial Y_1^i \partial Y_2^j \partial Y_3^k} \exp\left(-\frac{1}{2}\gamma(\underline{Y})\right) \tag{2.12}$$

with

$$\gamma(\underline{Y}) = \underline{Y}^T R\, \underline{Y} \tag{2.13}$$

is used.

It is of interest to note that the leading term in (2.4) is the Gaussian distribution. In this problem, when t approaches zero, the leading term provides the correct Gaussian solution; and changes to this are provided by higher order terms at later times. Since $x_2 = 0$ is a plane of symmetry, the structure of the

solution is such that

$$R = r_{ij} = \begin{pmatrix} 1 & 0 & r_{13} \\ 0 & 1 & 0 \\ r_{13} & 0 & 1 \end{pmatrix}, \tag{2.14}$$

and the principal axes of the inertia tensor of the contaminant cloud are given by

$$\begin{pmatrix} 0 \\ 1 \\ 0 \end{pmatrix}, \quad \begin{pmatrix} 1 \\ 0 \\ 1 \end{pmatrix}, \quad \begin{pmatrix} 1 \\ 0 \\ -1 \end{pmatrix}, \tag{2.15}$$

with the relative magnitudes, along the principal axes, of 1, $1+r_{13}(t)$, and $1-r_{13}(t)$ respectively.

The conventional way in which the function $C(\underline{x},t)$ is used to compute the coefficients D_{ijk} can not be applied here because $C(\underline{x},t)$ is unknown. Instead, the moments of $C(\underline{x},t)$ are used to calculate the coefficients. Substitution of the full expression for the adjoint Hermite polynomial in (2.11) shows that the coefficients are functions of the central moments, which are defined by

$$m_{l,m,n} = \int_{\substack{\text{all} \\ \text{space}}} \left(\frac{x_1-\bar{x}_1}{\sigma_1}\right)^l \left(\frac{x_2-\bar{x}_2}{\sigma_2}\right)^m \left(\frac{x_3-\bar{x}_3}{\sigma_3}\right)^n C(\underline{x},t)\,dV(\underline{x}). \tag{2.16}$$

The above central moments are calculated with the moments defined by

$$M_{m,n,p}(t) = \int_{\substack{\text{all} \\ \text{space}}} x_1^m x_2^n x_3^p C(\underline{x},t)\,dV(\underline{x}). \tag{2.17}$$

A method pioneered by Aris (1956) is here used in an alternate way to generate the moments required by (2.11). After suitable multiplication and partial integra-

tion over all space of each term in equation (2.1), one derives the following recurrence relationship:

$$M'_{m,n,p}(t) = m[(m-1)a_0 M_{m-2,n,p} + m a_1 M_{m-1,n,p} + (m+1)a_2 M_{m,n,p}]$$
$$+n(n-1)[b_0 M_{m,n-2,p} + b_1 M_{m+1,n-2,p} + b_2 M_{m+2,n-2,p}]$$
$$+p(p-1)[c_0 M_{m,n,p-2} + c_1 M_{m+1,n,p-2} + c_2 M_{m+2,n,p-2}]$$
$$+p[2m\varepsilon_0 M_{m-1,n,p-1} + \varepsilon_1(2m+1)M_{m,n,p-1}$$
$$+\varepsilon_2(2m+2)M_{m+1,n,p-1}] + p\sum_{i=1}^{q} d_i M_{m+i,n,p-i} \qquad (2.18)$$

Equation (2.18) is a system of first-order, ordinary, differential equations that can be approximated to $O(\tau^2)$, where τ is the non-dimensional time. The moments generated by that expression are normalized and converted into central moments using (2.16), which in turn are used to compute the coefficients D_{ijk}. The non-dimensional moments and coefficients D_{ijk} are provided in Appendix A.

To derive (2.18), the components of the diffusivity tensor and the mean velocity function in equation (2.1) were expanded in the following truncated Taylor series about the point of release:

$$\kappa_{11} = a_0 + a_1 x_1 + a_2 x_1^2, \qquad (2.19)$$

$$\kappa_{13} = \kappa_{31} = \varepsilon_0 + \varepsilon_1 x_1 + \varepsilon_2 x_1^2, \qquad (2.20)$$

$$\kappa_{22} = b_0 + b_1 x_1 + b_2 x_1^2, \qquad (2.21)$$

$$\kappa_{33} = c_0 + c_1 x_1 + c_2 x_1^2, \qquad (2.22)$$

$$U_3(x_1) = \sum_{i=1}^{q} d_i x_1^i, \qquad q \text{ finite.} \qquad (2.23)$$

The Taylor series expansions in (2.19-2.23) ensure that all continuous functions of κ_v and U_3 are locally represented by this scheme. When an instantaneous point-source is released for a sufficiently small-time interval, the resulting contaminant cloud will occupy only a small, finite region in space wherein the spatial variation of κ_v and U_3 are accurately described by (2.19-2.23). An estimate of the small-time interval in which κ_v is valid can be obtained by considering the typical length scale of the contaminant cloud to be $\sqrt{a_0 t}$ in time. In order for κ_{11} to be valid, the restriction

$$a_2 x_1^2 \gg a_0, \tag{2.24}$$

must be satisfied. Equation (2.24) then reduces to

$$t \ll \frac{1}{a_2}, \tag{2.25}$$

which, in non-dimensional variables, is

$$\tau^2 \beta^2 \ll 1. \tag{2.26}$$

With a small-time approximation to equation (2.18) and a truncated Taylor series expansion of κ_v, equation (2.4) is now a small-time solution without the consideration of boundaries. The zero-flux boundary condition relevant to environmental flows is considered in the next chapter. If one is interested in considering the effects of boundaries in a small-time approximation of the distribution of mean concentration, one could probably use one-dimensional Hermite polynomials and the method of eigenfunction expansions to determine the coefficients of the corresponding Hermite polynomials (see Smith, 1982b).

For small values of τ, most of the information is contained in the first few terms of (2.4). The use of higher order terms in expansion (2.4) often provides negative concentration values, which are unrealistic. Thus it is not the convergence of (2.4) that is of central importance, but rather to ensure that τ is small. However, theorems on the convergence of the Hermite-expansion are provided in Sansone (1959) and Mihaila (1968).

Chapter Three

Small-time Analyses and Method of Superposition

The principal aim of this chapter is to develop and verify a flexible solution-scheme that utilizes the basic solution derived in the previous chapter. The solution-scheme must be capable of describing the spread of contaminant in various environmental flows and have the capabilities of incorporating empirical information in the absence of good theoretical models. Before directing attention to the solution-scheme, it is of interest to examine the local (or small-time) behavior of a cloud of contaminant under the influence of variable diffusivities, cross-terms, and shear.

3.1 A small-time, instantaneous, point-source solution

The non-dimensional moments (to order τ^2), coefficients for the Hermite-polynomial expansion, and relevant non-dimensional parameters are provided in Appendix A. The following list includes some of the relevant moments for the Hermite-polynomial expansion:

$$\bar{x}_1 = a_1 t, \qquad \bar{x}_3 = \varepsilon_1 t \tag{3.1}$$

$$\sigma_1^2 = 2a_0 t + t^2(a_1^2 + 6a_0 a_2), \tag{3.2}$$

$$\sigma_2^2 = 2b_0 t + t^2(a_1 b_1 + 2a_0 b_2), \tag{3.3}$$

$$\sigma_3^2 = 2c_0 t + t^2(c_1 a_1 + 2a_0 c_2 + 2d_1 \varepsilon_0 + 4a_0 \varepsilon_2), \tag{3.4}$$

$$\overline{x_1 x_3} = \int_{\substack{\text{all} \\ \text{space}}} x_1 x_3 C(\underline{x},t)\, dV(\underline{x})$$

$$= 2\varepsilon_0 t + t^2(2a_2\varepsilon_0 + 2\varepsilon_1 a_1 + a_0 d_1 + 4a_0\varepsilon_2), \tag{3.5}$$

$$r_{13} = (\tau^2(\beta^2 h + \beta\phi + \psi + 4\xi) + h)/AE. \tag{3.6}$$

The non-dimensional concentration of contaminant, with non-zero D_{ijk} and non-zero r_{13} given by (3.6), is

$$\hat{C}(\underline{X},t) = \sigma_1\sigma_2\sigma_3 C(\underline{X},t)$$

$$= \frac{\exp(-\frac{1}{2}g(\underline{X}))}{(8\pi^3 |R|)^{1/2}}\left\{1 + \sum_{i+j+k=1}^{6}(-1)^{i+j+k} D_{ijk}(\tau) H_{ijk}(\underline{X}) + O(\tau^3)\right\}. \tag{3.7}$$

Equation (3.7) can now be used to examine the local behavior of a release of an instantaneous point-source. The surfaces $\hat{C} = constant$, when $\tau \to 0$, are concentric ellipsoids elongated in the direction of the principal axis which is inclined at $\pi/4$ to the horizontal axis x_3. Terms of order τ appear in the coefficients D_{ijk} with

$i+j+k \leq 3$ (see Appendix A), and distort the basic three-dimensional Gaussian distribution. At $O(\tau^2)$ the effects of dispersion come into play, evident from the non-dimensional parameter ψ in r_{13}, with further departures, due to the coefficients D_{ijk} with $3 \leq i+j+k \leq 6$, from normality. (Note that D_{ijk} with $i+j+k > 6$ are zero.) By setting $\kappa_{13} = 0$, it is clear that the effects of the non-zero gradient of κ appear at $O(\tau)$ following the strictly diffusive effects as $\tau \to 0$, and before the effects of dispersion which enter at $O(\tau^2)$. That sequence of events is consistent with the results of Chatwin (1976) who showed that the dominant mechanisms for small-time spread of contaminant were, sequentially, diffusion, diffusion-dispersion and, ultimately, dispersion. It is worth noting that for constant κ_y the center of masses given by (3.1) are zero; however, when a spatially varying κ_y is present, $\bar{x}_1$ and $\bar{x}_3$ are non-zero. Figure 2 shows the effects of the higher order terms in (3.7) on the location of the maximum concentration. The higher order terms tend to displace the location of the maximum value of $\hat{C}(\underline{X},\tau)$ from the origin. This salient feature is absent in Gaussian models (see Sutton, 1947; Hwang et al., 1979; Wilson et al., 1982; Fackrell and Robins, 1982), which is only the first term in expansion (2.4).

3.2 The effects of the cross-terms in the diffusivity tensor

In this section the salient features of a dispersing cloud of contaminant that are strictly due to κ_{13} and κ_{31} are singled out. It is clear, from Appendix A, that removal of the cross-terms in the moments and coefficients would result in a much

simpler expansion in (3.7). The one component of the inertial tensor given in (3.6) is also affected by the cross-term. The cross-terms in (3.6), represented by the coefficient h, are important when $\tau \to 0$. The most accessible feature of a dispersing cloud is its trajectory of the center of mass, which is

$$\bar{x}_3 = \left(\frac{\varepsilon_1}{a_1}\right)\bar{x}_1 + \frac{\overline{x_1^2}}{a_1^2}\left(a_0 d_2 + \frac{a_1 d_1}{2} + a_1 \varepsilon_2\right), \tag{3.8}$$

while

$$t \ll \frac{3(a_0 d_2 + a_1 d_1/2 + a_1 \varepsilon_2)}{2a_1^2 d_2 + a_2(6a_0 d_2 + a_1 d_1 + 2a_1 \varepsilon_2)} \tag{3.9}$$

and

$$t \ll \frac{1}{a_2}. \tag{3.10}$$

The ramification of the non-zero gradient cross-terms, represented by ε_1 and ε_2, is shown as a shift of origin of the parabolic profile given in (3.8), and shown on figure 3. Note that equation (3.8) and (3.9) reduce to the results obtained by Chatwin and Sullivan (eqn. 16 and 17b, 1981) in the absence of cross-terms (i.e., ε_1 and ε_2 are zero).

Another interesting feature that is affected by the cross-terms is the variance represented by equation (3.4). When cross-terms are included, the effects of shear, as represented by d_1, on this variance begin at order t^2. It is of interest to contrast this result with that of Smith (1982b), who calculated a small-time solution for the variance, to order t^3, without the inclusion of cross-terms and without cross-sec-

tional averaging of the concentration distribution. Smith's result (eqn. 4.12, 1982b) shows that the effects of shear on the variance begin at order t^3. Although Smith (1982b) has pointed out that cross-sectional averaging of the concentration distribution (see Chatwin, 1976) gives illusory evidence that effects of shear on the variance begin at order t^2, equation (3.4) shows that the inclusion of cross-terms could also cause the effects of shear on the variance to occur at order t^2

The solution (3.7) degenerates to an exact solution for a linear profile of velocity and values of constant κ_y (i.e., d_1, a_0, b_0, c_0 and ε_0 are non-zero in 2.19-2.23). This solution is

$$\hat{C}(\underline{X},T) = C(\underline{X},t)\sigma_1\sigma_2\sigma_3 = \frac{\exp(-\frac{1}{2}g(\underline{X}))}{(8\pi^3 \mid \underline{R} \mid)^{1/2}}, \tag{3.11}$$

$$\sigma_1^2 = 4a_0QT^2, \tag{3.12}$$

$$\sigma_2^2 = 4b_0QT^2, \tag{3.13}$$

$$\sigma_3^2 = 4c_0QT^2S^2, \tag{3.14}$$

where

$$T^2 = t/2Q, \tag{3.15}$$

$$Q = \frac{1}{d_1}\left(\frac{c_0}{a_0}\right)^{1/2}, \tag{3.16}$$

and

$$S^2 = 1 + 2hT^2 + 4T^4/3. \tag{3.17}$$

The r_{13} element of the correlation matrix R given by (2.14) is

$$r_{13} = (T^2 + h)/S. \tag{3.18}$$

It is easy to show that (3.11) is an exact solution to (2.1) when κ and the gradients of mean velocity are constant (Townsend, 1951; Yip, 1984). The exact solution is very simple and compact. Its description of a dispersing cloud of contaminant in an incompressible fluid, with a linear profile of velocity, is represented by just two parameters, T and h, the non-dimensional time and the cross-terms, respectively.

It is evident, from the presence of the parameter h in r_{13} and σ_1, that the effects of κ_{13} are most significant when $T \to 0$. As T increases, the entire process becomes dominated by the effects of shear, as can be seen from the presence of the coefficient d_1 in T. Also affected by the cross-terms are the following moments of the concentration distribution:

$$M_{1,0,1} = 2\varepsilon_0 t + a_0 d_1 t^2, \tag{3.19}$$

and

$$M_{0,0,2} = 2c_0 t + 2d_1 \varepsilon_0 t^2. \tag{3.20}$$

These effects are shown by the presence of the parameter ε_0, which occurs during $O(t)$ and $O(t^2)$ of the evolution of the cloud.

The exact solution (3.11), which is of Gaussian form and valid for all times, is useful for illustrating the qualitative effects of the cross-terms on $\hat{C}(X,T)$ (see Sullivan and Yip, 1985). By initializing $a_0 = b_0 = c_0$ to unity and h to zero, one can observe, in figure 4, that the surfaces of constant $\hat{C}$ are elongated along the

principal axis inclined $\pi/4$ from the horizontal axis x_3. As T increases, the ellipsoids are farther elongated in the same direction (see figure 4a). When $h=-1/2$, the surfaces of constant $\hat{C}$ are initially stretched out along the principal axis inclined at $3\pi/4$ from the x_3 axis, and as T increases the ellipsoidal surfaces evolve into surfaces qualitatively resembling the case $h=0$ at large T (see figure 4b).

The cross-terms in $\hat{C}(\underline{X},T)$, depending on the value of h relative to T, tend to suppress the effects of the linear velocity variation. This suggest that, in environmental flows, where the far-field distributions of contaminant are of interest, the effects of these cross-terms will be insignificant in the modeling process. However, in the study of small-time problems of dispersion, such as the injection of chemicals in blood vessels and the streamwise mixing in a small sample tube (Dewey and Sullivan, 1982), these cross-terms are likely to play a dominant role.

3.3 Large-time solutions and continuous source solutions: utility of the method of superposition

The linear property of the model equation (2.1) allows one to calculate a large-time solution, with superposition and the small-time, asymptotic solution (3.7), for an instantaneous source. That is, by considering the cloud of contaminant, at time t, to be made up of a large field of instantaneous sources, and the sum

of all the contributions from each source after a small-time interval Δt provides the concentration at $t + \Delta t$. In two dimensions, the cloud of contaminant is comprised of many instantaneous line-sources: in three dimensions, the cloud of contaminant is comprised of many instantaneous point-sources. The concentration of contaminant $\Gamma(\underline{x},t)$, after a small-time interval Δt, is

$$\Gamma(\underline{x},t+\Delta t) = \int_{\substack{\text{all}\\ \text{space}}} \Gamma(\underline{x}',t) C(\underline{x}-\underline{x}',\Delta t)\, dV(\underline{x}'), \tag{3.21}$$

where $C(\underline{x},t)$ is the small-time, asymptotic solution represented by the dimensional form of equation (3.7). Through the repeated use of (3.21), one can find the field of concentration $\Gamma(\underline{x},t)$ for individual clouds of contaminant for any time. The continuous-source solution $\bar{C}(\underline{x},t)$ is derived from the superposition of individual clouds convected downstream (see Csanady, pp.17, 1973). The solution for $\bar{C}(\underline{x},t)$ is expressed as

$$\bar{C}(\underline{x},t) = Q_s \int_{-\infty}^{t} \Gamma(\underline{x}, t-t')\, dt', \tag{3.22}$$

where Q_s is the steady source emission rate.

Equation (3.21) and (3.22) offer a simple and compact description of the spread of contaminant in environmental flows. The solution-scheme can describe distributions of arbitrary, finite sources, which can be continuous or instantaneous. Such distributions are more realistic, in practice, than instantaneous point-sources. Empirical information from the mean velocity and diffusivity profiles are utilized by the solution-scheme. However, these profiles must be

continuous before one can incorporate them into the solution-scheme. The calculation of equation (3.21) and (3.22) is a step-by-step procedure. This step-by-step approach is convenient because the unsteady feature of environmental flows can be taken into account by using update information from the flow-field during each stage of the calculations. Use of a vertical diffusivity profile adequately satisfies the inhomogeneity requirements discussed in chapter one. Thus the dominant features of environmental flows are well considered by this solution-scheme.

In practice, the cloud of contaminant is discretized into tiny square cells, and the application of the small-time solution is at the intersecting grid points. The summation of all the individual clouds that result from instantaneous releases at the various grid points then provides the solution for one discrete time-step. To advance to the next time-step, one repeats this procedure. It is important to ensure that the grid size is small with respect to the distance over which an appreciable change in concentration takes place, i.e.,

$$\Delta x_i \ll \left(\frac{1}{C} \frac{\partial C}{\partial x_i} \right)^{-1}, \tag{3.23}$$

and also small with respect to σ_i that occur in time $O(\tau^2)$ between steps. With κ_v and U_i dependent on z only, efficiency in the calculation of (3.21) is gained. By adopting a fixed grid representing the location of all the instantaneous sources, all of the small-time solutions, for each vertical location of a grid point, can be pre-tabulated, and the advance of the cloud by a small discrete time-step is

accomplished through the addition of pre-tabulated information. When an instantaneous source is released at each vertical grid point, its parameters, $\tau,\beta,\rho,\alpha,\omega,\gamma,\psi,h,\phi,\xi$, are changed to reflect the vertical change in κ_z and U_1, and the cloud of contaminant is convected downwind with the basic transformation, $x'' = x - Ut$. This transformation ensures a quick advancement of the cloud of contaminant on the fixed grid. The construction of a solution for a continuous source is simply the accumulation of the values of concentration from clouds over the previous discrete time-steps in the cloud evolution at the same grid points.

The standard no-flux condition at ground-level is satisfied by setting up a fully reflective barrier at $z = 0$. In practice, this is accomplished by placing an image source equidistant from the real source.

At this stage it is of interest to examine the errors arising from the calculation of (3.21). The field of concentration for one time step is expressed by equation (3.21), where

$$C(\underline{x},t) = \frac{\exp(-\frac{1}{2}g(\underline{X}))}{\sigma_1\sigma_2\sigma_3(8\pi^3 \mid R \mid)^{\frac{1}{2}}}\left\{1 + \sum_{i+j+k=1}^{6}(-1)^{i+j+k}D_{ijk}(\tau)H_{ijk}(\underline{X}) + O(\tau^3)\right\} \qquad (3.24)$$

and

$$\tau^2 = \frac{a_1^2 t}{2a_o} \quad X_i = \frac{x_i - \bar{x}_i}{\sigma_i} \qquad (3.25)$$

For convenience, let

$$L = 1 + \sum_{i+j+k=1}^{6} (-1)^{i+j+k} D_{ijk}(\tau) H_{ijk}(\underline{X}), \tag{3.26}$$

and let P represent the exponential part of (3.24). That is

$$C(\underline{x},\Delta t) = P(\underline{x},\Delta t)[L(\underline{x},\Delta t) + O(\tau^3)]. \tag{3.27}$$

Note that the error term in equation (3.27) is of order τ^3. For the first time-step,

$$\Gamma(\underline{x},\Delta t) = P[L + O(\tau^3)]. \tag{3.28}$$

That is, one starts a solution by using the small-time, asymptotic solution. Discretization of the cloud of contaminant, that is represented by equation (3.28), results in a field of seed-points. The next time-step involves the product of the value of concentration at $\underline{x}'$ and the asymptotic solution $C(\underline{x},t)$. The contribution from a seed-point located at $\underline{x}'$ is

$$P(\underline{x}',\Delta t)[L(\underline{x}',\Delta t) + O(\tau^3)] \cdot P(\underline{x} - \underline{x}',\Delta t)[L(\underline{x} - \underline{x}',\Delta t) + O(\tau^3)]. \tag{3.29}$$

The sum of the contributions from other sources within the marked fluid provides the field of concentration for the next time-step, $2\Delta t$. If τ is very small, expansion of the above equation results in errors that are of order τ^3 and τ^6 respectively. Thus errors incurred in the above expression will be very small. The largest error term in that expression is still of order τ^3. When calculating a continuous point-source solution, the errors will still be of order τ^3 because the solution is constructed by adding the clouds released.

The analysis shown above is a simple estimate of one source of error incurred during the superpositioning procedure. Another way (and perhaps more convenient) to verify (3.21) is to compare the results with some analytical solutions or finite-difference calculations. This is critical, especially before comparing the results of the solution-scheme with experimental data. One wants to be sure that the solution-scheme is in fact providing accurate solutions to (2.1). Even if the solutions are accurate, one wants to be assured that this procedure is as flexible and as efficient as a direct numerical solution to the convective-diffusion equation would be.

3.4 A comparison with a numerical and an analytical solution

For simplicity and computational efficiency, a two-dimensional equation was considered for comparison purposes. The steady-state, two-dimensional form of (1.1),

$$u(z)\frac{\partial C}{\partial x} = \frac{\partial}{\partial z}\left(\kappa(z)\frac{\partial C}{\partial z}\right), \tag{3.30}$$

for a continuous line-source at $z = H_1$ above an impermeable plane at $z = 0$, with velocity

$$u(z) = u_0 z^{1/2} \tag{3.31}$$

and diffusivity

$$\kappa(z) = \kappa_0 z^{1/2}, \tag{3.32}$$

where u_0 and κ_0 are constants, was solved analytically by Smith (1957). In (3.30), the streamwise (x) gradients in $C(x,z)$ were considered to be small with respect to the vertical (z) gradients and neglected. In (3.32) the value of $\kappa(z)$ at $z=0$ is unrealistic; however, the values of $C(x,0)$ were found to have a finite limit (see pp.134, Csanady, 1973) and shown on figure 5. The linear property of (2.1) simplifies the reduction of (3.7) to a two-dimensional, small-time solution, which allows for an efficient comparison with some exact solutions of Smith (1957) and a numerical finite-difference scheme. The solution represented by equation (3.7), without cross-terms in the diffusivity tensor, as required here, simplifies to

$$\sigma_1\sigma_3 C(\underline{X},t)=\frac{\exp(-\frac{1}{2}g(\underline{X}))}{2\pi\,|R|^{1/2}}\left\{1+\sum_{i+k=1}^{6}(-1)^{i+k}D_{ik}(\tau)H_{ik}(\underline{X})+O(\tau^3)\right\} \tag{3.33}$$

where

$$X_i=\frac{x_i-\bar{x}_i}{\sigma_i},\qquad i=1\&3, \tag{3.34}$$

$$g(\underline{X})=\underline{X}^T R^{-1}\underline{X}, \tag{3.35}$$

$$R=\begin{pmatrix}1 & r\\ r & 1\end{pmatrix}, \tag{3.36}$$

$$\bar{x}_i=\int_{\substack{\text{all}\\ \text{space}}} x_i C(\underline{x},t)\,dV(\underline{x})\qquad i=1\&3, \tag{3.37}$$

$$r=\int_{\substack{\text{all}\\ \text{space}}} X_1X_3 C(\underline{x},t)\,dV(\underline{x}), \tag{3.38}$$

and

$$\sigma_i^2 = \int_{\substack{\text{all} \\ \text{space}}} (x_i - \bar{x}_i)^2 C(\underline{x},t)\,dV(\underline{x}) \qquad i = 1\&3. \tag{3.39}$$

$|R|$ and R^{-1} represent the determinant and inverse of the correlation matrix R respectively. The requisite Taylor series for the diffusivities, κ_{11} and κ_{33}, and velocity $u(x_1)$, are represented by (2.19-2.22) and (2.23), respectively. Subscripts, 1 and 3, represent the vertical and horizontal directions respectively. The following is a list of non-zero coefficients $D_{\mu}(\tau)$, to order τ^2, of the corresponding two-dimensional Hermite polynomial H_{μ}:

$$D_{0,0} = 1, \tag{3.40}$$

$$D_{1,2} = -\tau(2\gamma^2/2)/AE^2, \tag{3.41}$$

$$D_{2,2} = \tau^2(2\gamma^2/3 + \beta^2\omega^2/3)/A^2E^2, \tag{3.42}$$

$$D_{3,0} = -\tau(1/2)/A^3, \tag{3.43}$$

$$D_{2,4} = \tau^2(\gamma^4/8)/A^2E^4, \tag{3.44}$$

$$D_{0,4} = \tau^2(\gamma^4/6)/E^4, \tag{3.45}$$

$$D_{4,2} = \tau^2(\gamma^2/4)/A^4E^2, \tag{3.46}$$

$$D_{4,0} = \tau^2(1/2 + \beta^2/3)/A^4, \tag{3.47}$$

$$D_{6,0} = \tau^2(1/8)/A^6. \tag{3.48}$$

The non-dimensional parameters that appear in (3.40-3.48) are defined in Appendix A. Without cross-terms, the parameter E in Appendix A is now

$$E^2 = 1 + \tau^2(\gamma^2 + \omega^2\beta^2). \tag{3.49}$$

Relevant moments for the two-dimensional distribution (3.33) are

$$\bar{x}_1 = a_1 t, \qquad \bar{x}_3 = 0, \qquad r = \tau^2\psi/AE, \tag{3.50a}$$

$$\sigma_1^2 = 2a_0 t + t^2(a_1^2 + 6a_0 a_2), \tag{3.50b}$$

$$\sigma_3^2 = 2c_0 t + t^2(c_1 a_1 + 2a_0 c_2). \tag{3.50c}$$

Equation (3.21) and (3.22) were used to obtain a solution for a continuous, elevated line-source represented by equations (3.30-3.32). The grid sizes employed in this comparison were $\Delta x_1 = 0.5$ and $\Delta x_3 = 0.5$. A comparison is made in figure 6 and figure 7, of the values of concentration along fixed vertical and horizontal lines respectively, between the Smith (1957) solution to (3.30-3.32) and the solution-scheme outlined in the previous section. The source was placed sufficiently away from the impermeable boundary so that any appreciable amount of contaminant did not arrive at $z = 0$ over the distances downstream specified in the figures. Note that the trajectory of the vertical location of the maximum concentration in figure 6 moves toward $z = 0$. Furthermore, there is a slight shift between the Smith (1957) solution and values from the solution-scheme in figure 6 because the streamwise diffusivity was included in the solution-scheme where as it was neglected in Smith's (1957) model equation. Near the source, bumps appear in the solution generated with (3.21) and (3.22). These bumps were an artifact of the solution procedure. In using the discrete representation of a continuous source, (3.22), it was efficient to use a fixed value of Δt that was comparable with the largest time interval for which the the small-time, asymptotic solution (3.7) was valid. However, near the source and circumstances when the cloud size was comparable with its convective displacement during Δt, slight anomalies appeared. Unlike the growing oscillations that often result from numerical methods em-

ploying central differencing schemes on parabolic equations (see Patel, Markatos and Gross, 1980), these anomalies were reduced with increasing cloud size downstream. One can rectify this problem by using a variable time step which increases with time during the evaluation of (3.22). In this comparison the modified Bessel function appearing in the Smith (1957) solution becomes singular at the source and the series approximation used could only be confidently applied at the downstream distances given in the figures.

In order to assess the effects of the (unrealistic) zero-diffusivity feature of the Smith (1957) profile, (3.32), a low source-height of $H_1 = 2$ was used. For this case, where a significant amount of contaminant has reached the solid boundary, a fully reflective boundary with an image source equidistant below the boundary was used in the solution-scheme to satisfy the no-flux condition at the ground: That is, the diffusivity and velocity profiles were made into even functions as

$$u(z) = u_0\left((z^2 + \dot{\varepsilon}_1)^{1/4} - \dot{\varepsilon}_1^{1/4}\right) \tag{3.51}$$

and

$$\kappa(z) = \kappa_0(z^2 + \dot{\varepsilon}_2)^{1/4}, \tag{3.52}$$

where $\dot{\varepsilon}_1$ and $\dot{\varepsilon}_2$ are O(1) constants, and thus ensured a rapid approach, with increasing z, to the form (3.31) and (3.32). The curves of concentration at fixed values of z and illustrating the interaction of contaminant with the solid boundary are shown on figure 5. The ground-level, steady-state concentration could not be computed with the solution-scheme for very low values of $\dot{\varepsilon}_1 = \dot{\varepsilon}_2 = 0.1$ (used here to compare with values of $\dot{\varepsilon}_1 = \dot{\varepsilon}_2 = 0$ in (3.31) and (3.32)), and this difficulty

appears to be consistent with discussion of the convergence of (3.22) given in pp.16, Csanady (1973). Following a sufficient downstream distance, high values of concentration appear near the wall, and this important region warrants further investigation.

To assess whether or not the solution-scheme is capable of describing concentration of contaminant in the near wall region, a simple finite difference scheme was used to compare the results from the solution-scheme. An alternating-direction, implicit method (A.D.I.) was used to obtain a numerical solution for

$$\frac{\partial C}{\partial t} + u(z)\frac{\partial C}{\partial x} = \kappa(z)\frac{\partial^2 C}{\partial x^2} + \frac{\partial}{\partial z}\left(\kappa(z)\frac{\partial C}{\partial z}\right), \tag{3.53}$$

with boundary conditions,

$$C(\pm\infty, z, t) = 0, \tag{3.54}$$

$$C(x, \infty, t) = 0 \tag{3.55}$$

and

$$\left(\frac{\partial C}{\partial z}\right)_{z=0} = 0, \tag{3.56}$$

and initial condition,

$$C(x, z, 0) = \delta(x - x_0)\delta(z - z_0). \tag{3.57}$$

The profiles of $\kappa(z)$ and $u(z)$ are prescribed by (3.51) and (3.52). Boundaries were chosen to be sufficiently far away from the cloud centers at all times to satisfy, to a good approximation, the zero concentration boundary conditions, (3.54-3.55).

The asymptotic, small-time solution (3.33) was used in place of the delta function initial condition (3.57). The steady-state, continuous-source solution was then compiled using (3.21) and (3.22). This procedure avoids the difficult downstream boundary condition that occurs in the direct solution of (3.30). In the numerical scheme, each implicit scheme in a particular direction involved the direct solution of a tri-diagonal set of equations when central differencing was used on the diffusion terms and a backward difference scheme was used on the convective term. With this approach, oscillations did not appear in the solutions (see Mitchell and Griffith, 1980). Although the local spatial resolution was only first order, one could use a higher-order scheme. Patel et al. (1980) and Gupta et al. (1984) provide higher-order schemes for the steady-state equation. In the context of environmental flows the model equation (3.30), with empirical data for the diffusivities and velocity profiles, with attendant experimental errors, does not in itself warrant further accuracy, and the additional accuracy is pertinent to the stability and convergence of the numerical procedures. The success of any scheme for the numerical solution of the convective-diffusion equation will be reasonably specific to the choice of velocity and diffusivity profiles that one wishes to use, and these profiles usually adopt a wide variety of shapes in environmental flows.

The following algorithms provided stable, non-oscillatory, numerical solutions:

Solving x implicitly and z explicitly

$$-a_i C_{i-1,j,n+1} + b_i C_{i,j,n+1} - c_i C_{i+1,j,n+1} = d_i, \tag{3.58}$$

where

$$a_i = \frac{\Delta t}{\Delta x} u(z) + \kappa(z) \frac{\Delta t}{(\Delta x)^2}, \tag{3.59}$$

$$b_i = 1 + 2\kappa(z) \frac{\Delta t}{(\Delta x)^2} + u(z) \frac{\Delta t}{\Delta x}, \tag{3.60}$$

$$c_i = \kappa(z) \frac{\Delta t}{(\Delta x)^2}, \tag{3.61}$$

and

$$d_i = \left(1 - 2\kappa(z) \frac{\Delta t}{(\Delta z)^2}\right) C_{i,j,n} + \left(\kappa(z) \frac{\Delta t}{(\Delta z)^2} + \kappa'(z) \frac{\Delta t}{2\Delta z}\right) C_{i,j+1,n}$$

$$+ \left(\kappa(z) \frac{\Delta t}{(\Delta z)^2} - \kappa'(z) \frac{\Delta t}{2\Delta z}\right) C_{i,j-1,n}. \tag{3.62}$$

Advancing to the next time-step by solving z implicitly and x explicitly.

$$-a_j C_{i,j-1,n+2} + b_j C_{i,j+1,n+2} - c_j C_{i,j,n+2} = d_j, \tag{3.63}$$

where

$$a_j = \kappa(z) \frac{\Delta t}{(\Delta z)^2}, \tag{3.64}$$

$$b_j = \kappa(z) \frac{2\Delta t}{(\Delta z)^2} + \kappa'(z) \frac{\Delta t}{\Delta z} + 1, \tag{3.65}$$

$$c_j = \kappa(z)\frac{\Delta t}{(\Delta z)^2} + \kappa'(z)\frac{\Delta t}{\Delta z}, \tag{3.66}$$

and

$$d_j = \left(u(z)\frac{\Delta t}{\Delta x} + \kappa(z)\frac{\Delta t}{(\Delta x)^2}\right)C_{i-1,j,k+1} + \left(1 - u(z)\frac{\Delta t}{\Delta x} - \kappa(z)\frac{2\Delta t}{(\Delta x)^2}\right)C_{i,j,k+1}$$

$$\left(\kappa(z)\frac{\Delta t}{(\Delta x)^2}\right)C_{i+1,j,k+1}. \tag{3.67}$$

After each time-step, mass conservation was monitored using

$$\int_{\substack{\text{all}\\ \text{space}}} C(\underline{x},t)\,d\mathcal{V}(\underline{x}) = 1 \tag{3.68}$$

An immediate comparison can be made between the efficiency of the solution-scheme and the use of the A.D.I. method, where, in both methods, superposition of individual clouds at intervals of 0.25 seconds was used. To produce a cloud with the A.D.I. method, 25 time-steps ($\Delta t = .01$) were used for each successive time interval whereas that same cloud is produced in one time-step with the superposition procedure of the solution-scheme.

The results from using the solution-scheme and the results from using the A.D.I. method are shown in figure 8, and appear to be in good agreement with each other. The values of concentration in figure 8 decreased rapidly with distance from the source because only 45 individual clouds were used for the comparison. The large downstream range specified in figure 8 allowed a signifi-

cant amount of contaminant to reach the solid boundary, and this critical region in which the solutions from the scheme could not be compared with Smith's (1957) analytical solution is now encompassed.

The fact that environmental flows are often unsteady suggest that using the solution-scheme to solve (3.53) is a better choice than solving the steady-state equations. The scheme is so flexible that any temporal changes in the flow-field can be incorporated (see Sullivan, 1983). The use of (3.22) to find values of steady-state concentration shows that the length of time required for steady-state values will increase with distance downstream and with proximity to the wall. The time required for steady-state, wall-level concentrations to be achieved is shown as a function of downstream distance on figure 9. This figure illustrates how far downstream a steady-state value would be reached for a given time-scale of change in the flow conditions.

A theoretical framework is now established, and the validity of the model equation (1.1), especially with regards to the description of the spread of contaminant in environmental flows, can be assessed.

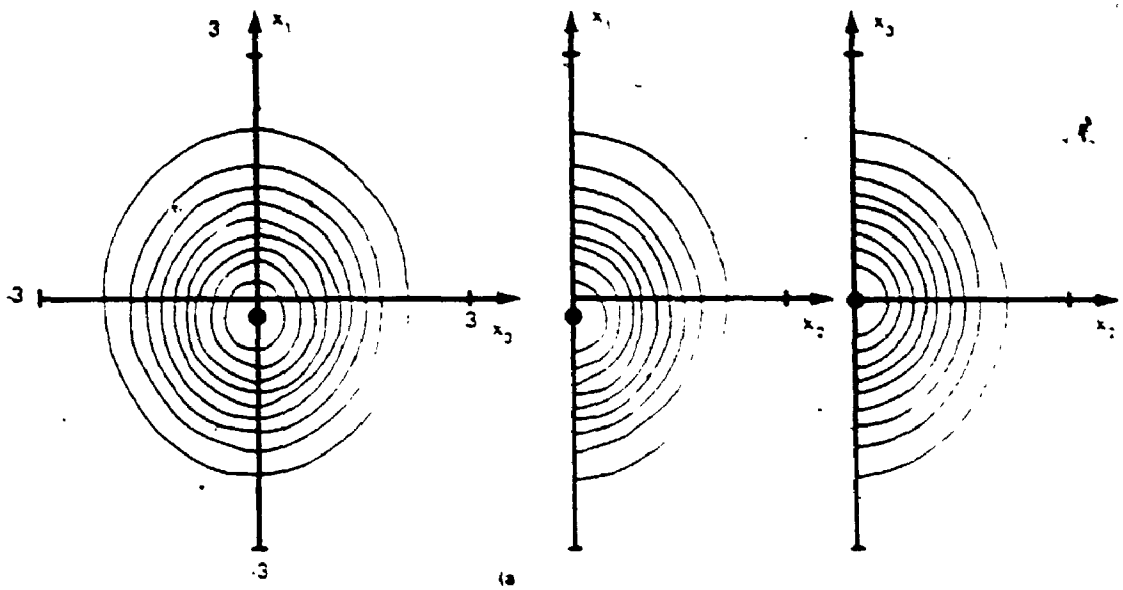

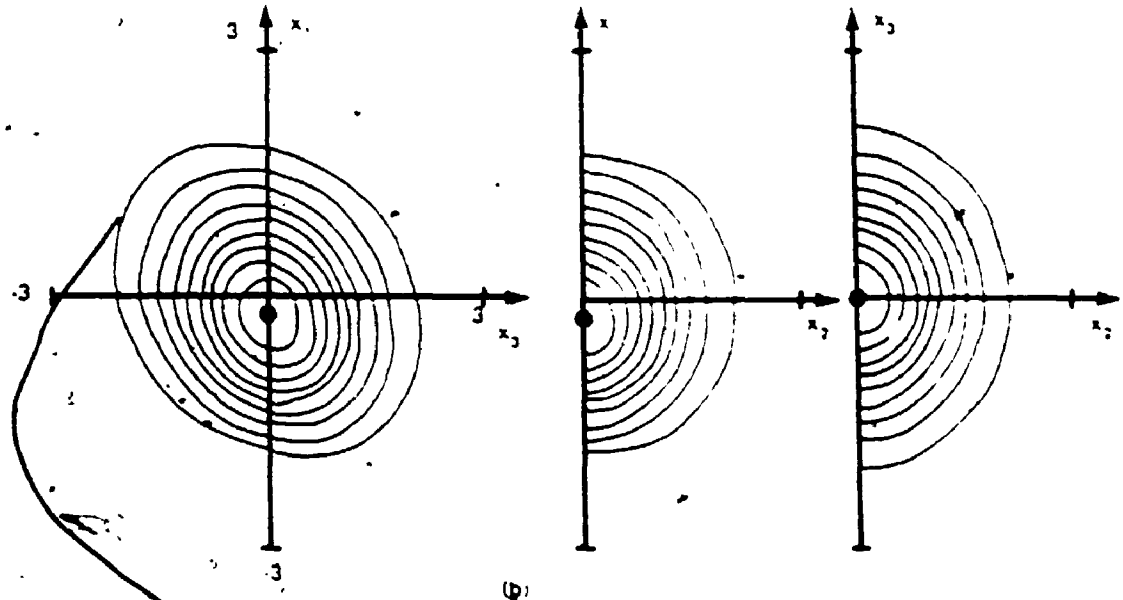

Figure 2
Concentric curves enclose values of concentration that were 90%, 80%, 70% etc. of the maximum value (indicated by) on the planes $X_2 = 0$, $X_3 = 0$, $X_1 = 0$ at $\tau = 0.1$. In (a), $\beta = \rho = \alpha = \omega = \gamma = \psi = 1$ and $h = \phi = \xi = 0$. In (b), h, ϕ and ξ were set to -0.2.

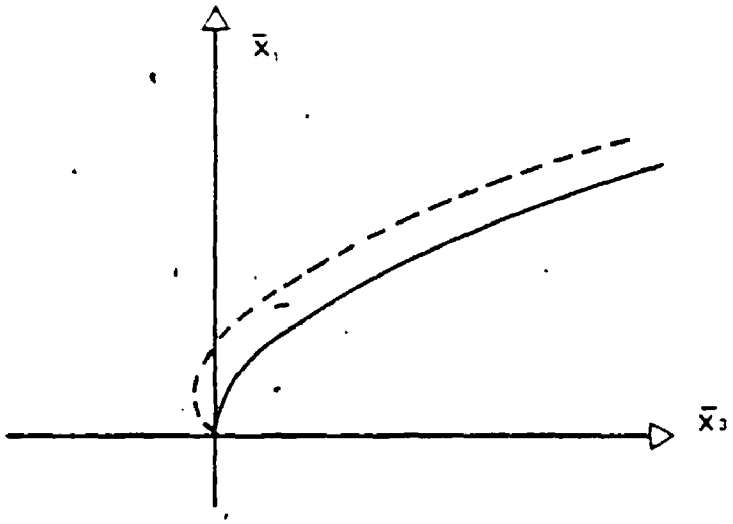

Figure 3
The trajectory of the centre-of-mass of a contaminant cloud with cross-terms included (----), and cross-terms excluded (——).

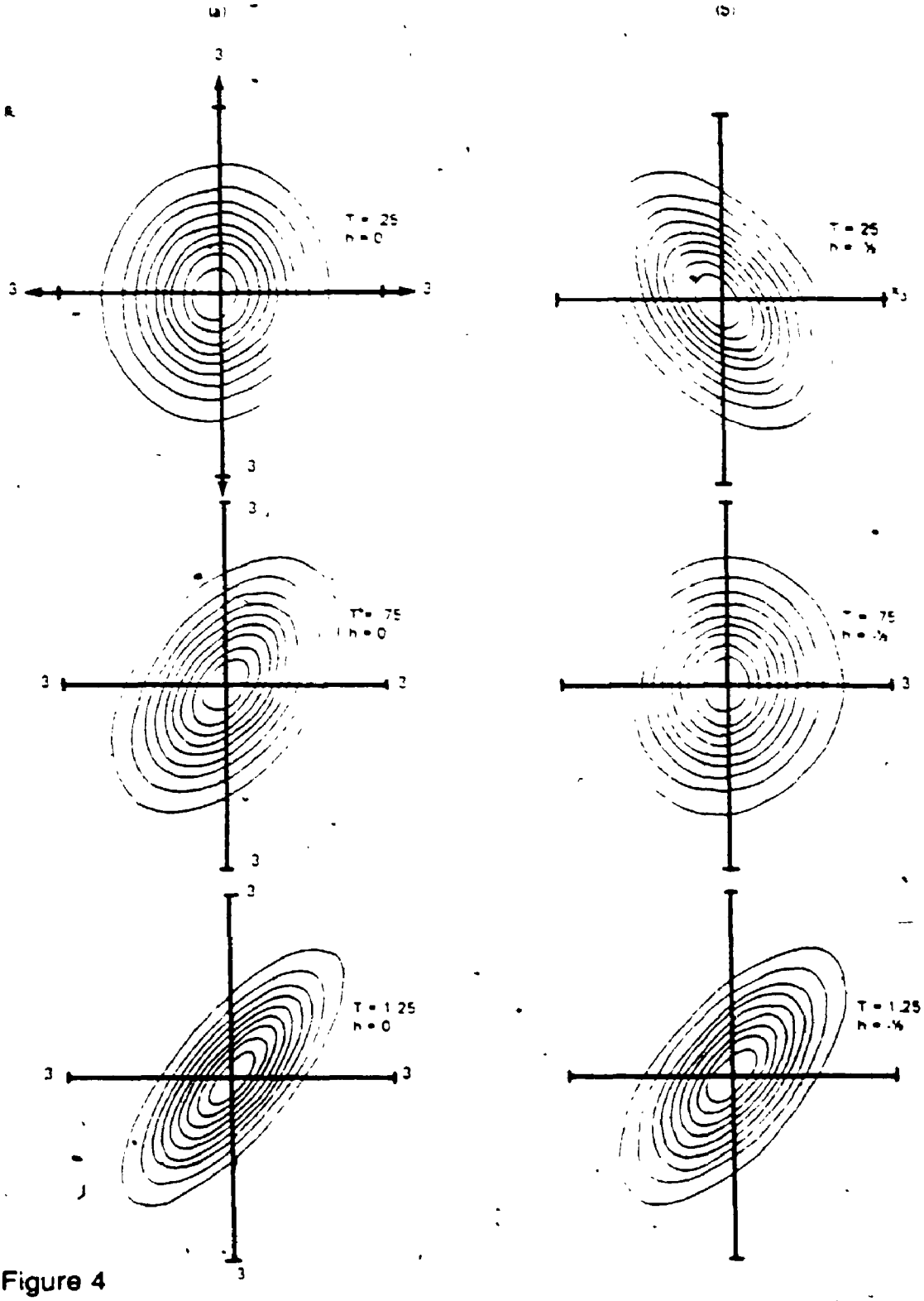

Figure 4
A comparison of the exact solution given in equation (3.11) on the $X_2 = 0$ plane with $h = 0$ in (a) and $h = -1/2$ in (b), at $T = 0.25, 0.75, 1.25$ starting at the top of the figure. Scale and notation as in Figure 2.

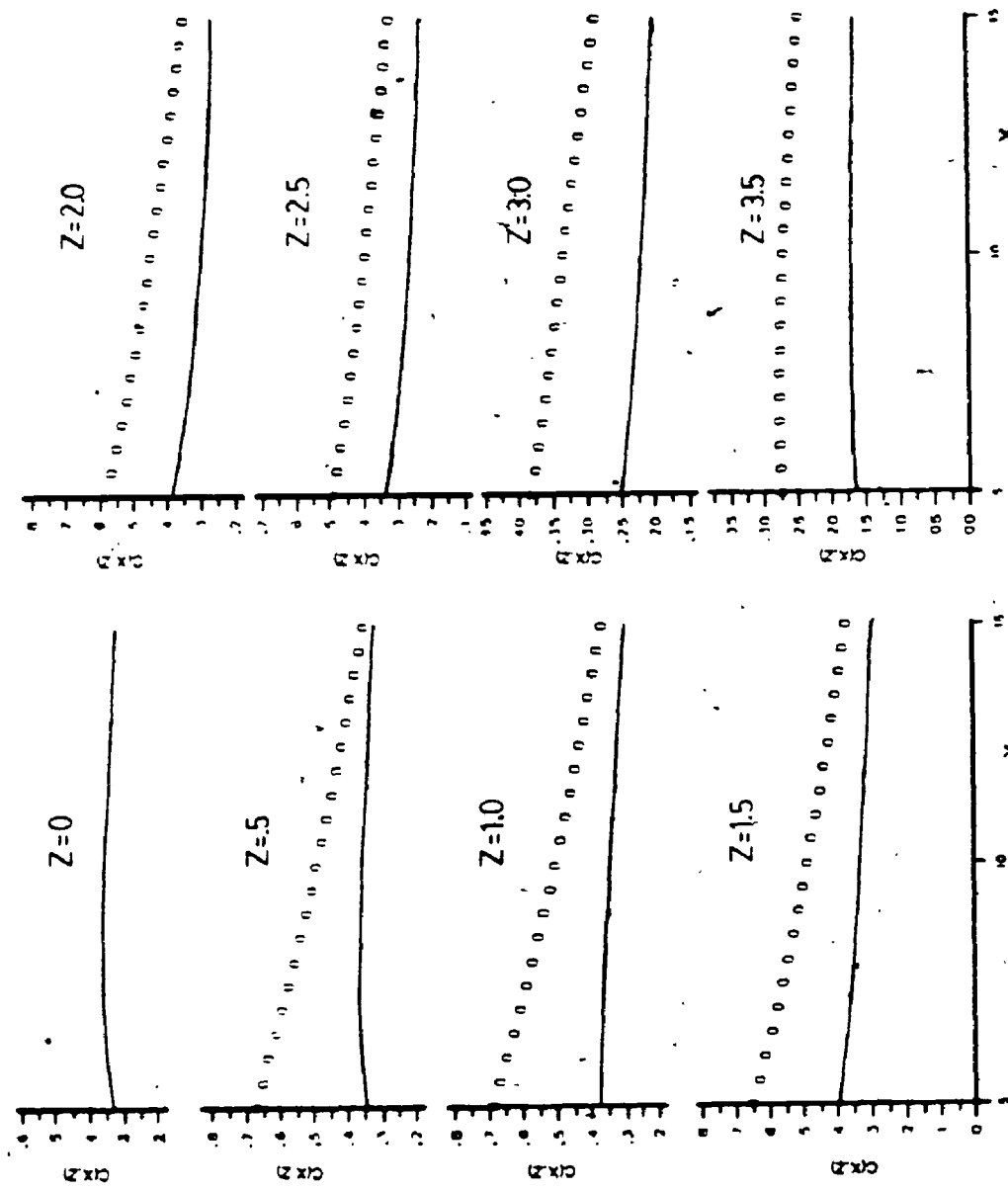

Figure 5
Horizontal concentration profiles at various heights in arbitrary but consistent units with Smith (1957). $Q_s = 5, h \pm 2, \mu_0 = 3, \kappa_0 = 0.5, \dot{\varepsilon}_1 = \dot{\varepsilon}_2 = 0.1$ (——) Smith, (0 0 0 0) solution-scheme. Note, $\varepsilon_i = 0$ $(i = 1,2)$ in Smith's solutions.

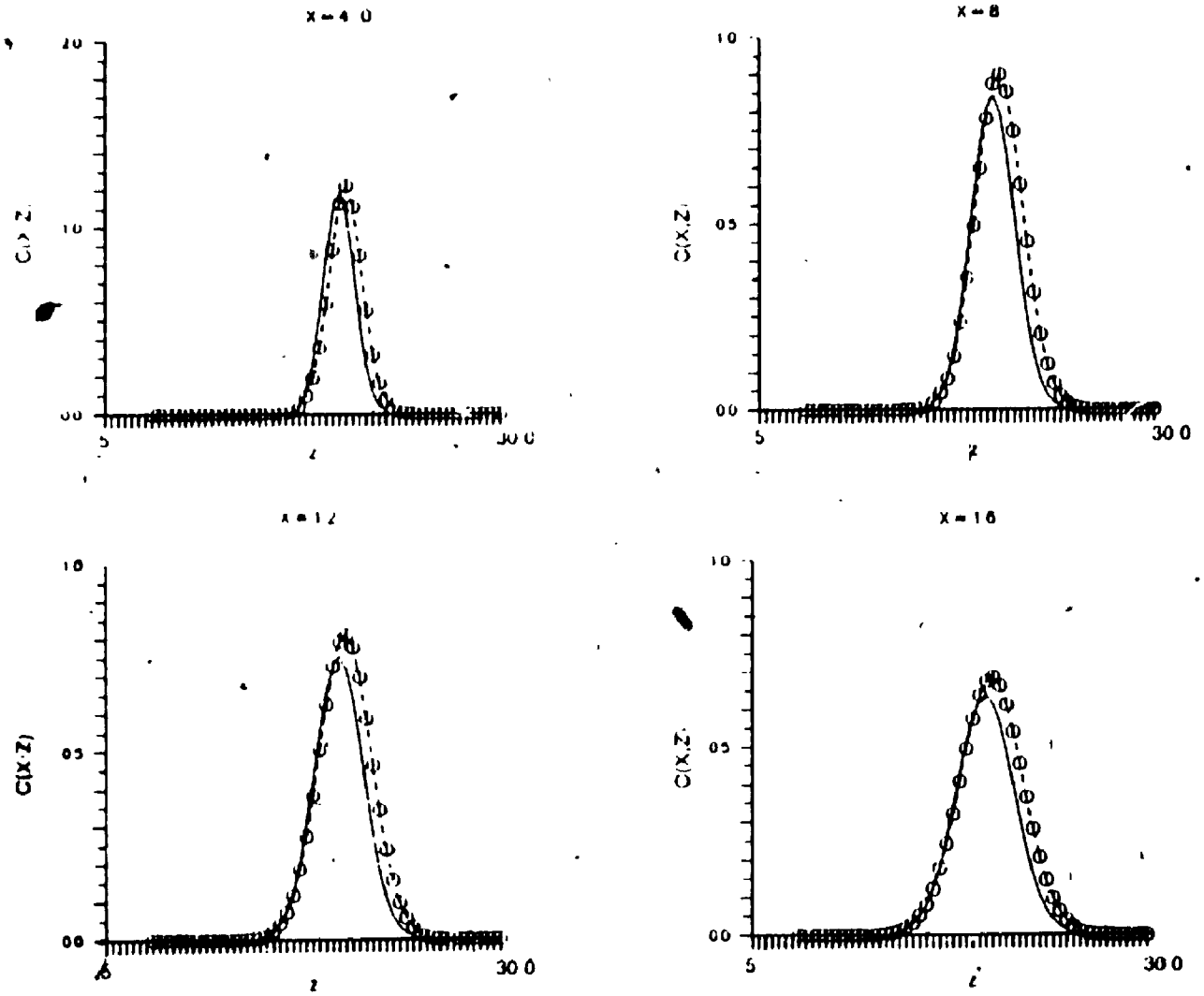

Figure 6
Vertical concentration profiles at various downstream distances in arbitrary but consistent units with Smith (1957). $Q_s = 4, h = 15, u_0 = 3, \kappa_0 = 0.5$, $\varepsilon_1 = \varepsilon_2 = 0.1$ (——) Smith, (0 0 0) solution-scheme.

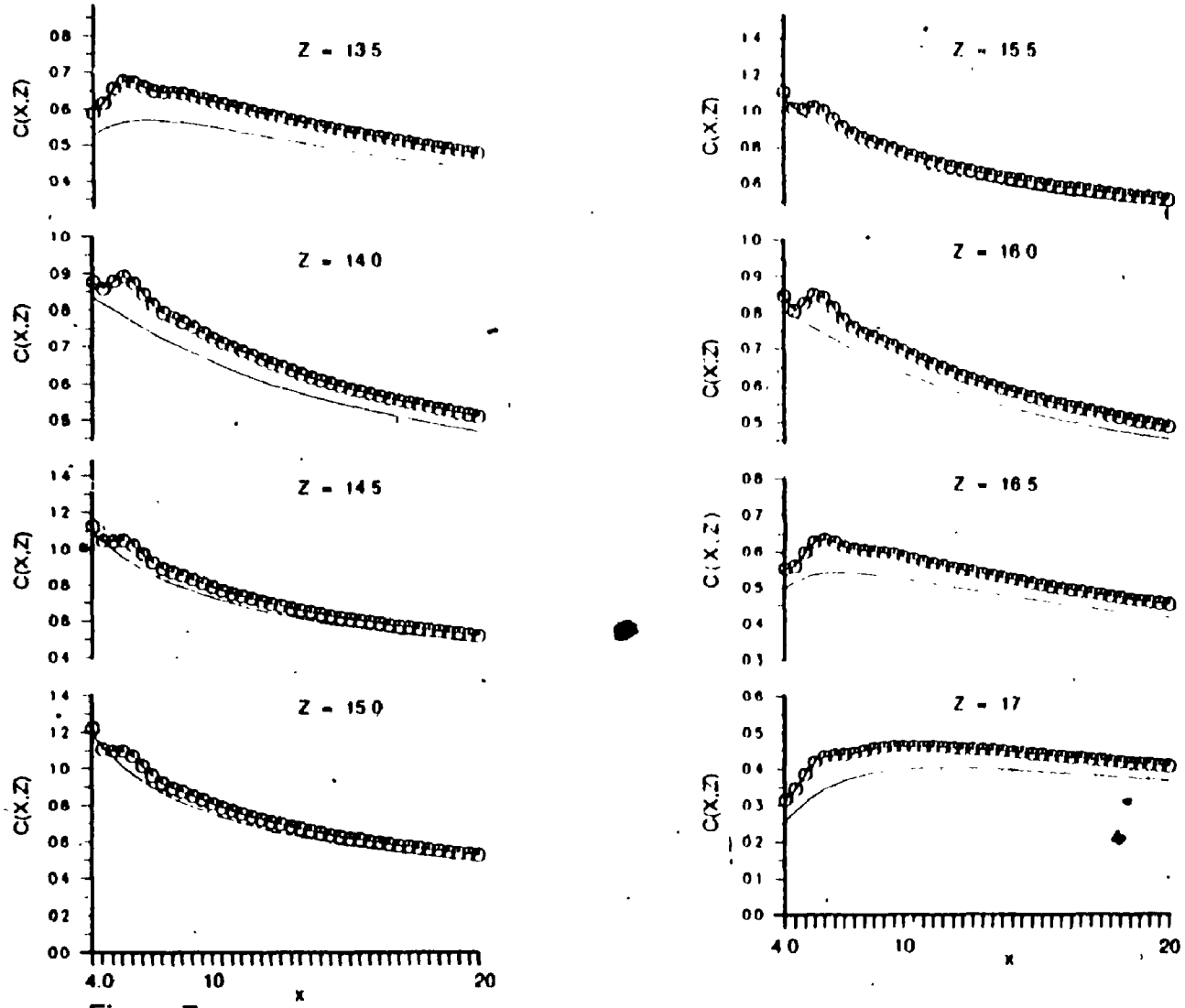

Figure 7
Horizontal concentration profiles at various heights. Parameters and symbols as in figure 6.

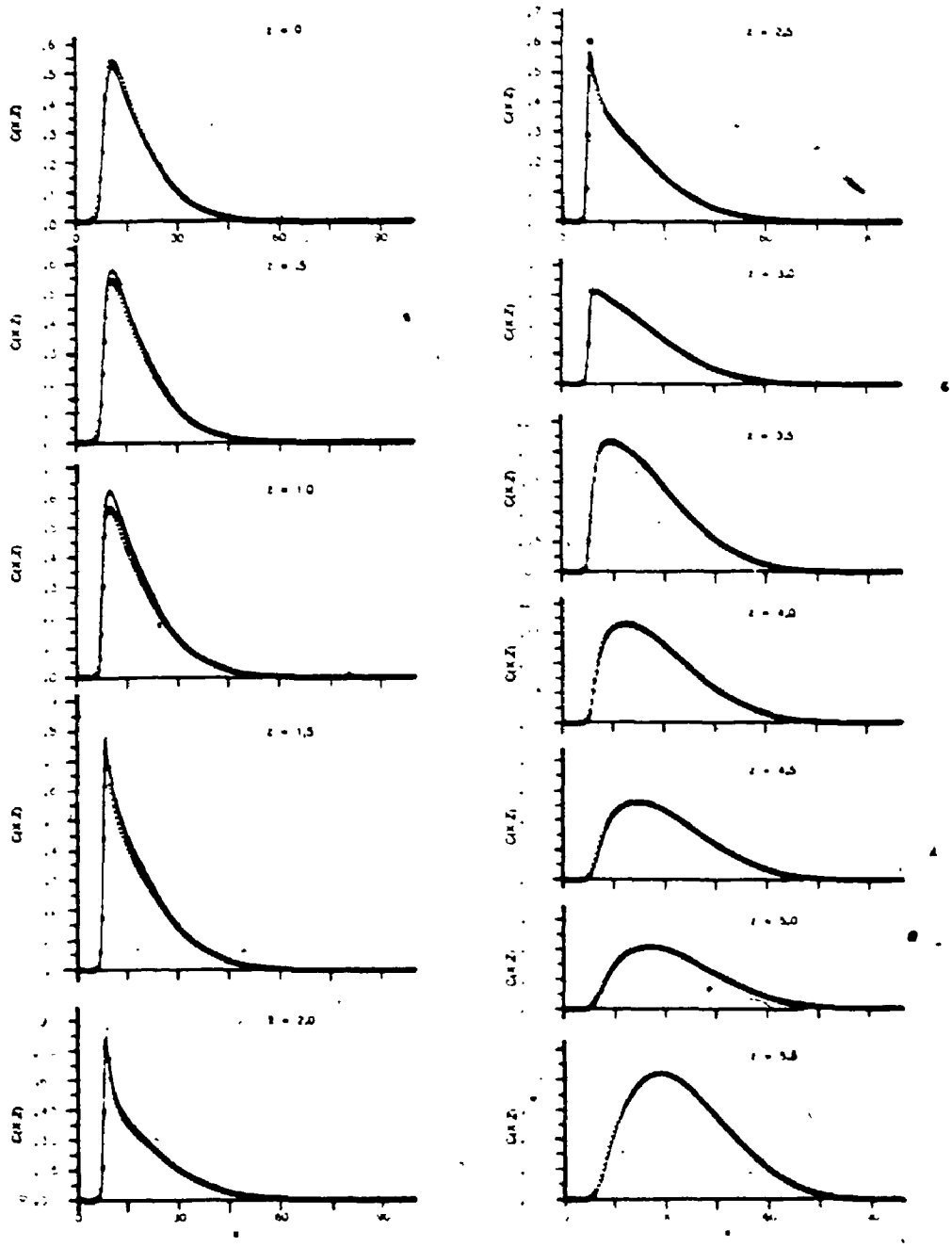

Figure 8
A comparison of concentration profiles for various vertical planes between solution-scheme values (——) and a numerical solution (0-0-0) given in equations (3.58-3.67). $Q_e = 4, h = 2, \varepsilon_1 = \varepsilon_2 = 0.1, \mu_0 = 3, \kappa_0 = 0.5$. The horizontal source location was at $x = 5$ and 45 individual clouds were used in equation (3.22).

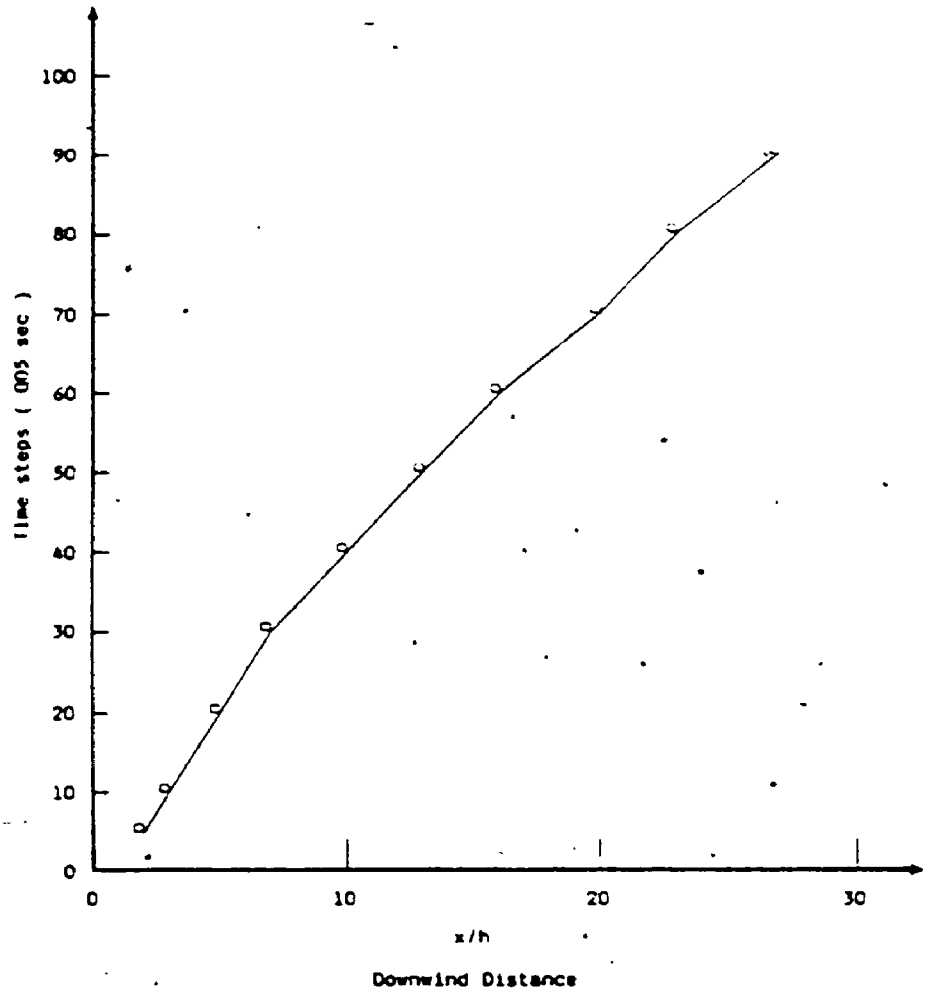

Figure 9
The time required to reach steady-state values of ground-level concentration for the solution-scheme values given in figure 11.

Chapter Four

Experimental Verification

In chapter three, a numerical validation of a robust and versatile solution-scheme was provided. What follows now is an assessment of the model equation (1.1) using recent experimental data from Raupach and Legg (1983), and Fackrell and Robins (1982). Both experiments are concerned with the dispersion of a passive contaminant in the region of constant stress within a neutral, turbulent boundary-layer. This is one flow-configuration for which the model equation (1.1) is thought to be on a reasonably firm theoretical foundation (see pp.4, Pasquill, 1974). Such a practically important and relatively simple flow-configuration presents a good occasion to illustrate the utility of the solution-scheme and to test the model equation (1.1). In particular, the controversy over the inclusion of the cross-terms in that simple flow-configuration can be examined.

4.1 A comparison with Raupach and Legg (1983) data

Raupach and Legg (1983) have made detailed measurements of the velocity profile and values of temperature (i.e., temperature was used a passive scalar) in the relatively sensitive region, at moderate distances downstream from an elevated line-source, within a two-dimensional, turbulent boundary-layer. The flow in the wind tunnel was over a gravel bed with a nominal gravel size of $7mm$. The source used in their experiment was a heated wire located at $h_1 = 60mm$ above a rough wall. The temperature of the wire was reported to be low enough to avoid any buoyancy effects. The measured velocity profile was found to coincide with the theoretical, law-of-the-wall profile,

$$u(z) = \frac{u_*}{k} \ln(z/z_0), \tag{4.1}$$

where $u_* = 48cms^{-1}$ is the friction-velocity, $k = 0.38$ is von Karman's constant, and the roughness parameter $z_0 = 0.12mm$. Profiles of mean concentration of contaminant $C(z/h_1)$, at downstream locations of $x/h_1 = 2.5, 7.5, 15.0, 30.0$, are provided in Raupach and Legg (1983) and reproduced here in figure 11.

In order to apply the solution-scheme to that flow-configuration, the velocity,

$$u(z) = \frac{u_*}{2k} \ln((z/z_0)^2 + \exp(-(z/z_0)^2)), \tag{4.2}$$

and diffusivity,

$$\kappa(z) = u_* z_0 k (C_0^2 (z_1/z_0)^2 + (z/z_0)^2)^{1/2}, \tag{4.3}$$

where z_1 is the nominal size of the gravel and $C_0 = O(1)$ is a constant, were used with (3.21) and (3.22). The even distributions, (4.2) and (4.3), were necessary for the implementation of the no-flux condition at the wall. Equations (4.2) and (4.3) only departed from the standard velocity profile (4.1) and diffusivity profile,

$$\kappa(z) = k u_* z \,, \tag{4.3a}$$

which represents the normal Reynold's analogy, over a thin region adjacent to the wall. The no-slip boundary condition was also satisfied by (4.2) at the wall, and the value of κ was approximately constant for $z < z_1$. Figure 10 is a sketch illustrating the conditions near the rough boundary.

The condition that the non-dimensional time τ be small in (3.33), requires

$$\tau^2 = \frac{a_1^2 t}{2a_0} \sim \frac{u_* k}{z} t \qquad z > z_1 \tag{4.4}$$

be small. At the boundary, the form of $\kappa(z)$ given in (4.3) gives rise to $\tau = 0$ because of the zero value of a_1. The criterion given by (2.26) was reasonably met in that

$$a_2 \sim 0 \quad \text{for} \quad z > z_1, \tag{4.5}$$

and

$$a_2 \sim 0.1 \quad \text{for} \quad 0 < z < z_1. \tag{4.6}$$

In this pilot study, grid sizes of $\Delta z = 0.5$ and $\Delta x = 0.5$ were used with $\Delta t = 0.005$. This value of Δt was sufficiently small to satisfy (4.4-4.6), and large enough to provide a reasonable cloud-size for a source located at any z.

In the comparison between the measured and computed values of concentration shown on figure 11, the solution-scheme variables were normalized following Raupach and Legg (1983). That is, vertical and downstream distances were normalized with source height h_1, and the values of concentration were normalized with the temperature scale,

$$\theta_* = \frac{F}{h_1 u(h_1)}, \tag{4.7}$$

where F is the constant flux of contaminant through a plane normal to the flow.

The comparison shown on figure 11 is remarkably good considering the fact that the basic differential equation is a model equation and the solution-scheme is an approximate solution. Moreover, there are no adjustable constants in (4.2) and (4.3) apart from C_0, which does not have a significant effect on the profiles shown in figure 11, except at very small values of x.

At $x/h_1 = 2.5$, the values of concentration from the solution-scheme are shown to be much smaller than the measured values. The discrepancies that appear in this profile are anticipated because of the formulation of the model equation. If one ignores the effects of shear, one would expect an increasing value of κ with elapsed time from release until convergence of the Lagrangian velocity autocorrelation integral (Taylor, 1921; Batchelor, 1949). In the model, κ was used to represent the hypothetical converged value, and hence was over estimated at small times and distances downstream. One could overcome this obstacle by incorporat-

ing a time-dependent diffusivity into the solution-scheme (see Appendix B). Another possible explanation for the discrepancy in the profile of concentration at $x/h_1 = 2.5$ is the absence of the cross-terms in the model. It was shown in section 3.2 that the effects of the cross-terms are important during the early stages of the cloud evolution and qualitatively insignificant at later times. Indeed, it is interesting to observe the good comparison achieved in figure 11, for $x/h_1 > 2.5$, without cross-terms in the model equation.

The constant-flux of contaminant used in the temperature scale (4.7) was monitored in the solution-scheme. The flux loss from the solution-scheme was less than 5 per cent for the first three stations and less than 10 per cent for the farthest downstream station whereas the measurements exhibited a 10 per cent and 20 per cent flux loss respectively at these stations. Thus the comparisons for $x/h_1 > 2.5$ would appear to be within experimental error.

In figure 12, the computed values of ground-level concentrations are shown to be less than the measured values. This could be a result of a large diffusivity value. Moreover, there is a degree of uncertainty over the value of z that represents the ground-level in the gravel bed (in the Raupach and Legg experiment, ground-level was taken to be $6mm$ whereas $z_1 = 7mm$). It is unlikely that the complex and important region at the wall can be characterized by a simple length-scale z_1; however, the results shown on figure 12 for a value of the one adjustable constant $C_0 = 1.25$ do appear to be in reasonable qualitative agreement.

4.2 A Comparison with Fackrell and Robins (1982) data

In the Fackrell and Robins (1982) experiment, a neutrally-buoyant mixture of propane and helium was continuously emitted ($1.63 \cdot 10^{-4} m^3 s^{-1}$) at $z = 23cm$ within the fully developed, rough-walled, turbulent boundary-layer (boundary-layer height $H = 120cm$). Unlike the gravel surface in the Raupach and Legg experiment, Lego blocks, with a nominal height of 1.1 to 1.8 cm, were used as rough elements. Values of concentration were measured at up to 34.3 release heights downstream with a flame ionization technique (see Fackrell, 1978, 1980). The logarithmic profile of velocity, with $z_0 = .0288cm$, $u_* = 17.86cm\ s^{-1}$, and von Karman's constant, $k = 0.38$, were shown to be a very good representation of the measured profile of mean velocity. Experiments led Robins and Fackrell (1978) to conclude that the diffusivity profile is a linear function of height over the thin region adjacent to the rough wall. Thus one can use (4.2) and (4.3) to represent the velocity profile and diffusivity profile respectively.

In the solution-scheme, (4.3) was used with $C_0 = 1.25$ and $z_1 = 1.8\ cm$ to represent the vertical, lateral, and streamwise components of κ_y while the off-diagonal components of κ_y were taken to be zero.

The use of (3.21) and (3.22) with the dimensional form of (3.7) to describe the Fackrell and Robins (1982) elevated point-source within a neutral, turbulent boundary-layer requires enormous amounts of computational time and storage. For example, to adopt a fixed grid, which represents the spatial dimension of the

wind tunnel, approximately 5.8×10^8 elements are required for a wind tunnel with physical dimensions of 270 cm high, 910 cm wide and 2400 cm long. This is a substantial amount of computational memory, even when employing single precision. There can, however, be a reduction in the amount of computational memory if emphasis is placed on obtaining the solution for the ensemble-mean along a streamwise, central plane of the wind tunnel, where vertical profiles of concentration at the various downstream stations were measured in the Fackrell and Robins (1982) experiment.

During the calculation of the steady-state solution, an optimum number of grid points was used so that the effects on the solutions at the center of the wind tunnel were minimal. A linear dimension of 1 cm for cubical elements was found to give adequate resolution throughout, and the extent of the cubical array was 75 cm in the vertical until the first downstream sampling station, and thereafter changed to 65 cm. Further computational efficiency was gained when symmetry in the cross-stream direction was taken into account. Contaminants passing the center line of the wind tunnel were reflected back to one side in the scheme. The extent of the lateral array, used to represent one-half of the plume, was 40 cm throughout. Although this caused the solution-scheme lateral half-widths to be less than the measured values of Fackrell and Robins of 30 *cm* at the station located at 25.2 release-heights downstream, the solution-scheme and experimental vertical half-widths remained in good agreement (see figure 13). Note that the half-width is defined, in Fackrell and Robins (1982), as the distance where the

concentration falls to one-half of its maximum. Figure 16 shows the surfaces of concentration $C(x,y,z)$, from the solution-scheme, at the x_i measurement sampling stations. The value of Q_o in equation (3.22) was $0.1205 g s^{-1}$.

After each discrete time-step, the cloud of contaminant enlarged. To further reduce the computational time, values of concentration less than .25% of the maximum concentration of the cloud of contaminant were removed after each discrete time-step. The prescribed cut-off values decreased after each discrete cloud because the maximum concentration in each cloud also decreased. Only values of concentration at the periphery of the cloud, which have insignificant effects on the values of concentration at the center of the wind tunnel, were removed by that method. The removal of each seed-point eliminated approximately 1700 steps of addition. Here, computational efficiency is gained at the expense of introducing some error. For calculations of values of concentration very far downstream, where the prescribed cut-off value must be small, the use of a supercomputer would be more appropriate. The steady-state continuous solutions, at the furthest downstream station, presented in figure 15, required approximately 200 hrs. on a VAX 8550 computer with 5 megabytes of memory.

The boundary-layer growth over the distance between release and the farthest downstream sampling station was negligible, therefore, no account was taken of this change. In circumstances where one is confronted with a growing boundary-layer, the versatility of the solution-scheme can accommodate the re-scaling

feature of the velocity profile. To ensure that the convective displacement of a cloud was small relative to its own dimensions, a time step of .01s was used until the first experimental sampling station and then changed to .015s thereafter.

The no-flux condition at the ground was implemented by reflecting values of concentration of contaminant which fell below the solid barrier. This procedure was easy to apply because the diffusivity and velocity profiles were even functions. Computationally, if j represents the level of the barrier, then values of concentration at the j+k level are added with values of concentration at the j-k level. After all the calculations were completed, the concentration at the j level was multiplied by a factor of two. A factor of two was necessary only at the ground level because the reflection method used here does not provide any identical contributions to the ground from the fictitious source. An alternate approach for modeling the no-flux boundary condition is to use a source directly below the real source, but this method requires more computing time. In a situation (a purely hypothetical situation) where a boundary does not have any effect on a cloud of contaminant, and $t \rightarrow \infty$, this cloud of contaminant will spread until the location of its maximum concentration coincides with the location of the boundary. If the reflection principle is used here to represent the effects of the boundary, a portion of the cloud of contaminant below the boundary is reflected and the ground values of concentration are multiplied by two. This is consistent with the result of Csanady (pp.14, 1973), who showed, using a simple plane

source solution, and for large t, the ground-level concentration, in the presence of a solid boundary, is equal to twice the maximum concentration from a plane source diffusing in the absence of a reflecting barrier.

Figure 14 shows a comparison of measured and solution-scheme values of the vertical distribution of mean concentration $C(x_i,0,z)$, where x_i are taken at the sampling stations within the plume. Figure 15 shows that same comparison except the distributions were normalized with the maximum concentration at each station. Values from the solution-scheme appear to have already reached the anticipated, asymptotic, self-similar distribution of a ground-level release by about 25 release-heights downstream. The Fackrell and Robins data do not appear to reach this asymptotic state until approximately 40 release-heights downstream. In Figure 17a, the distribution of mean concentration from the solution-scheme at a downstream distance of 25.2 release-heights is shown to be in very good agreement with the Fackrell and Robins (1982) measurements of concentration from a ground-level release, and with the Wilson et al. (1982) Gaussian model. Overall, the comparison between the experimental data and results from the solution-scheme is quite acceptable when the measurement error and the steps taken in the three-dimensional solution-scheme to increase computational efficiency are considered. Again, one adjustable parameter C_0 was used, and its effect on the solutions were minimal.

Based on the experimental evidence presented in this chapter, the model equation is certainly valid for the simple flow-configuration investigated. The general solution-scheme, which provided the framework to validate the model equation, is shown to be applicable for the flow-configurations considered.

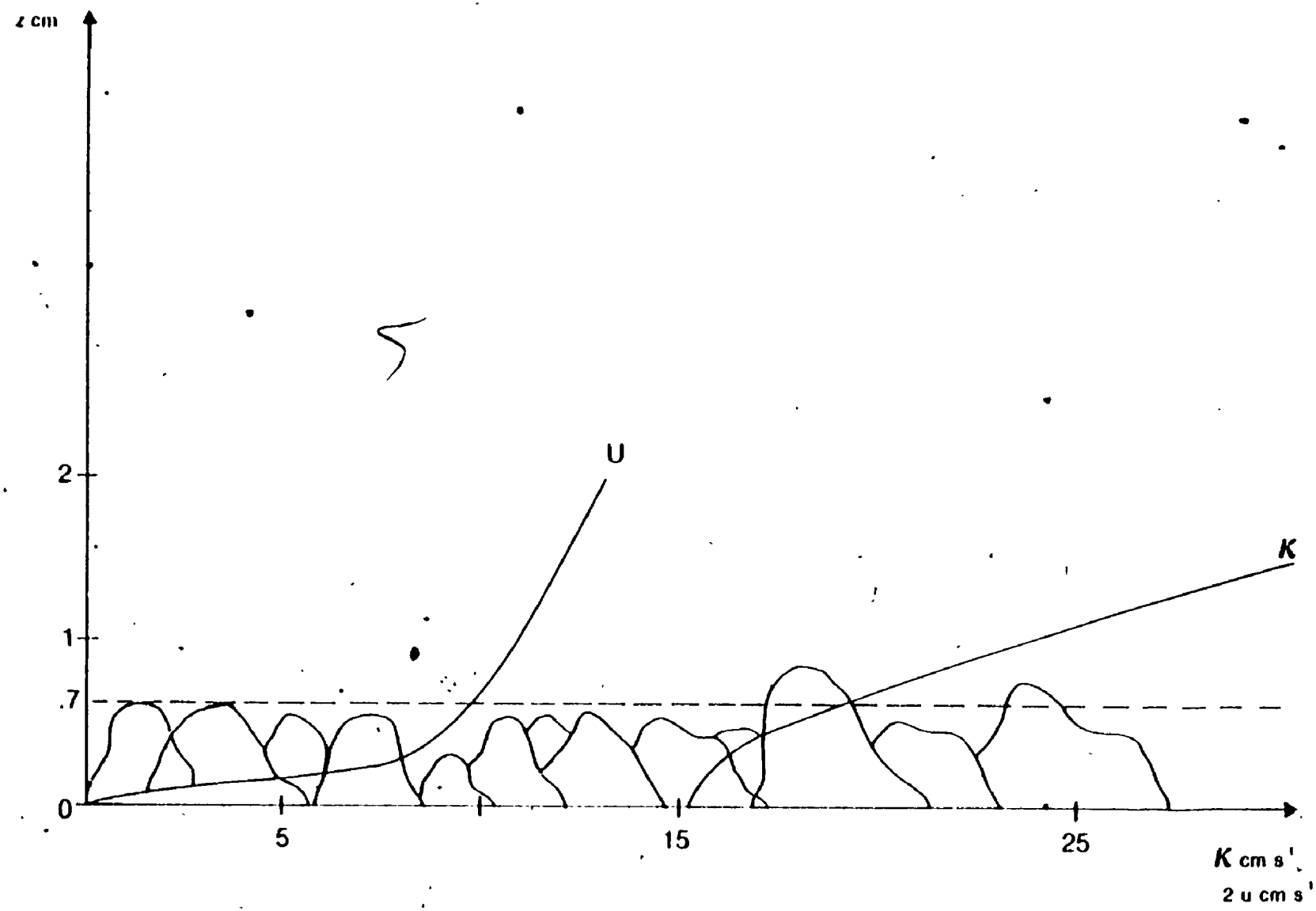

Figure 10
A sketch of the rough-wall conditions showing equation (4.2) and (4.3).

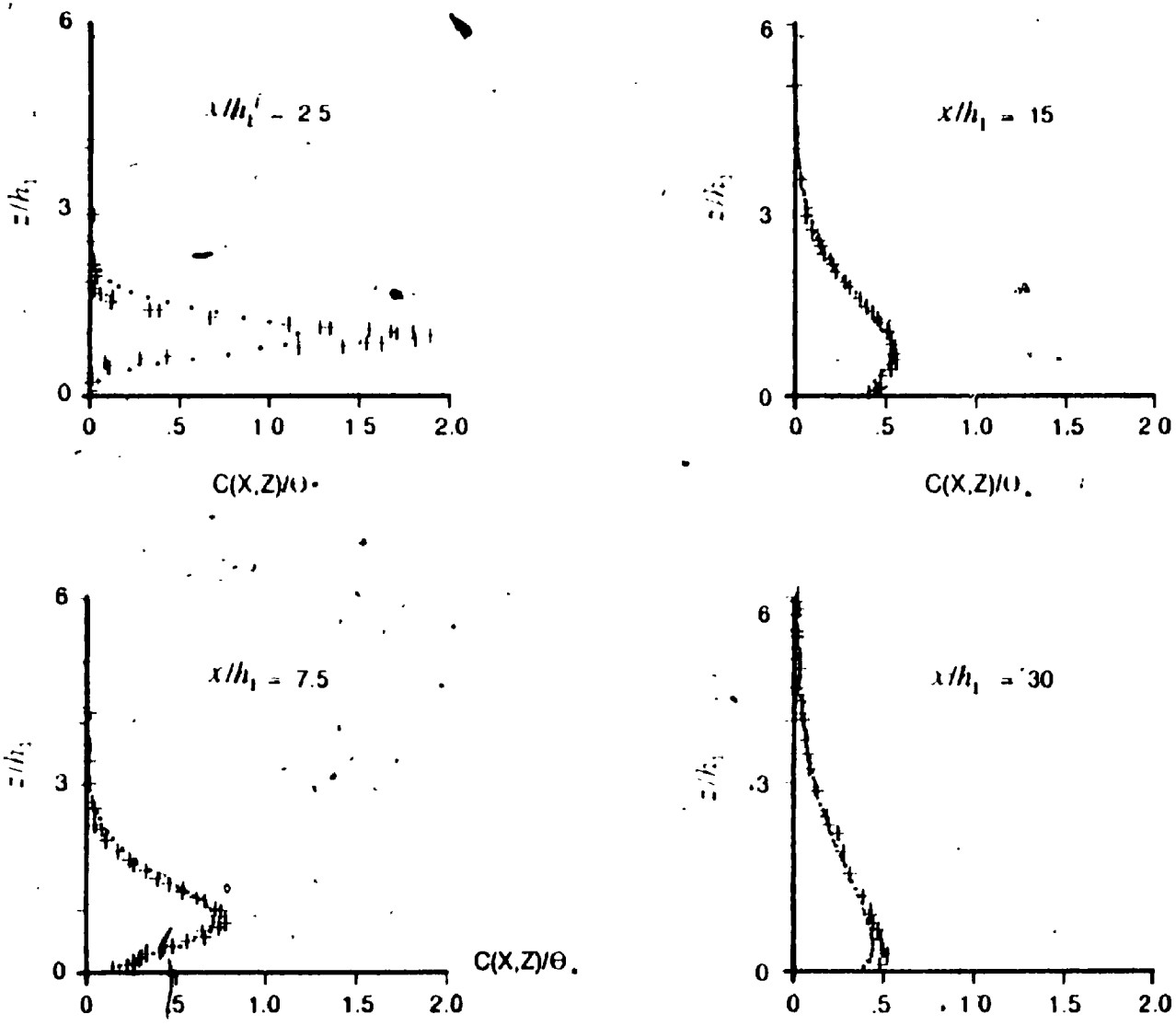

Figure 11
A comparison between the non-dimensional concentration profiles at various downstream distances found in the experiments of Raupach and Legg (1983) (++++) and solution-scheme values (· · · ·).

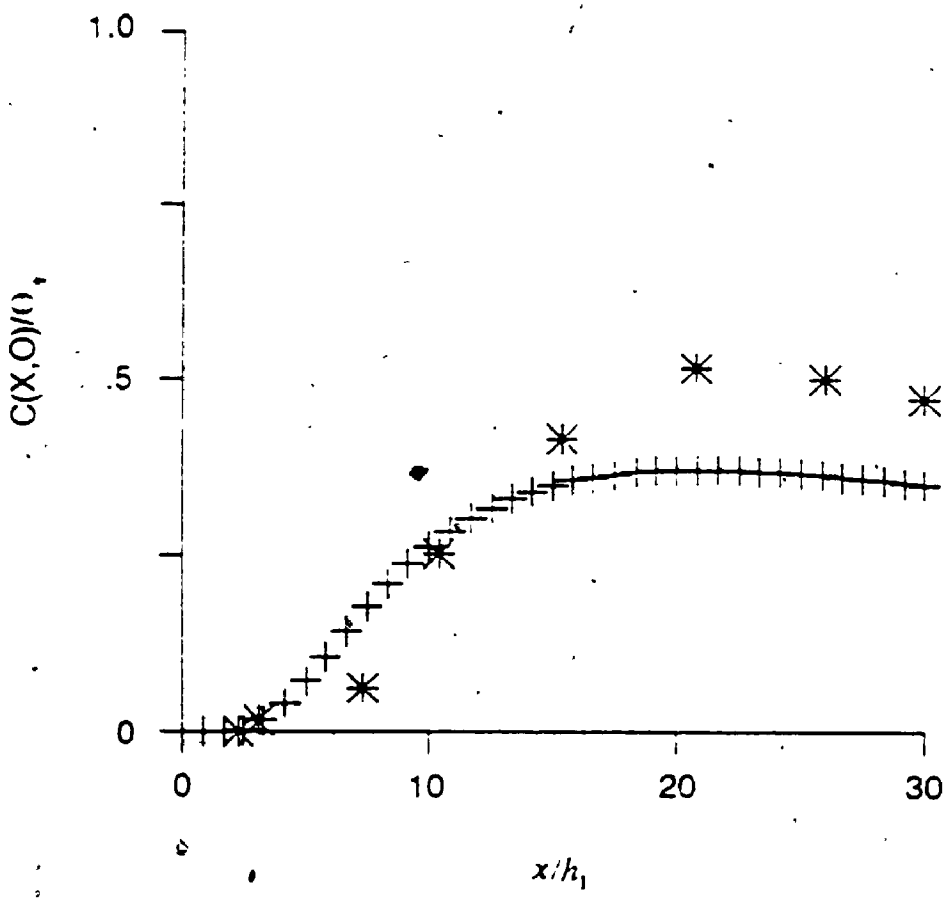

Figure 12
A comparison between the non-dimensional, ground-level concentration values found in the experiments of Raupach and Legg (1983) (***) and solution-scheme values (++++).

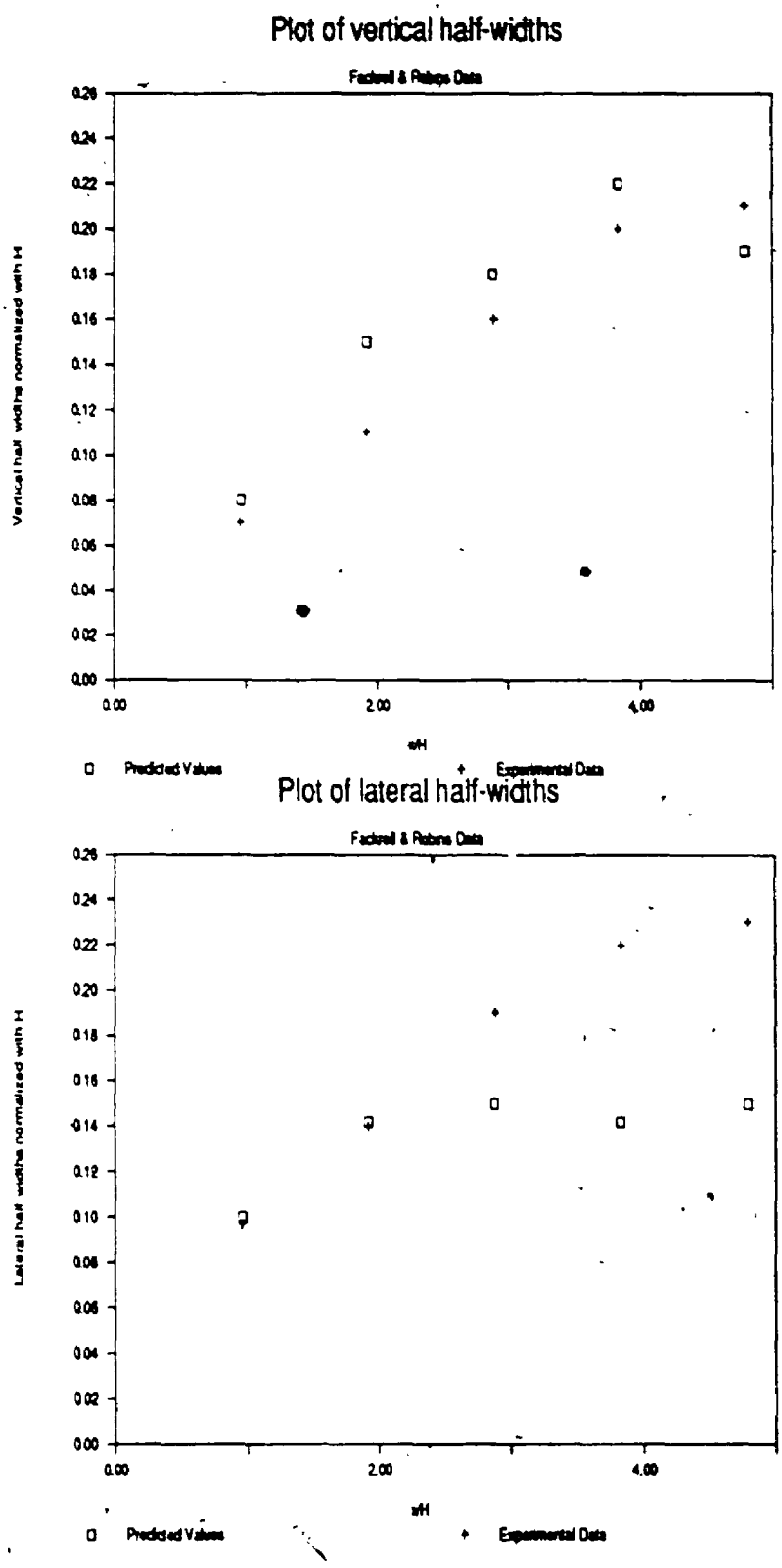

Figure 13
A comparison between the vertical and lateral half-widths found in the experiments of Fackrell and Robins (1982) and solution-scheme values.

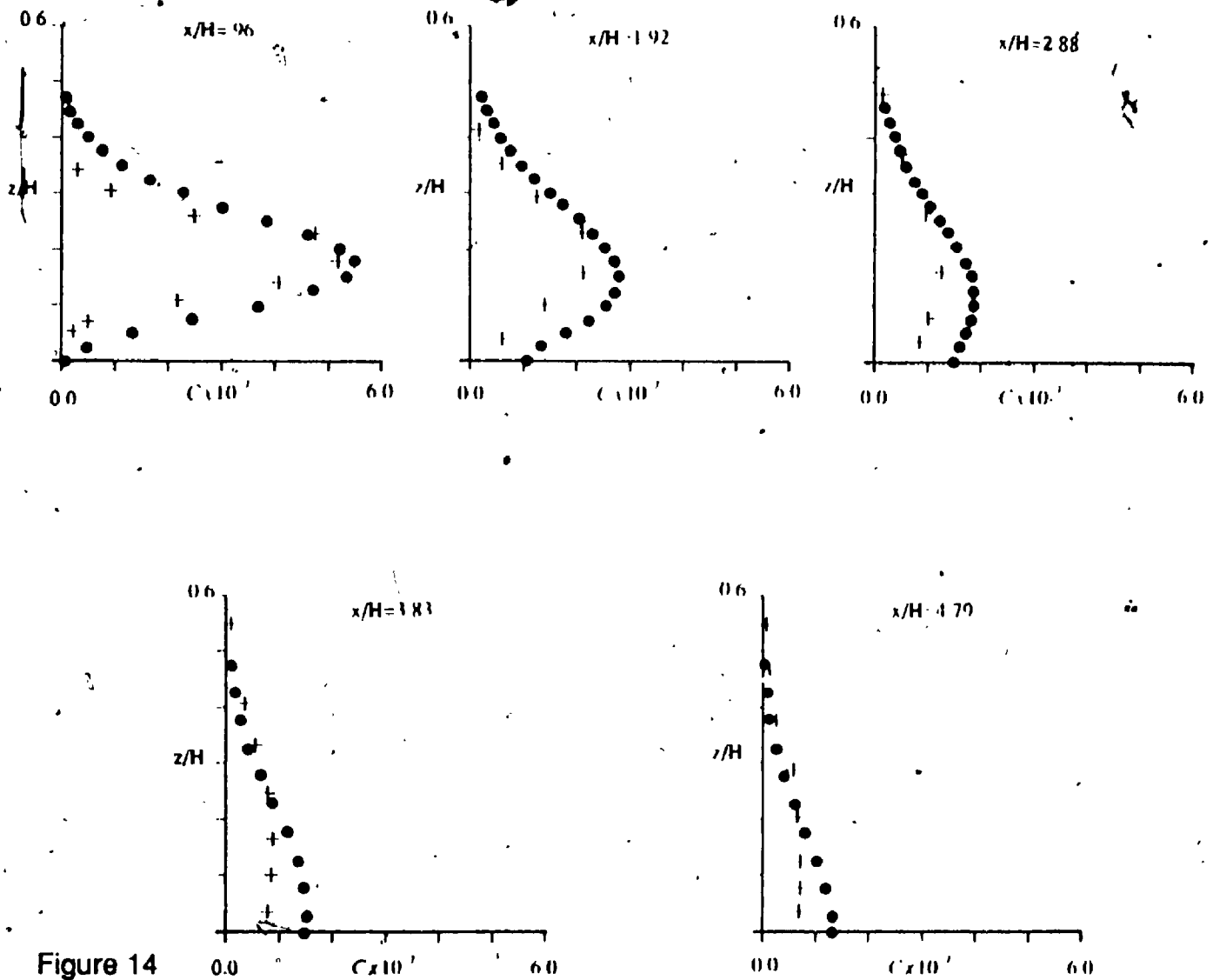

Figure 14
A comparison between the experimental mean-concentration values in $gm \cdot cm^{-3}$ of Fackrell and Robins (1982), +, and those of the solution-scheme,(· · · ·) .

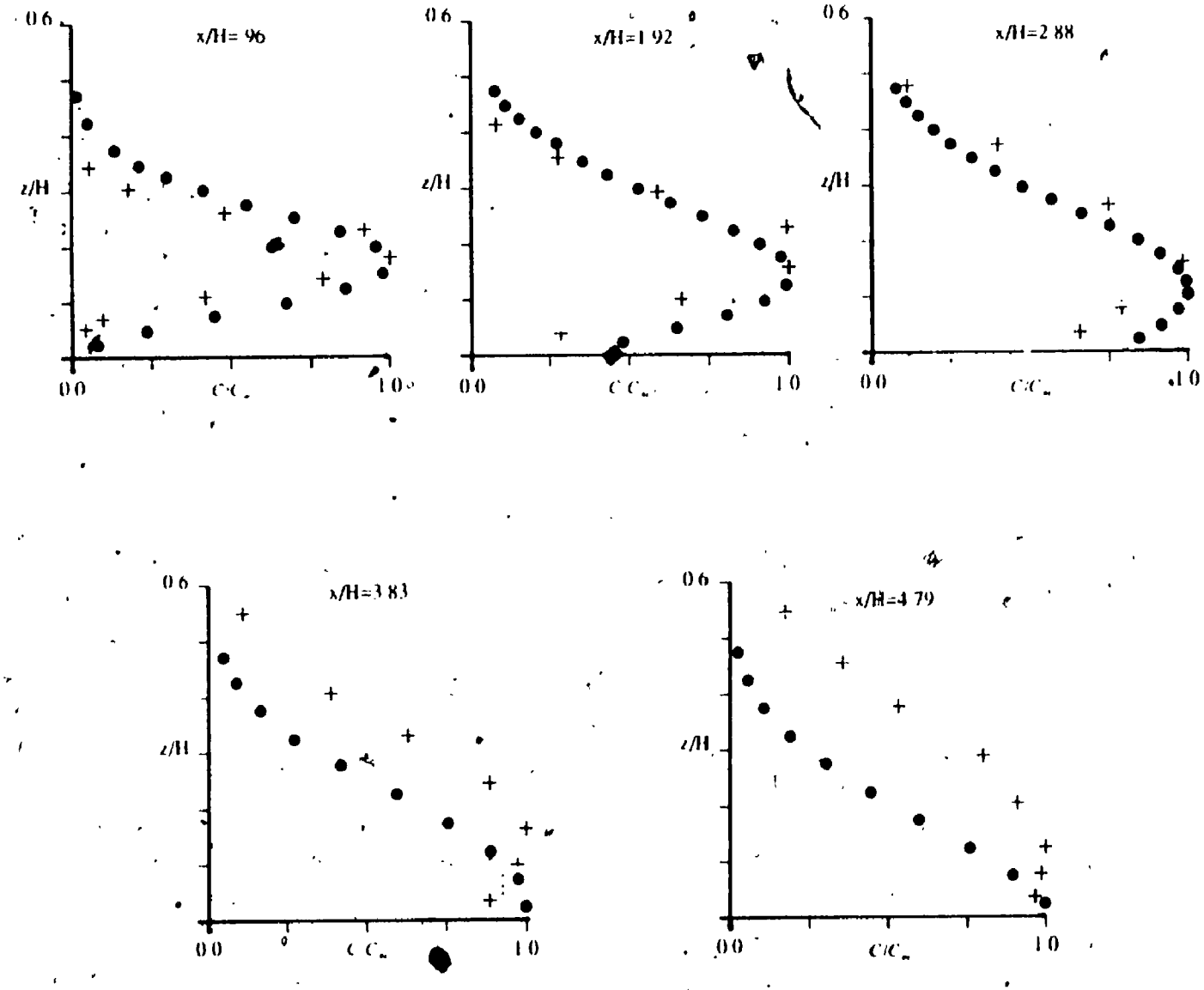

Figure 15
Values shown on figure 14 when normalized with the respective maximum concentration.

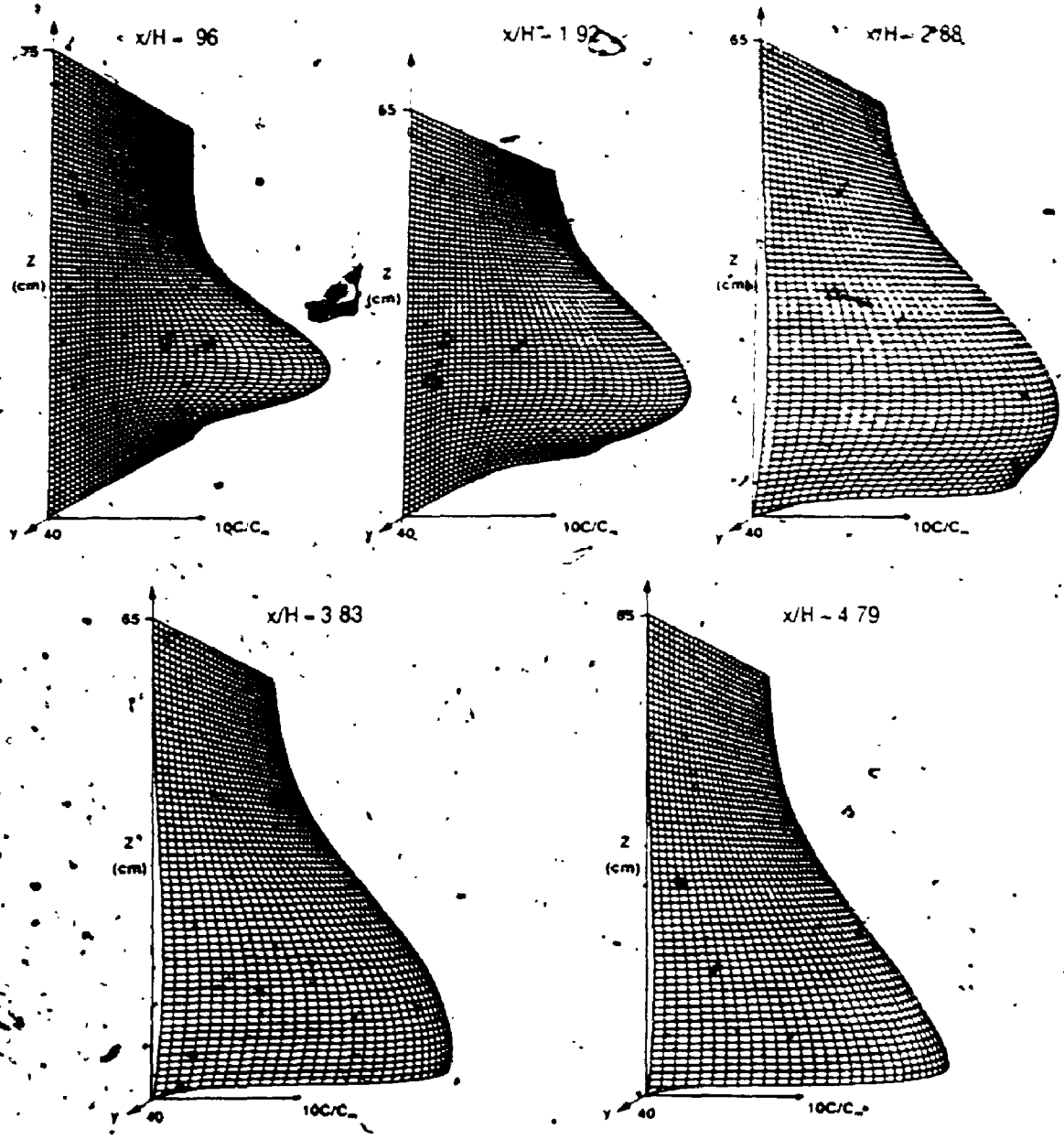

Figure 16
Solution-scheme surfaces of mean-concentration

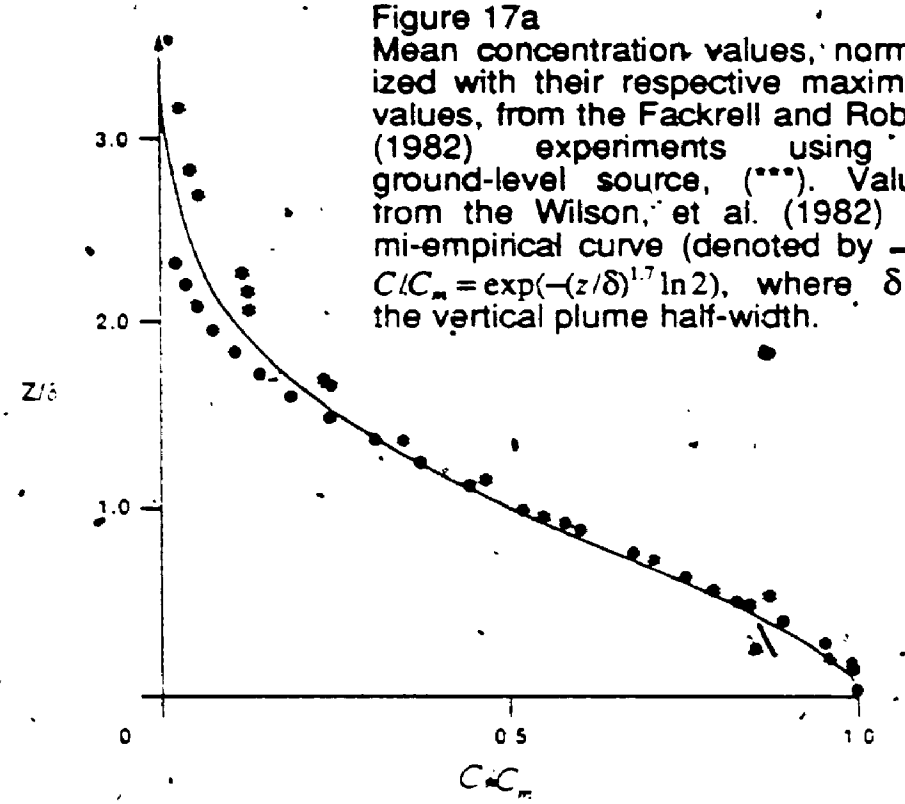

Figure 17a
Mean concentration values, normalized with their respective maximum values, from the Fackrell and Robins (1982) experiments using a ground-level source, (***). Values from the Wilson, et al. (1982) semi-empirical curve (denoted by ——) $C/C_m = \exp(-(z/\delta)^{1.7}\ln 2)$, where δ is the vertical plume half-width.

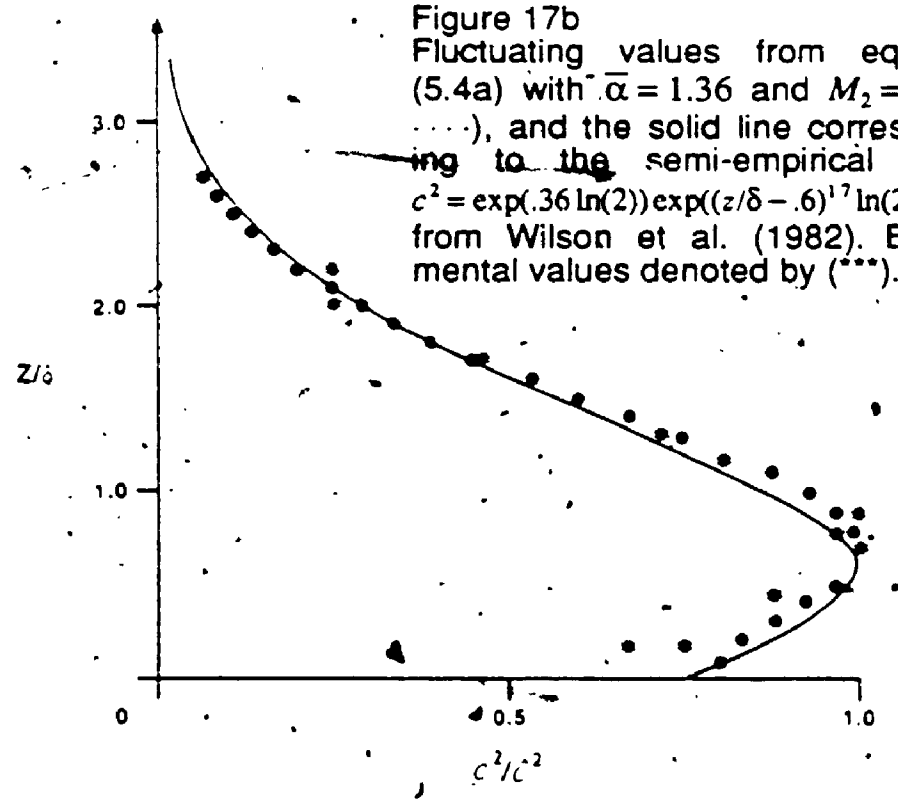

Figure 17b
Fluctuating values from equation (5.4a) with $\bar{\alpha} = 1.36$ and $M_2 = 1.2$, (· · · ·), and the solid line corresponding to the semi-empirical curve $c^2 = \exp(.36\ln(2))\exp((z/\delta - .6)^{1.7}\ln(2))$ from Wilson et al. (1982). Experimental values denoted by (***).

Chapter Five

Other Useful Statistics

The awareness of the importance of scalar fluctuations and concentration probability density functions is increasing. These fundamental statistical properties are relevant to the study of turbulent flames (Cheng et al., 1987), reacting flows (Saetran et al., 1987), and risk exposure problems (Wilson, 1982). Such fundamental statistics are critical elements in a hazard assessment of an accidental release of lethal contaminants. An ultimate aim is to have a framework with similar capabilities as the solution-scheme in chapter three, but this is rather difficult at the present moment due to the laek of available experimental information regarding these statistical properties in environmental flows. This chapter provides a simple approach to describe the field of fluctuating concentra-

tion using information provided by the solution-scheme in chapter three. The work herein is the beginning of another framework that could provide a global understanding of the way these statistical properties behave.

5.1 Fluctuations

A model is often tested with experimental data. This data must be reliable before a comparison can be made. When modeling fluctuations, that comparison may not be simple because the measured fluctuations are sensitively affected by molecular diffusion and the spatial and temporal resolution of the instrument (Chatwin and Sullivan, 1985). However, the measured distribution of mean concentration is relatively unaffected by the instrumentation and molecular diffusion (Chatwin, 1984; Sullivan, 1984). While the exact causes of the discrepancy between the values of measured fluctuations and theoretical fluctuations are still unresolved, and more experimentation regarding the effects of instrumentation on the mean-squared concentration is necessary, it does seem appropriate, at the present moment, for one to adopt an approach that is considerably simpler than second-order modeling procedures (e.g.; Sykes et al., 1984).

Here one exploits a knowledge of the field of mean concentration $C(\underline{x},t)$ to enable predictions on the field of fluctuating concentration $c(\underline{x},t)^2$, where

$$c(\underline{x},t)^2 = \int_0^{\infty} [\theta - C(\underline{x},t)]^2 p(\theta;\underline{x},t) d\theta. \qquad (5.1)$$

$p(\theta;\underline{x},t)$ is the probability density function of concentration, which has a form,

$$p(\theta;\underline{x},t) = \pi(\underline{x},t)\delta(\theta-\theta_0) + (1-\pi(\underline{x},t))\delta(\theta), \tag{5.2}$$

in the absence of molecular diffusion (Chatwin, 1984; Sullivan, 1984). $p(\theta;\underline{x},t)d\theta$ is the probability of finding values of concentration between θ and $\theta+d\theta$, and $\pi(\underline{x},t)$ is the probability of a point, located by the vector $\underline{x}$, at time t, being in marked fluid. θ_0 represents the initial concentration value. The relationship between $C(\underline{x},t)$ and $\pi(\underline{x},t)$ is $\pi=\theta_0 C$ (i.e., D has no effect on $C(\underline{x},t)$ generally). Equation (5.1) with (5.2) reduces to

$$c(\underline{x},t)^2 = C(\underline{x},t)(\theta_0 - C(\underline{x},t)), \tag{5.3}$$

which is a general result (see Chatwin and Sullivan 1985). It has been shown by Chatwin and Sullivan (1987a,b) that equation (5.1) can be applied in self-similar flows, when molecular diffusion (D) is important, by replacing θ_0 with a local concentration scale, $\hat{\theta}=\overline{\alpha}C(0)$, which scales out the effects of D. That is, equation (5.1) reduces to

$$c(\underline{x},t)^2 = \frac{C(\underline{x},t)}{M_2^2}(\overline{\alpha}C(0) - C(\underline{x},t)). \tag{5.4}$$

Equation (5.4) provides a relationship between the fluctuations $c(\underline{x},t)^2$ and mean concentration $C(\underline{x},t)$. $\overline{\alpha}$ and M_2 are O(1) constants, and $C(0)$ is the maximum concentration. For the case of a continuous, point-source release in a steady flow, equation (5.4) can be expressed as

$$c(r)^2 = \frac{C(r)}{M_2^2}(\overline{\alpha}C(0) - C(r)), \tag{5.4a}$$

where r is the vertical distance normalized with the mean concentration half-width. Figure 17b shows the excellent agreement between measured fluctuations and the values from equation (5.4a) with a value of $\bar{\alpha} = 1.36$ appropriate to the ground-level source. Thus the fluctuations are well described by (5.4a) at many release-heights downstream where the field of fluctuating concentration of an elevated-source degenerates into the self-similar result of a ground-level source. The value of M_2 was unnecessary in figure 17b because the vertical profile of mean-squared concentration was normalized with its maximum mean-squared concentration.

Although equation (5.4) confidently predicts vertical, self-similar profiles of mean-squared concentration, such profiles are unlikely to be found in environmental flows because of the unsteady nature of these flows. The principle aim of this section is to extend the use of equation (5.4) to describe the field of fluctuating concentration in the intermediate region, which is between the near-source and far-field region. This is a critical region in the assessment of environmental hazards, particularly when any living organisms are affected; certainly more important than the far-field region in this case.

In the very near region of the source (or small-times after release) and before the effects of molecular diffusion become important, equation (5.3) provides a relationship between the values of fluctuations and mean concentration. In equation (5.3), there will be a surface of maximum $c(\underline{x},t)^2$ located by $C(\underline{x},t) = \theta_0/2$.

There is experimental data to support this feature of equation (5.3). Axial profiles of mean and r.m.s. concentration from a methane jet experiment of Birch et al. (1978) show that a pronounced maximum of $c(\underline{x},t)^2$ occurs at approximately where $C(\underline{x},t) = \theta_0/2$. The value of $\bar{\alpha}$ in the zero molecular-diffusion regime of equation (5.4) is, upon comparison with equation (5.3),

$$\bar{\alpha} = \theta_0/C(0), \tag{5.5}$$

and $M_2 = 1$. Thus the maximum value in the mean distribution $C(\underline{x},t)$ will initially be coincident with the location of the maximum value in the fluctuations $c(\underline{x},t)^2$. Thereafter, the location of the respective modal values will separate and return to coincidence when $\bar{\alpha} = 2$ to close the zero molecular-diffusion region. Figure 18 presents a sketch of the anticipated form of $\bar{\alpha}$ and M_2 in the region where the asymptotic, $x \to 0$, behavior given by equation (5.3) is joined by the asymptotic, $x \to \infty$, behavior given by equation (5.4). Note that the value of M_2 in figure 18 may not have reached its asymptotic form in the region specified in this figure.

In the region where molecular diffusion is likely to play an important role (i.e., when the cloud of contaminant is stretched into very thin strands by the velocity field), equation (5.4) is used. $\bar{\alpha}$ and M_2 are to be determined experimentally. Since the Fackrell and Robins (1982) elevated-source data show the modal values of $C(x,z)$ and $c(x,z)^2$ to be coincident within experimental error, a value of $\bar{\alpha} = 2$ was used in equation (5.4) with the experimental values for c^2 and C to

determine the value of M_2. Figure 19 is a plot of

$$M_2 = \frac{(C(2C(0) - C))^{1/2}}{c}. \qquad (5.6)$$

The values of M_2 appear reasonably constant over each sampling station within the plume. The near-wall measurements at the furthermost sampling stations ($x/H = 3.83, 4.79$) exhibit the largest departure from the constant value of M_2 (see figure 19). This is most evident in figure 20, where a comparison is shown between the measured values of $c(\underline{x},t)^2$ and those generated by equation (5.4) with $\overline{\alpha} = 2$. It is possible that the instrument used for measuring $c(\underline{x},t)^2$ could be responsible for the discrepancies in Figures 19 and 20.

In any experiments where measurements of concentration are made, a finite volume of sample is examined, and the quantity measured is averaged over this volume of sample. Instrument averaging can affect the quantity of $c(\underline{x},t)^2$ by filtering the high-wave number (or fine-scale structure) contributions to $c(\underline{x},t)^2$. This can cause the measured values of $c(\underline{x},t)^2$ to be lower than the true theoretical values, and the theoretical framework of Chatwin (1984) confirms the significance of that effect. The flame ionization detector used in the Fackrell and Robins (1982) experiment was unable to measure the fine-scale structure. This effect could have contributed to some of the observed discrepancies in the near-wall comparison illustrated in figures 19 and 20. However, the good comparison in the main of figures 19 and 20, particularly when the experimental errors in making these difficult measurements are taken into account, certainly encourages the

belief that the second moment $c(\underline{x},t)^2$ can be determined with the values of mean concentration (which are reliable and easily measured) along with the slowly varying values of $\bar{\alpha}$ and M_2.

5.2 Probability density functions

The ensemble-mean concentration and mean-squared concentration may not be useful for studying flammability problems (see Birch et al., 1978). In dealing with such problems, one is interested in the probability of exceeding an unsafe level of concentration; a cumulative density function is appropriate in this context. Thus it is useful to obtain a probability density function of concentration.

An approach taken herein to find the probability density function relies on a simple approximation provided by the Beta distribution, which depends on the values of $\bar{\alpha}$ and M_2 from the previous section. One could take an alternate approach by using an orthogonal polynomial expansion on a finite interval, $0 \le \theta \le \theta_0$, and expressing its corresponding coefficients in terms of central moments generated with (5.2). This, however, may be an inefficient procedure, and the use of a Beta distribution, which can provide some insights into the physics, is a more convenient approach.

Here the Beta distribution

$$p(\theta) = \frac{1}{B(p,q)} \theta^{p-1}(1-\theta)^{q-1}, \tag{5.7}$$

with

$$p, q > 0$$

and

$$B(p,q) = \int_0^1 t^{p-1}(1-t)^{q-1} dt, \tag{5.8}$$

is used to represent the probability density function of concentration when the random variable (i.e., concentration) takes on values within a finite range, $0 \le \theta \le 1$. The first four central moments of the Beta distribution are approximately equal to the first four central moments derived from equation (5.2), and the constraint $p + q + 1 = M_2$ is generated when the first two moments are used to find p and q (see Sullivan and Chatwin, 1987b). Moreover, if one uses the same concentration scale (i.e., $\hat{\theta} = \bar{\alpha} C(0)$) as in the previous section to normalize the n^{th} moment with $\hat{\theta}^n$, the skewness changes sign at $C/\hat{\theta} = 1/2$ (see eqn. 11, Chatwin and Sullivan, 1987b). Experimental data of La Rue et al. (1974) and Birch et al. (1978) support this qualitative behavior of the skewness.

The mean of the Beta distribution is

$$\frac{p}{p+q} = \frac{C}{\hat{\theta}} = \frac{C}{\bar{\alpha} C(0)}, \tag{5.9}$$

and the ratio of the first two moments is

$$\frac{p}{p+q+1}=\frac{1}{M_2^2}\left\{1+\frac{(M_2^2-1)}{\bar{\alpha}}\frac{C}{C(0)}\right\}. \tag{5.10}$$

For compactness, let the right hand side of equation (5.9) and (5.10) be $\overline{A}$ and $\overline{B}$ respectively. Solving for p and q, one obtains the following:

$$q=p\left(\frac{1-\overline{A}}{\overline{A}}\right) \tag{5.11}$$

where

$$p=\frac{\overline{A}\,\overline{B}}{\overline{A}-\overline{B}}. \tag{5.12}$$

Thus a probability density function can be obtained with the knowledge of M_2, $\bar{\alpha}$ and $C/C(0)$.

Measured probability density functions downstream from a ground level source (Flow C, Robins and Fackrell, 1978) are available for comparison with the Beta distribution. With the exception of the boundary-layer height (denoted by H_r), the flow-field and measuring system in the Robins and Fackrell (1978) and Fackrell and Robins (1982) experiments are similar. The probability density functions were measured at $x/H_r = 20.8$, which corresponds to a non-dimensional downstream distance of $x/H = 6.24$ from the source when x is normalized with the boundary-layer height in the Fackrell and Robins (1982) experiment. Vertical profiles of mean concentration at various downstream distances in both experiments were shown to collapse on to the same curve when each vertical profile was

normalized with its respective maximum mean concentration (Fackrell and Robins,, 1980). In addition, the vertical profiles of mean-squared concentration from both experiments are similar when each downstream profile was normalized with their respective maximum mean-squared concentration (see figure 14, Robins and Fackrell, 1978 and figure 6, Fackrell and Robins, 1982). Thus one can use the vertical profiles of mean concentration and vertical profiles of mean-squared concentration from the Fackrell and Robins (1982) experiment to find the values of M_2 and $\bar{\alpha}$ for the Beta distribution, which will be compared with the measured probability density functions given in Robins and Fackrell (1978).

The value of $\bar{\alpha}$ was found by using the normalized value of mean concentration at a vertical location ($z/\delta = 0.75$) where the modal value of the vertical distribution of c^2 occurs, i.e.,

$$\frac{C}{C(0)} = \frac{\bar{\alpha}}{2} = .68 \qquad (5.13)$$

$$\bar{\alpha} = 1.36 \qquad (5.14)$$

A similar method used to find M_2 in figure 19 was adopted here. Equation (5.4) was rearranged as

$$M_2^2 = (1/(c^2/\hat{c}^2))\left(\frac{C(0)^2}{\hat{c}^2}\right)\left(\frac{C}{C(0)}\right)\left(\bar{\alpha} - \frac{C}{C(0)}\right), \qquad (5.15)$$

where $\hat{c}^2$ is the maximum mean-squared concentration. The values of M_2 in figure 21 were derived from normalized values of mean and mean-squared concentration at downstream distances of x/H = 1.67,3.33,5.00,5.92 from a ground-level source of

Fackrell and Robins (1982). The value of M_2 appears relatively constant in the vertical direction. An asymptotic value of 2.86 for the ratio $C(0)/\hat{c}$ was used in equation (5.15) to produce the M_2 values in figure 21. This asymptotic value was selected at a downstream distance $x/H_r = 20.8$, where the measurements of the probability density functions were made (see figure 20, Robins and Fackrell, 1978). Figure 22 shows a comparison between the Beta distribution and the measured probability density functions of Robins and Fackrell (1978). The Beta distribution appears to give the correct qualitative behavior of the probability density functions, with the exception of the near ground concentration probability density function. It is possible that the limitations of the flame ionization detector are responsible for the discrepancies in the probability density functions of concentration near the wall; the effective radius of the instrument was 5 to 10 times the Kolmogorov micro-scale (Robins and Fackrell, 1978).

The measured concentration probability density function of Robins and Fackrell (1978) were renormalized with a local concentration scale $\hat{\theta}$. The following equation was used during the renormalization process:

$$\theta = \frac{1}{\alpha} \frac{C}{C(0)} \left(\frac{\hat{c}}{C} \eta + 1 \right), \tag{5.16}$$

where η represents the random variable in the Robins and Fackrell (1978) probability density functions. It is interesting to observe from figure 22 that, after renormalization, some values of concentration greater than one and less than zero appeared. The concentration scale $\hat{\theta}$ is unlikely to be inappropriate here because

of the relatively good comparison between the Beta distribution and the measured probability density functions of concentration at heights greater than $z/\delta = 0.05$. Although the use of $\bar{\alpha}$ and M_2 in the Beta distribution provided good results here, more experimentation regarding the effects of instrumentation on the values of $\bar{\alpha}$ and M_2 is necessary before equation (5.4) can be adopted in general. Moreover, a thorough experimental assessment of the ratio $C(0)/\hat{c}$ is necessary, especially with regards to its asymptotic value, because the asymptotic value of M_2 in equation (5.15) depends on that ratio. It is rather odd to observe that the approaches to asymptotic values for $C(0)/\hat{c}$, illustrated in figure 5 of Fackrell and Robins (1982) and figure 20 of Robins and Fackrell (1978), are different whereas the vertical profiles of mean and mean-squared concentration from both experiments all collapse on to the same curve after the appropriate normalization.

An alternate technique which uses a Beta-Jacobi orthogonal polynomial expansion to find the probability density function of concentration is under investigation (Derksen and Sullivan, 1988). This expansion is

$$P(\theta) = \sum_{n=0}^{\infty} \frac{\theta^{p-1}(1-\theta)^{q-1}}{B(p,q)} a_n G_n(p,q,\theta), \tag{5.17}$$

where

$$G_n(p,q,\theta) = \frac{\theta^{1-q}(1-\theta)^{q-1}}{q(q+1)\cdots(q+n-1)} \frac{d^n}{d\theta^n}(\theta^{q+n-1}(1-\theta)^{p+n-q}) \tag{5.18}$$

are the Jacobi polynomials that are orthogonal in the interval, $0 < \theta < 1$, and a_n are the corresponding coefficients (pp.90, Sansone, 1959). $B(p,q)$ is represented by equation (5.8). This expansion uses the Beta distribution as a weighting function, and the method does not require the local concentration scale $\hat{\theta}$. The coefficients in the expansion given by equation (5.17) are expressed in terms of the moments of the concentration distribution. Figure 23 shows a comparison between the measured probability density function and the Beta-Jacobi expansion. In that comparison, the moments were obtained from the measured probability density function provided by Robins and Fackrell (1978). The relatively good comparison in figure 23 provides some support that the Beta-Jacobi expansion is capable of representing probability density functions if the first four moments are known. It is of interest to note that, at $z/\delta = 0.05$, the measured probability density function is predicted with greater precision by the Beta-Jacobi expansion than by the Beta distribution (see figure 22 and 23). The relatively good comparison over the remaining probability density functions in figure 22 suggests that the Beta distribution, which is the first term of the expansion represented by equation (5.17), could be used to describe the asymptotic forms of the probability density functions of concentration. One cannot be sure whether the discrepancies at $z/\delta = 0.05$ are the effects of instrumentation or arise because the probability density function has not reached its asymptotic form. Certainly, more experimentation in these two areas are needed. However, should the probability density function at $z/\delta = 0.05$ not be in its asymptotic form, the Beta-Jacobi expansion could be used.

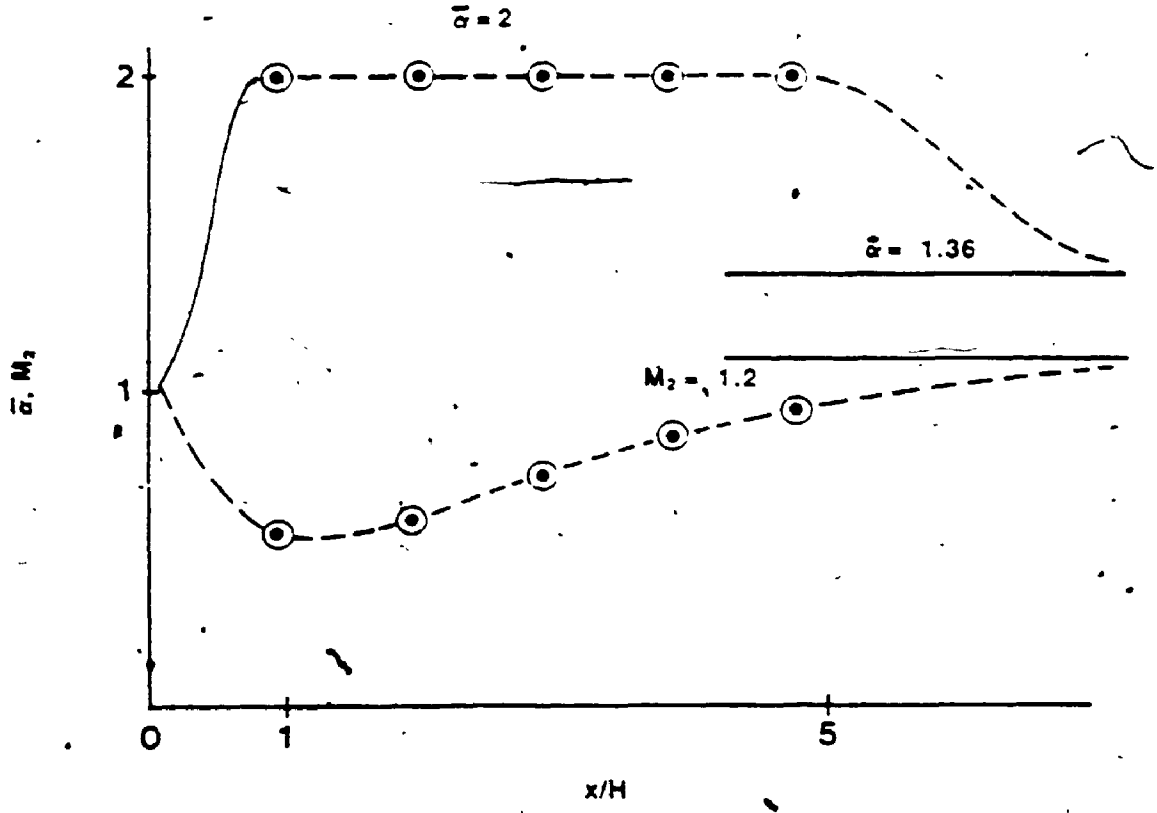

Figure 18
Experimental values of $\bar{\alpha}$ and M_2 from equation (5.4) and figure 19 that occur between the asymptotic (solid line) near-source region and far-field regions.

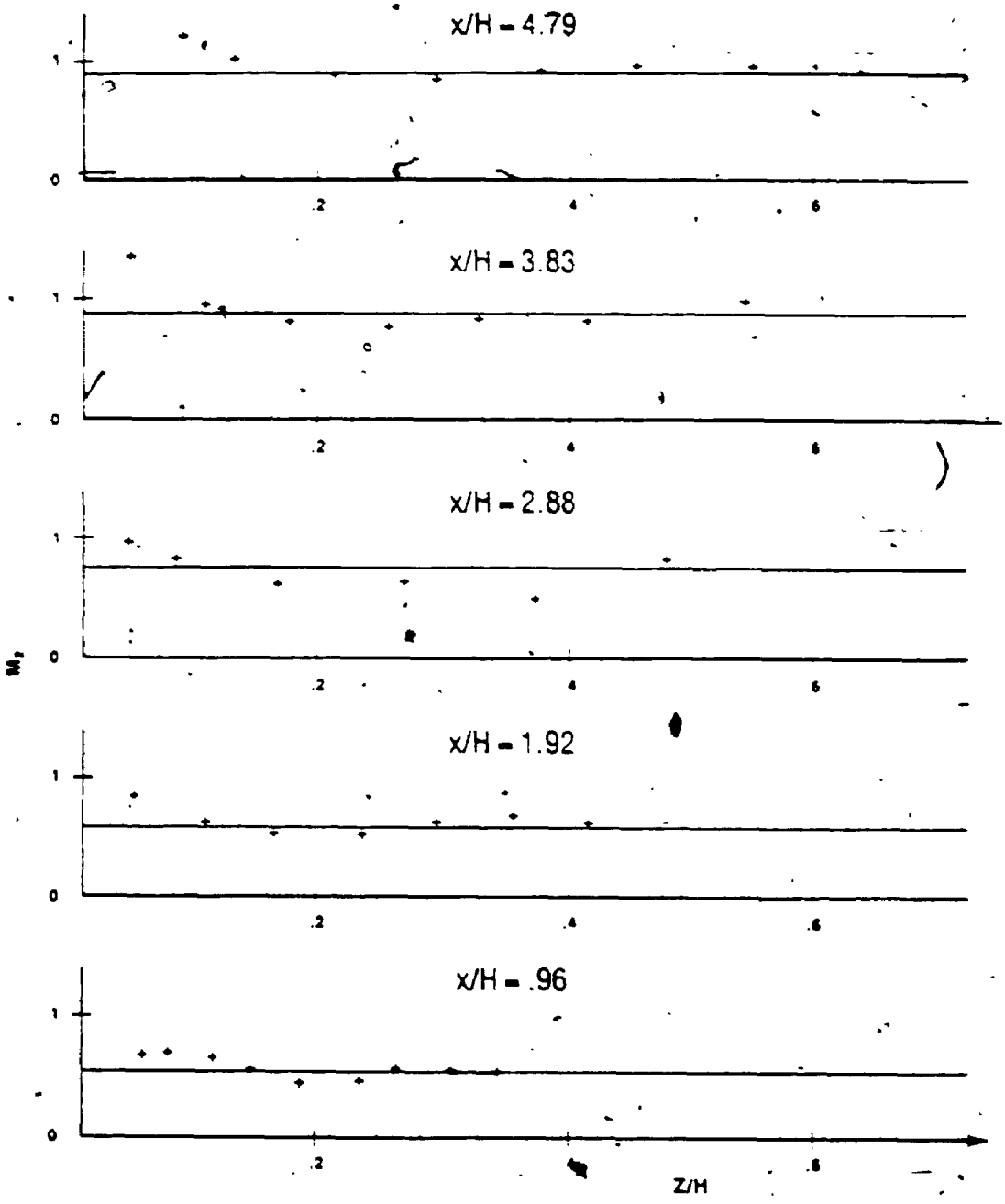

Figure 19
A display of Fackrell and Robins (1982) experimental values using equation (5.6).

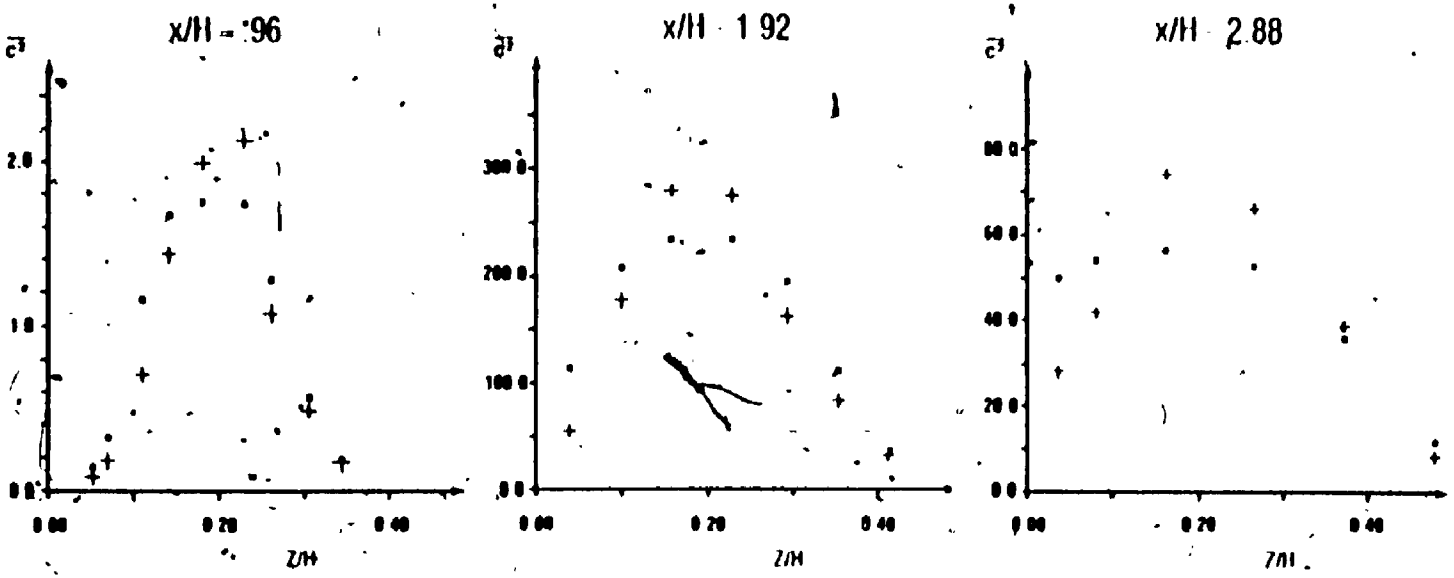

Figure 20
A comparison between Fackrell and Robins (1982) experimental values of fluctuation in $(ppm)^2$, +, and those generated using values of $\bar{\alpha}$ and M_2 of Figure 18 and equation (5.4), (■). A vertical scale factor of 10^4 at $x/H = 0.96$, and 10^3 for the remaining stations was used.

Figure 21
A plot of the square root of equation (5.15) using normalized mean and mean-squared concentration values at downstream distances of $x/H = 1.67, 3.33, 5.00, 5.92$ from a ground level source of Fackrell and Robins (1982). The asymptotic value of $C(0)/\hat{c}$ at $x/H_r = 20.8$ was selected from figure 20 of Robins and Fackrell (1978).

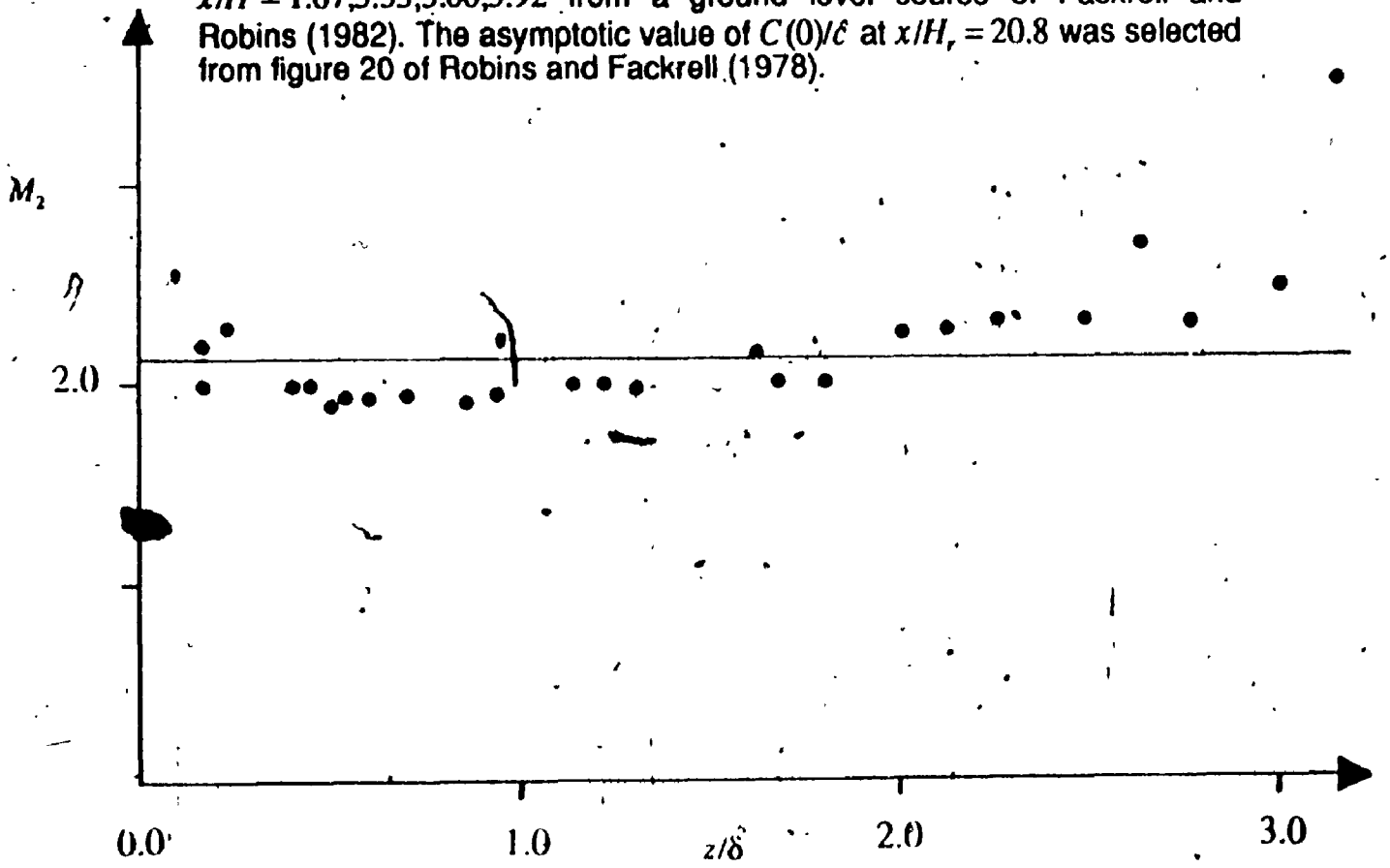

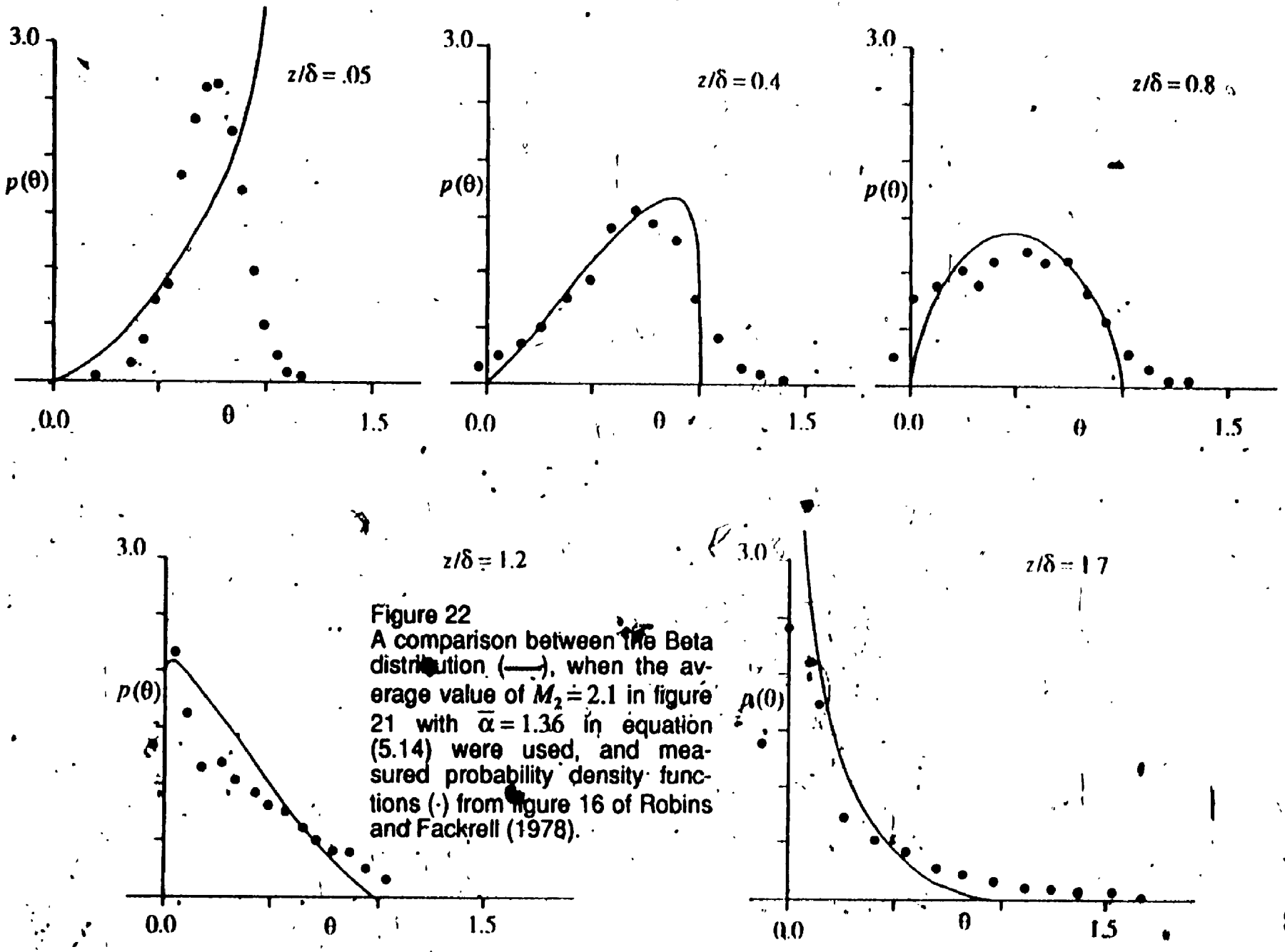

Figure 22
A comparison between the Beta distribution (—), when the average value of $M_2 = 2.1$ in figure 21 with $\bar{\alpha} = 1.36$ in equation (5.14) were used, and measured probability density functions (·) from figure 16 of Robins and Fackrell (1978).

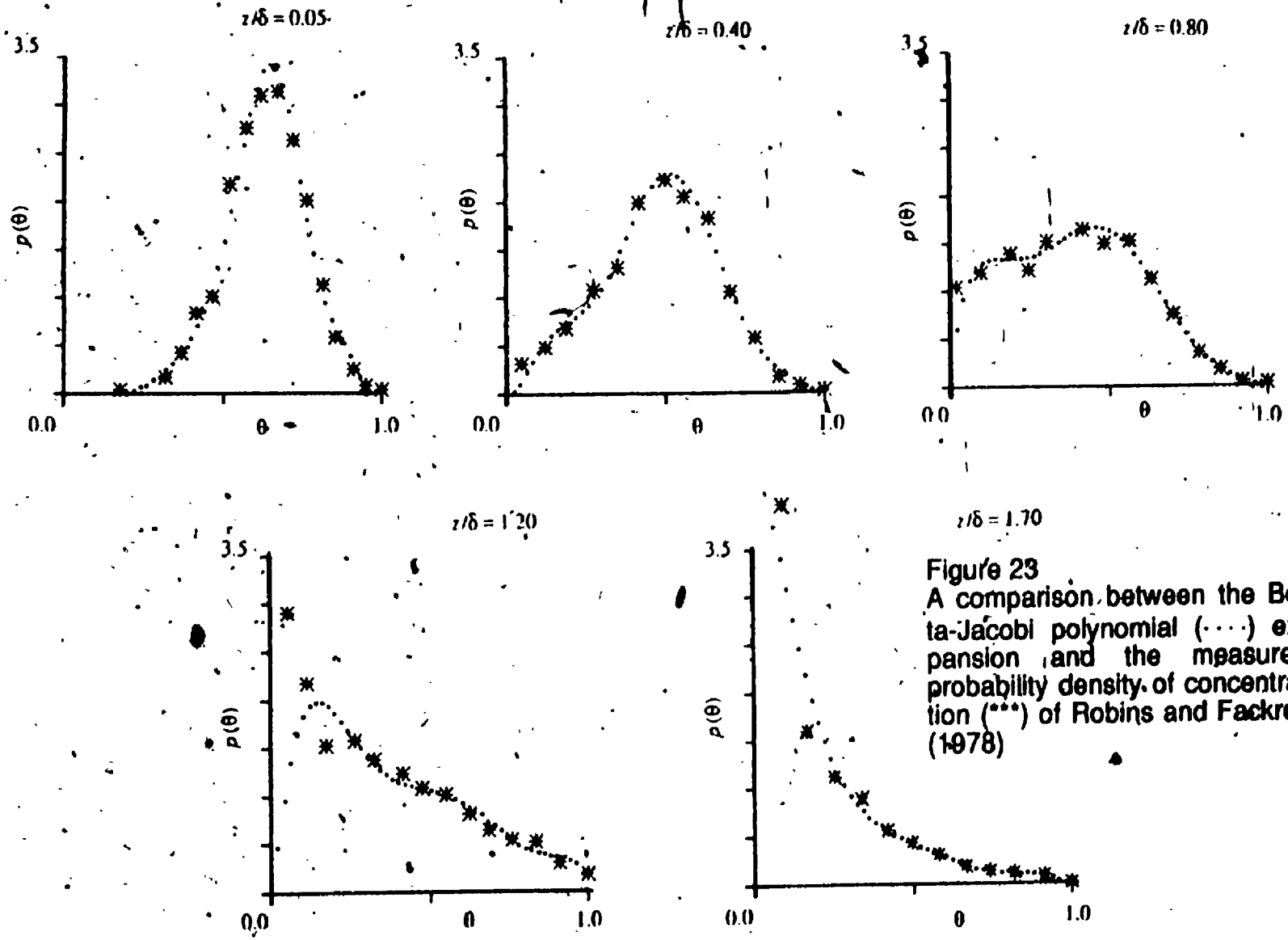

Figure 23
A comparison between the Beta-Jacobi polynomial (····) expansion and the measured probability density of concentration (***) of Robins and Fackrell (1978)

Appendix A

This appendix provides detailed information for the generalized, small-time, asymptotic solution to the convective-diffusion equation.

A.1 Calculated Non-dimensional moments

The moments calculated from the recurrence relationship, (2.18), were normalized as

$$\overline{M}_{mnp} = \frac{M_{mnp}}{\sigma_1^m \sigma_2^n \sigma_3^p}.$$

The following non-dimensional parameters were used in this thesis for compactness:

$$\tau^2=\frac{a_1^2 t}{2a_0}\ ,\quad \beta^2=\frac{2a_2a_0}{a_1^2}\ ,\quad \rho^2=\frac{a_0b_2}{a_2b_0}\ ,\quad \alpha^2=\frac{a_0b_1}{a_1b_0}\ ,\quad \omega^2=\frac{a_0c_2}{a_2c_0}$$

$$\gamma^2=\frac{a_0c_1}{a_1c_0}\ ,\quad \psi^2=\frac{a_0^3d_1^2}{a_1^4c_0}\ ,\quad h^2=\frac{\varepsilon_0^2}{a_0c_0}\ ,\quad \phi^2=\frac{\varepsilon_1^2}{2a_2c_0}\ ,\quad \xi^2=\frac{a_0^3\varepsilon_2^2}{a_1^4c_0}\ ,$$

$$A^2=\tau^2(1+3\beta^2)+1,$$

$$B^2=\tau^2(\alpha^2+\beta^2\rho^2)+1,$$

$$E^2=\tau^2(\gamma^2+\omega^2\beta^2+2h\psi+4h\xi)+1.$$

The following is a list of the non-dimensional moments, to order τ^2, calculated from the recurrence relation (2.18):

$$\overline{M}_{1,0,0}=\tau/A$$

$$\overline{M}_{0,1,0}=0$$

$$\overline{M}_{0,0,1}=(\tau\phi\beta)/E$$

$$\overline{M}_{1,0,1}=(\tau^2\beta^2h+2\tau^2\beta\phi+\tau^2\psi+4\tau^2\xi+h)/AE$$

$$\overline{M}_{2,0,0}=(2\tau^2+3\beta^2\tau^2+1)/A^2$$

$$\overline{M}_{0,0,2}=1+(\tau^2\beta^2\phi^2)/E^2$$

$$\overline{M}_{3,0,0}=6\tau/A^3$$

$$\overline{M}_{2,0,1}=(3\tau\beta\phi+3\tau h)/A^2E$$

$$\overline{M}_{1,0,2}=(\tau\gamma^2+\tau+4\tau\beta\phi h)/AE^2$$

$$\overline{M}_{0,2,0}=(\tau\beta\phi+\tau\alpha^2h)/B^2E$$

$$\overline{M}_{0,0,3}=3\tau(\beta\phi+\gamma^2h)/E^3$$

$$\overline{M}_{4,0,0}=(3+36\tau^2+26\tau^2\beta^2)/A^4$$

$$\overline{M}_{3,0,1}=(16\tau^2\beta^2h+25\tau^2\beta\phi+11\tau^2h+3\tau^2\psi+20\tau^2\xi+3h)/A^3E$$

$$\overline{M}_{1,2,1} = (\tau^2\beta^2 h + 2\tau^2\beta\phi + 8\tau^2\alpha^2 h/3 + \tau^2\psi + 3\tau^2\alpha^2\beta\phi + 4\tau^2\xi + 7\tau^2\beta^2\rho^2 h/3 + h)/AB^2E$$

$$\overline{M}_{2,0,2} = (\tau^2(17\gamma^2/3 + 7\beta^2\omega^2/3 + 6\psi h + 31\beta^2\phi^2/3 + 92h\xi/3 + 18\beta\phi h + 2 + 3\beta^2 + 16\beta^2 h^2/3) + 1 + 2h^2)/A^2E^2$$

$$\overline{M}_{0,2,2} = (\tau^2(\gamma^2 + \beta^2\omega^2 + 2\psi h + \beta^2\phi^2 + 10\alpha^2\beta\phi h/3 + 4h\xi + 4\gamma^2\alpha^2/3 + \alpha^2 + \beta^2\rho^2 + 4\beta^2\rho^2 h^2/3) + 1)/B^2E^2$$

$$\overline{M}_{1,0,3} = (\tau^2(3\beta^2 h + 6\beta\phi + 8\gamma^2 h + 3\psi + 12\xi + 9\beta\gamma^2\phi + 7\beta^2\omega^2 h + 6h^2\psi + 13\beta^2\phi^2 h + 20\xi h^2) + 3h)/AE^3$$

$$\overline{M}_{0,0,4} = (\tau^2(6\gamma^2 + 6\beta^2\omega^2 + 12\psi h + 6\beta^2\phi^2 + 24\xi h + 4\gamma^4 + 20\gamma^2\beta\phi h + 8\beta^2 h^2\omega^2) + 3)/E^4$$

$$\overline{M}_{5,0,0} = (45\tau)/A^5$$

$$\overline{M}_{4,0,1} = (15\tau\beta\phi + 30\tau h)/A^4E$$

$$\overline{M}_{1,0,4} = \tau(3 + 6\gamma^2 + 24\beta\phi h + 12\gamma^2 h^2)/AE^4$$

$$\overline{M}_{2,2,1} = 3\tau(\beta\phi + \alpha^2 h + h)/A^2B^2E$$

$$\overline{M}_{3,0,2} = \tau(3\gamma^2 + 6 + 24\beta\phi h + 12h^2)/A^3E^2$$

$$\overline{M}_{2,0,3} = \tau(9\beta\phi + 9\gamma^2 h + 9h + 18\beta\phi h^2)/A^2E^3$$

$$\overline{M}_{0,0,5} = \tau(15\beta\phi + 30\gamma^2 h)/E^5$$

$$\overline{M}_{1,2,2} = \tau(1 + \gamma^2 + 4\beta\phi h + \alpha^2 + 2\alpha^2 h^2)/AB^2E^2$$

$$\overline{M}_{0,4,1} = \tau(3\beta\phi + 6\alpha^2 h)/B^4E$$

$$\overline{M}_{0,2,3} = \tau(3\beta\phi + 3\gamma^2 h + 3\alpha^2 h)/B^2E^3$$

$$\overline{M}_{6,0,0} = (15 + 255\tau^2\beta^2 + 540\tau^2)/A^6$$

$$\overline{M}_{5,0,1} = (\tau^2(185\beta^2 h + 280\beta\phi + 260h + 15\psi + 140\xi) + 15h)/A^5E$$

$$\overline{M}_{4,0,2} = (\tau^2(26\beta^2 + 100\beta^2h^2 + 43\gamma^2 + 11\beta^2\omega^2 + 30\psi h + 83\beta^2\phi^2 + 236\xi h + 308\beta\phi h + 36 + 70h^2) + 12h^2 + 3)/A^4E^2$$

$$\overline{M}_{3,0,3} = (\tau^2(30\beta^2h^3 + 48\beta^2h + 75\beta\phi + 84\gamma^2h + 9\psi + 60\xi + 45\beta\gamma^2\phi + 36\psi h^2 + 33\beta^2\omega^2h + 159\beta^2\phi^2h + 228\xi h^2 + 33h + 144\beta\phi h^2) + 9h + 6h^3)/A^3E^3$$

$$\overline{M}_{2,0,4} = (\tau^2(32\beta^2h^2 + 9\beta^2 + 34\gamma^2 + 14\beta^2\omega^2 + 36\psi h + 62\beta^2\phi^2 + 184\xi h + 10\gamma^4 + 140\gamma^2\beta\phi h + 52\beta^2h^2\omega^2 + 6 + 108\beta\phi h + 64\gamma^2h^2 + 24\psi h^3 + 116\beta^2\phi^2h^2 + 112\xi h^3) + 3 + 12h^2)/A^2E^4$$

$$\overline{M}_{1,0,5} = (\tau^2(15\beta^2h + 30\beta\phi + 80\gamma^2h + 15\psi + 90\gamma^2\beta\phi + 60\xi + 70\beta^2\omega^2h + 60\psi h^2 + 130\beta^2\phi^2h + 200\xi h^2 + 50\gamma^4h + 40\beta^2\omega^2h^3 + 160\gamma^2\beta\phi h^2) + 15h)/AE^5$$

$$\overline{M}_{0,0,6} = (\tau^2(45\gamma^2 + 45\beta^2\omega^2 + 90\psi h + 45\beta^2\phi^2 + 180\xi h + 60\gamma^4 + 300\gamma^2\beta\phi h + 120\beta^2\omega^2h^2 + 90\gamma^4h^2) + 15)/E^6$$

$$\overline{M}_{3,2,1} = (\tau^2(16\beta^2h + 25\beta\phi + 28\alpha^2h + 3\psi + 15\alpha^2\beta\phi + 20\xi + 11\beta^2\rho^2h + 11h) + 3h)/A^3B^2E$$

$$\overline{M}_{1,4,1} = (\tau^2(3\beta^2h + 6\beta\phi + 16\alpha^2h + 3\psi + 18\alpha^2\beta\phi + 12\xi + 10\alpha^4h + 14\beta^2\rho^2h) + 3h)/AB^4E$$

$$\overline{M}_{2,2,2} = (\tau^2(16\beta^2h^2/3 + 3\beta^2 + 17\gamma^2/3 + 7\beta^2\omega^2/3 + 6\psi h + 31\beta^2\phi^2/3 + 70\alpha^2\beta\phi h/3 + 92\xi h/3 + 10\alpha^2\gamma^2/3 + 17\alpha^2/3 + 7\beta^2\rho^2/3 + 26\beta^2\rho^2h^2/3 + 2 + 18\beta\phi h + 32\alpha^2h^2/3) + 1 + 2h^2)/A^2B^2E^2$$

$$\overline{M}_{0,4,2} = (\tau^2(3\gamma^2 + 3\beta^2\omega^2 + 6\psi h + 3\beta^2\phi^2 + 20\alpha^2\beta\phi h + 12\xi h + 8\alpha^2\gamma^2 + 6\alpha^2 + 6\beta^2\rho^2 + 8\beta^2h^2\rho^2 + 4\alpha^4 + 6\alpha^4h^2) + 3)/B^4E^2$$

$$\overline{M}_{1,2,3} = (\tau^2(3\beta^2 h + 6\beta\phi + 8\alpha^2 h + 8\gamma^2 h + 3\psi + 12\xi + 9\gamma^2\beta\phi + 7\beta^2\omega^2 h + 6\psi h^2 + 13\beta^2\phi^2 h + 20\xi h^2 + 9\alpha^2\beta\phi + 10\alpha^2\gamma^2 h + 16\alpha^2\beta\phi h^2 + 7\beta^2\rho^2 h + 4\beta^2\rho^2 h^3) + 3h)/AB^2C^3$$

$$\overline{M}_{0,2,4} = (\tau^2(6\gamma^2 + 6\beta^2\omega^2 + 12\psi h + 6\beta^2\phi^2 + 8\beta^2\omega^2 h^2 + 3\alpha^2 + 8\alpha^2\gamma^2 + 20\alpha^2\beta\phi h + 24\xi h + 4\gamma^4 + 20\gamma^2\beta\phi h + 12\alpha^2\gamma^2 h^2 + 3\beta^2\rho^2 + 8\beta^2\rho^2 h^2) + 3)/B^2E^4$$

$$\overline{M}_{7,0,0} = (420\tau)/A^7$$

$$\overline{M}_{6,0,1} = 105\tau(\beta\phi + 3h)/A^6E$$

$$\overline{M}_{4,0,3} = \tau(45\beta\phi + 45\gamma^2 h + 90h + 180\beta\phi h^2 + 60h^3)/A^4E^3$$

$$\overline{M}_{3,0,4} = \tau(18 + 18\gamma^2 + 144\beta\phi h + 72\gamma^2 h^2 + 72h^2 + 96\beta\phi h^3)/A^3E^4$$

$$\overline{M}_{2,0,5} = \tau(45\beta\phi + 90\gamma^2 h + 45h + 180\beta\phi h^2 + 60\gamma^2 h^3)/A^2E^5$$

$$\overline{M}_{4,2,1} = \tau(15\beta\phi + 15\alpha^2 h + 30h)/A^4B^2E$$

$$\overline{M}_{2,4,1} = \tau(18\alpha^2 h + 9\beta\phi + 9h)/A^2B^4E$$

$$\overline{M}_{3,2,2} = \tau(6 + 3\gamma^2 + 24\beta\phi h + 3\alpha^2 + 12\alpha^2 h^2 + 12h^2)/A^3B^2E^2$$

$$\overline{M}_{2,2,3} = \tau(9\beta\phi + 9h\gamma^2 + 9\alpha^2 h + 9h + 18\beta\phi h^2 + 6\alpha^2 h^3)/A^2B^2E^3$$

$$\overline{M}_{1,0,6} = \tau(15 + 45\gamma^2 + 180\beta\phi h + 180\gamma^2 h^2)/AE^6$$

$$\overline{M}_{0,0,7} = \tau(105\beta\phi + 315\gamma^2 h)/E^7$$

$$\overline{M}_{0,6,1} = \tau(15\beta\phi + 45\alpha^2 h)/B^6E$$

$$\overline{M}_{1,2,4} = \tau(3 + 6\gamma^2 + 24\beta\phi h + 12\gamma^2 h^2 + 3\alpha^2 + 12\alpha^2 h^2)/AB^2E^4$$

$$\overline{M}_{0,2,5} = \tau(15\beta\phi + 30\gamma^2 h + 15\alpha^2 h)/B^2E^5$$

$$\overline{M}_{1,4,2} = \tau(3 + 3\gamma^2 + 12\beta\phi h + 6\alpha^2 + 12\alpha^2 h^2)/AB^4E^2$$

$$\overline{M}_{0,4,3} = \tau(9\beta\phi + 9\gamma^2 h + 18\alpha^2 h)/B^4E^3$$

$$\overline{M}_{5,0,2} = \tau(15\gamma^2 + 45 + 180\beta\phi h + 180h^2)/A^5E^2$$

$$\overline{M}_{8,0,0} = (105 + 2940\tau^2\beta^2 + 8400\tau^2)/A^8$$

$$\overline{M}_{7,0,1} = (\tau^2(2310\beta^2 h + 3465\beta\phi + 4935h + 105\psi + 1260\xi) + 105h)/A^7E$$

$$\overline{M}_{8,0,0} = (105 + 2940\tau^2\beta^2 + 8400\tau^2)/A^8$$

$$\overline{M}_{6,0,2} = (\tau^2(1500\beta^2 h + 255\beta^2 + 405\gamma^2 + 75\beta^2\omega^2 + 795\beta^2\phi^2 + 210\psi h + 2220\xi h + 4530\beta\phi h + 2130h^2 + 540) + 15 + 90h^2)/A^6E^2$$

$$\overline{M}_{5,0,3} = (\tau^2(720\beta^2 h^3 + 555\beta^2 h + 840\beta\phi + 900\gamma^2 h + 45\psi + 420\xi + 315\beta\phi\gamma^2 + 270h^2\psi + 225\beta^2\omega^2 h + 1755\beta^2\phi^2 h + 2460h^2\xi + 780h + 3300\beta\phi h^2 + 510h^3) + 45h + 60h^3)/A^5E^3$$

$$\overline{M}_{4,0,4} = (\tau^2(78\beta^2 + 600\beta^2 h^2 + 192\beta^2 h^4 + 258\gamma^2 + 66\beta^2\omega^2 + 180\psi h + 498\beta^2\phi^2 + 1416\xi h + 48\gamma^4 + 1068\gamma^2\beta\phi h + 384\beta^2\omega^2 h^2 + 108 + 1848\beta\phi h + 1008\gamma^2 h^2 + 240\psi h^3 + 1944\beta^2\phi^2 h^2 + 1824\xi h^3 + 420h^2 + 1200\beta\phi h^3) + 9 + 72h^2 + 24h^4)/A^4E^4$$

$$\overline{M}_{5,2,1} = (\tau^2(185\beta^2 h + 280\beta\phi + 300\alpha^2 h + 15\psi + 105\alpha^2\beta\phi + 140\xi + 75\beta^2\rho^2 h + 260h) + 15h)/A^5B^2E$$

$$\overline{M}_{4,2,2} = (\tau^2(100\beta^2 h^2 + 26\beta^2 + 43\gamma^2 + 11\beta^2\omega^2 + 30\psi h + 83\beta^2\phi^2 + 178\alpha^2\beta\phi h + 236\xi h + 16\alpha^2\gamma^2 + 43\alpha^2 + 11\beta^2\rho^2 + 64\beta^2\rho^2 h^2 + 36 + 308\beta\phi h + 168\alpha^2 h^2 + 70h^2) + 12h^2 + 3)/A^4B^2E^2$$

$$\overline{M}_{3,0,5} = (\tau^2(240\beta^2 h + 300\beta^2 h^3 + 375\beta\phi + 840\gamma^2 h + 300\xi + 450\gamma^2\beta\phi + 330\beta^2\omega^2 h + 360\psi h^2 + 1590\beta^2\phi^2 h + 2280\xi h^2 + 240\gamma^4 h + 420\beta^2\omega^2 h^3 + 1740\gamma^2\beta\phi h^2 + 165h + 1440\beta\phi h^2 + 540\gamma^2 h^3 + 45\psi + 120\psi h^4 + 1020\beta^2\phi^2 h^3 + 720\xi h^4) + 45h + 60h^3)/A^3E^5$$

$$\overline{M}_{2,0,6} = (\tau^2(240\beta^2h^2 + 45\beta^2 + 105\beta^2\omega^2 + 270\psi h + 465\beta^2\phi^2 + 1380\xi h + 150\gamma^4 + 2100\gamma^2\beta\phi h + 780\beta^2\omega^2h^2 + 810\beta\phi h + 960\gamma^2h^2 + 360\psi h^3 + 1740\beta^2\phi^2h^2 + 1680\xi h^3 + 570h^2\gamma^4 + 1320\gamma^2\beta\phi h^3 + 240\beta^2\omega^2h^4 + 30 + 255\gamma^2) + 15 + 90h^2)/A^2E^6$$

$$\overline{M}_{1,0,7} = (\tau^2(105\beta^2h + 210\beta\phi + 840\gamma^2h + 105\psi + 420\xi + 945\gamma^2\beta\phi + 735\beta^2\omega^2h + 630\psi h^2 + 1365\beta^2\phi^2h + 2100\xi h^2 + 1050\gamma^4h + 840\beta^2\omega^2h^3 + 3360\gamma^2\beta\phi h^2 + 630\gamma^4h^3) + 105h)/AE^7$$

$$\overline{M}_{0,2,6} = (\tau^2(15\alpha^2 + 60\alpha^2\gamma^2 + 150\alpha^2\beta\phi h + 180\alpha^2\gamma^2h^2 + 15\beta^2\rho^2 + 60\beta^2\rho^2h^2 + 45\beta^2\omega^2 + 45\beta^2\phi^2 + 180\xi h + 60\gamma^4 + 300\gamma^2\beta\phi h + 120\beta^2\omega^2h^2 + 90\gamma^4h^2 + 45\gamma^2 + 90\psi h) + 15)/B^2E^6$$

$$\overline{M}_{0,6,2} = (\tau^2(15\gamma^2 + 15\beta^2\omega^2 + 30\psi h + 15\beta^2\phi^2 + 150\alpha^2\beta\phi h + 60\xi h + 60\alpha^2\gamma^2 + 45\alpha^2 + 45\beta^2\rho^2 + 60\beta^2\rho^2h^2 + 60\alpha^4 + 90\alpha^4h^2) + 15)/B^6E^2$$

$$\overline{M}_{3,2,3} = (\tau^2(48\beta^2h + 30\beta^2h^3 + 75\beta\phi + 84\alpha^2h + 84\gamma^2h + 9\psi + 60\xi + 45\gamma^2\beta\phi + 33\beta^2\omega^2h + 36\psi h^2 + 159\beta^2\phi^2h + 228\xi h^2 + 45\alpha^2\beta\phi + 48\alpha^2\gamma^2h + 174\alpha^2\beta\phi h^2 + 33\beta^2\rho^2h + 42\beta^2\rho^2h^3 + 33h + 144\beta\phi h^2 + 54\alpha^2h^3) + 9h + 6h^3)/A^3B^2E^3$$

$$\overline{M}_{2,2,4} = (\tau^2(9\beta^2 + 32\beta^2h^2 + 34\gamma^2 + 14\beta^2\omega^2 + 36\psi h + 62\beta^2\phi^2 + 184\xi h + 10\gamma^4 + 140\gamma^2\beta\phi h + 52\beta^2\omega^2h^2 + 17\alpha^2 + 20\alpha^2\gamma^2 + 140\alpha^2\beta\phi h + 76\alpha^2\gamma^2h^2 + 7\beta^2\rho^2 + 52\beta^2\rho^2h^2 + 6 + 108\beta\phi h + 64\gamma^2h^2 + 64\alpha^2h^2 + 24\psi h^3 + 116\beta^2\phi^2h^2 + 112\xi h^3 + 88\alpha^2\beta\phi h^3 + 16\beta^2\rho^2h^4) + 3 + 12h^2)/A^2B^2E^4$$

$$\overline{M}_{1,6,1} = (\tau^2(15\beta^2h + 30\beta\phi + 120\alpha^2h + 15\psi + 135\alpha^2\beta\phi + 60\xi + 150\alpha^4h + 105\beta^2\rho^2h) + 15h)/AB^6E$$

$$\overline{M}_{3,4,1} = (\tau^2(48\beta^2 h + 75\beta\phi + 168\alpha^2 h + 9\psi + 90\alpha^2\beta\phi + 60\xi + 48\alpha^4 h + 66\beta^2\rho^2 h + 33h) + 9h)/A^3B^4E$$

$$\overline{M}_{0,4,4} = (\tau^2(18\gamma^2 + 18\beta^2\omega^2 + 36\psi h + 18\beta^2\phi^2 + 72\xi h + 12\gamma^4 + 60\gamma^2\beta\phi h + 24\beta^2\omega^2 h^2 + 18\alpha^2 + 48\alpha^2\gamma^2 + 120\alpha^2\beta\phi h + 72\alpha^2\gamma^2 h^2 + 18\beta^2\rho^2 + 48\beta^2\rho^2 h^2 + 12\alpha^4 + 36\alpha^4 h^2) + 9)/B^4E^4$$

$$\overline{M}_{1,4,3} = (\tau^2(9\beta^2 h + 18\beta\phi + 24\gamma^2 h + 48\alpha^2 h + 9\psi + 36\xi + 27\gamma^2\beta\phi + 21\beta^2\omega^2 h + 18\psi h^2 + 39\beta^2\phi^2 h + 60\xi h^2 + 54\alpha^2\beta\phi + 60\alpha^2\gamma^2 h + 96\alpha^2\beta\phi h^2 + 42\beta^2\rho^2 h + 24\beta^2\rho^2 h^3 + 30\alpha^4 h + 18\alpha^4 h^3) + 9h)/AB^4E^3$$

$$\overline{M}_{0,0,8} = (\tau^2(420\gamma^2 + 420\beta^2\omega^2 + 840\psi h + 420\beta^2\phi^2 + 1680\xi h + 840\gamma^4 + 4200\gamma^2\beta\phi h + 1680\beta^2\omega^2 h^2 + 2520\gamma^4 h^2) + 105)/E^8$$

$$\overline{M}_{1,2,5} = (\tau^2(15\beta^2 h + 30\beta\phi + 80\gamma^2 h + 40\alpha^2 h + 15\psi + 60\xi + 90\gamma^2\beta\phi + 70\beta^2\omega^2 h + 60\psi h^2 + 130\beta^2\phi^2 h + 200h^2\xi + 50\gamma^4 h + 40\beta^2\omega^2 h^3 + 160\gamma^2\beta\phi h^2 + 45\alpha^2\beta\phi + 100\alpha^2\gamma^2 h + 160\alpha^2\beta\phi h^2 + 60\alpha^2\gamma^2 h^3 + 35\beta^2 h\rho^2 + 40\beta^2\rho^2 h^3) + 15h)/AB^2E^5$$

$$\overline{M}_{9,0,0} = (4725\tau)/A^9$$

$$\overline{M}_{10,0,0} = (945 + 39375\tau^2\beta^2 + 141750\tau^2)/A^{10}$$

A.2 Calculated coefficients of Hermite polynomial expansion

The following is list of the non-zero coefficients, to order τ^2, of the Hermite polynomial expansion:

$$D_{000} = 1$$

$$D_{120} = -\tau(\alpha^2/2)/AB^2$$

$$D_{102} = -\tau(\gamma^2/2 + \beta\phi h)/AE^2$$

$$D_{201} = -\tau(\beta\phi + h/2)/A^2E$$

$$D_{021} = -\tau(\alpha^2 h/2)/B^2E$$

$$D_{300} = -\tau(1/2)/A^3$$

$$D_{003} = -\tau(\gamma^2 h/2)/E^3$$

$$D_{004} = \tau^2(\gamma^4/6 + \gamma^2\beta\phi h/3 + \beta^2 h^2\omega^2/3)/E^4$$

$$D_{400} = \tau^2(1/2 + \beta^2/3)/A^4$$

$$D_{040} = \tau^2(\alpha^4/6)/B^4$$

$$D_{301} = \tau^2(2\beta^2 h/3 + 5\beta\phi/3 + h/3 + 4\xi/3)/A^3E$$

$$D_{103} = \tau^2(\gamma^2 h/3 + \beta\phi\gamma^2 + 2\beta^2\omega^2 h/3 + 2\beta^2\phi^2 h/3 + 4h^2\xi/3)/AE^3$$

$$D_{022} = \tau^2(\alpha^2\beta\phi h/3 + \alpha^2\gamma^2/3 + \beta^2\rho^2 h^2/3)/B^2E^2$$

$$D_{202} = \tau^2(2\gamma^2/3 + \beta^2\omega^2/3 + 4\beta^2\phi^2/3 + 8h\xi/3 + \beta\phi h + \beta^2 h^2/3)/A^2E^2$$

$$D_{220} = \tau^2(2\alpha^2/3 + \rho^2\beta^2/3)/A^2B^2$$

$$D_{121} = \tau^2(\alpha^2 h/3 + \alpha^2\beta\phi + 2\beta^2\rho^2 h/3)/AB^2E$$

$$D_{024} = \tau^2(\alpha^2\gamma^2 h^2/4)/B^2E^4$$

$$D_{204} = \tau^2(\gamma^4/8 + \gamma^2\beta\phi h + \gamma^2 h^2/4 + \beta^2\phi^2 h^2/2)/A^2E^4$$

$$D_{420} = \tau^2(\alpha^2/4)/A^4B^2$$

$$D_{240} = \tau^2(\alpha^4/8)/A^2B^4$$

$$D_{042} = \tau^2(\alpha^4 h^2/8)/B^4E^2$$

$$D_{402} = \tau^2(\gamma^2/4 + \beta\phi h + h^2/8 + \beta^2\phi^2/2)/A^4E^2$$

$$D_{222} = \tau^2(\alpha^2\beta\phi h + \alpha^2\gamma^2/4 + \alpha^2 h^2/4)/A^2B^2E^2$$

$$D_{600} = \tau^2(1/8)/A^6$$

$$D_{006} = \tau^2(\gamma^4 h^2/8)/E^6$$

$$D_{105} = \tau^2(\gamma^4 h/4 + \gamma^2 h^2 \beta\phi/2)/A\,E^5$$

$$D_{501} = \tau^2(h/4 + \beta\phi/2)/A^5 E$$

The coefficients, with $i + j + k > 6$, were found to be zero when only coefficients to order τ^2 were retained.

Appendix B

This appendix provides detailed information concerning the use of a time-dependent diffusivity in the general solution-scheme.

B.1 A time-dependent diffusivity

It was recognized, and evident upon comparison with experimental results of Raupach and Legg (1983), that some form of time dependence should be incorporated in the eddy-diffusivity to affect a better representation of the data at the closest measuring station from the source. Formerly the solution-scheme had but one empirical constant and here it is shown that the time-dependent aspect of the near-source diffusivity can be adequately included at the expense of one additional empirical constant.

The statistics of the motion of fluid particles in a turbulent shear flow are non-stationary. The variance growth-rate was shown in Dewey and Sullivan (1979) to depend on the integral over time of the Lagrangian autocorrelation function of the particle velocity and that this integral could be decomposed into three distinct components. These components are in essence made up of the change in location of the mean displacement, the correlation over the turbulent fluctuating velocities, and the correlation between the turbulent fluctuating velocities and the variation in the mean velocity field sampled by the particles. Of relevance here, in using an eddy-diffusivity, is the time-dependent integral of the correlation over the fluctuating velocity field. It is to be noted that, following a small time interval from release, the dominant mechanism for the variance growth-rate of a contaminant cloud is spreading due to turbulent fluctuations convecting contaminant into regions with different values of mean velocity (i.e., the third term in the Dewey and Sullivan (1979) decomposition, see also figure 4). In modeling turbulent diffusion with an eddy-diffusivity one anticipates dominant effects to arise from the presence of impermeable boundaries and that the interaction between cross-stream mixing and mean velocity gradients does not depend critically on the detailed structure of the turbulent fluctuating velocities.

The eddy-diffusivity arising from the streamwise (x) component of the Lagrangian fluctuating velocity field $u(t;h_1)$ as given in Dewey and Sullivan (1979) can be expressed as,

$$K(t;h_1) = (\overline{u(h_1)^2})^{1/2} (\overline{u(\bar{z}(t))^2})^{1/2} \int_0^t R(\tau;h_1) d\tau, \tag{1}$$

where,

$$R(t;h_1) = \frac{\overline{u(0;h_1)u(t;h_1)}}{(\overline{u(h_1)^2})^{1/2} (\overline{u(\bar{z}(t))^2})^{1/2}}, \tag{2}$$

when $\overline{u(h_1)^2}$ and $\overline{u(\bar{z}(t))^2}$ are the mean-square Eulerian values at release height h_1 at $t = 0$ and at the location of the mean cross-stream displacement $\bar{z}(t)$ at time interval t following release respectively.

On the expectation that the integral of (2) appearing in (1) converges to the value $T(h_1)$ as $t \to \infty$ and further that,

$$T(h_1) \propto h_1 / (\overline{u(h_1)^2})^{1/2}, \tag{3}$$

then from (1),

$$K(t;h_1) \propto (\overline{u(\bar{z}(t))^2})^{1/2} h_1. \tag{4}$$

Within the constant-stress layer (see Csanady pp.115, 1973)

$$\overline{u(z)^2} \propto u_*^2, \tag{5}$$

where u_* is the constant friction velocity such that,

$$\kappa(h_1) \propto k u_* h_1, \tag{6}$$

and the Reynold's analogy with k approximately equals to von Karman's constant is recovered. An estimate of the Lagrangian integral time scale for the vertical component of the fluctuating velocities in the neutral atmospheric boundary layer of

$$T \doteq (b_4/b_2)(h_1/u_*), \tag{7}$$

where $b_4 = 0.33 \pm 0.15$ and $b_2 = 1.3 \pm 0.1$, was given by Hunt and Weber (1979). This estimate suggests the correlation to be short-lived and comparable with the time h_1/u_* required for fluid particles to reach the boundary.

The form of the autocorrelation for a Markov process,

$$R(\tau) = e^{-\alpha\tau}, \tag{8}$$

is found to be a reasonable representation of experimental data except for very small values of τ (see Csanady pp.54, 1973; Taylor, 1921, and measurements of Sullivan, 1971). For the variable eddy-diffusivity it is useful to use (8), in (1) and take into account (6) to retrieve

$$K(z,t) = \kappa(z)(1 - e^{-t/T}), \tag{9}$$

where release height h_1 is contained in T and it is expected that the time required for the cloud to sample an appreciable variation in $\kappa(z)$ is larger than T. The relative change in K over the interval $t = T$ in the constant-stress layer is,

$$\frac{dK}{dz}\sqrt{\kappa(h_1)T} = \sqrt{(.19)k} \doteq 0.27, \tag{10}$$

when (7) is used for T with $b_4/b_2 = .19$.

In figure 24 the concentration as a function of vertical distance z/h_1 for an elevated, continuous, line-source as measured by Raupach and Legg (1983) are shown to be in rather good agreement with the solution-scheme when (9) is used with $\kappa(z)$ given by equation (4.3) and the ratio $b_4/b_2 = 0.19$ used in (7). This

value of the b_1/b_2 ratio is within the range given by Hunt and Weber (1979) and leads to agreement that is within the experimental accuracy given by Raupach and Legg (1983).

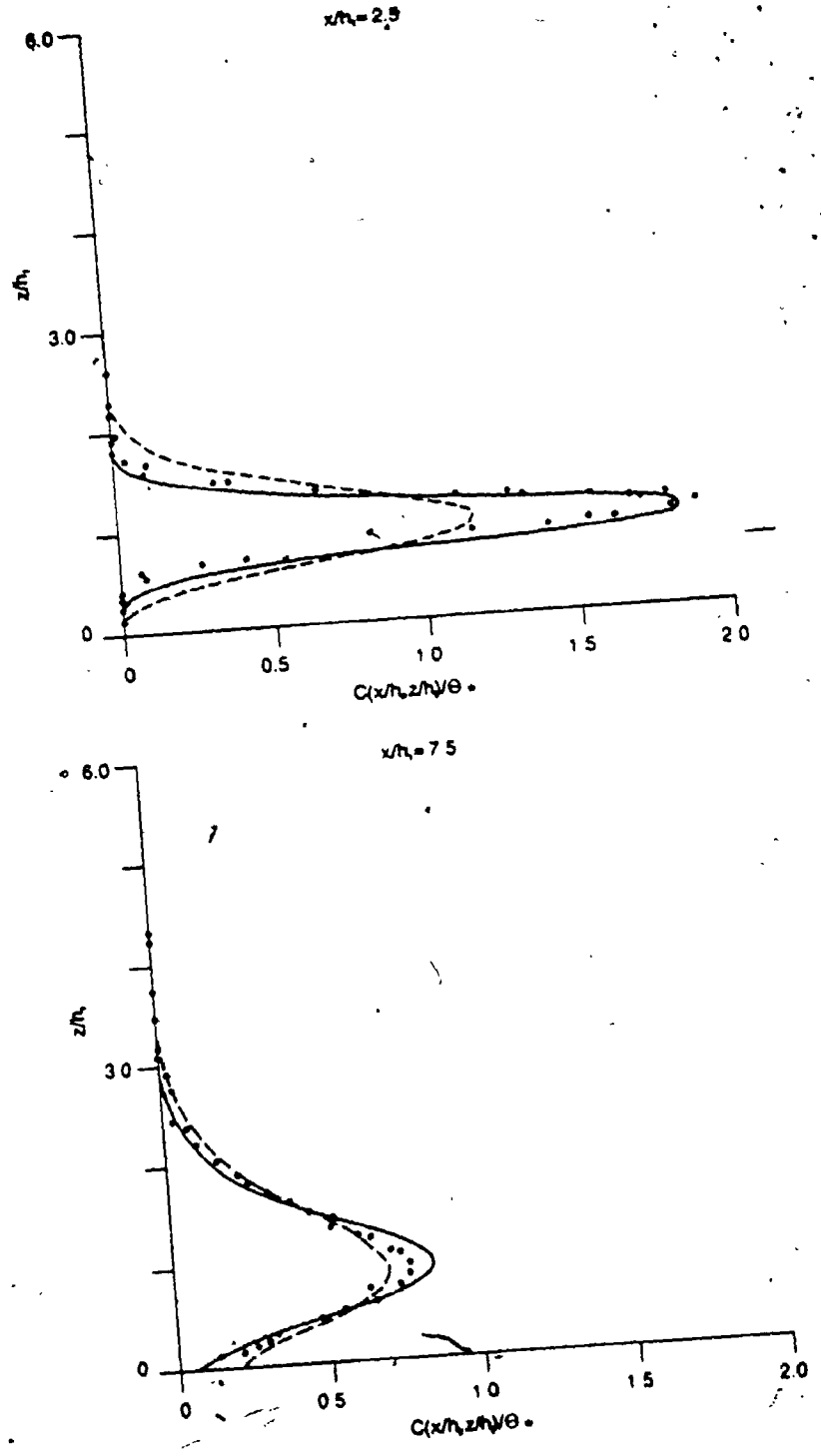

Figure 24
A comparison between the measured concentration values of Raupach and Legg (1983) (·) and the concentration values from the solution-scheme (—), when a time dependent diffusivity was used, at $x/h_1 = 2.5$ and $x/h_1 = 7.5$ respectively. The dashed lines represent the concentration values from the solution-scheme without a time-dependent diffusivity. At $x/h_1 = 2.5$ and 7.5, $t/T \doteq 1.26$ and 5.47 respectively.

References

Aris, R. (1956). On the dispersion of a solute in a fluid flowing through a tube. Proc. R. Soc. Lond. A 235, 67-77.

Batchelor, G.K. (1949). Diffusion in a field of homogeneous field of turbulence. Aust. J. Sci. Res. A, 2, 437-450.

Batchelor, G.K. (1964). Diffusion from sources in a turbulent boundary layer. Archiwum Mechaniki Stosowanej 3, 16, 661-670.

Birch, A.D., Brown, D.R., Dodson, M.G. and Thomas, J.R. (1978). The turbulent concentration field of a methane jet. J. Fluid Mech. 88, 431-449.

Cermak, J.E. (1963). Lagrangian similarity hypothesis applied to diffusion in turbulent shear flow. J. Fluid Mech. 15, 49-63.

Chamberlain, A.C. (1966). Transport of gases to and from grass and grass-like surfaces. Proc. R. Soc. Series A, 290, 236-265.

Chatwin, P.C. (1968). The dispersion of a puff of passive contaminant in the constant stress region. Q. J. R. Met. Soc. 94, 350-360.

Chatwin, P.C. (1976). The initial dispersion of contaminant in Poiseuille flow and the smoothing of the snout. J. Fluid Mech. 77, 593-602.

Chatwin, P.C. (1984). Modelling and measuring concentration fluctuations: the effects of different types of averaging. Proc. fourth joint conference on applications of air pollution meteorology, Portland, Oregon, 111-114.

Chatwin, P.C. and Sullivan, P.J. (1979). Measurements of concentration fluctuations in relative turbulent diffusion. J. Fluid Mech. 94, 83-101.

Chatwin, P.C. and Sullivan, P.J. (1981). Diffusion from an elevated source within the atmospheric boundary layer. Proc. 3rd Symp. on Turbulent Shear Flows, Univ. of California, Davis, 9.1-9.6.

Chatwin, P.C. and Sullivan, P.J. (1985). Effects of instrumentation and averaging on turbulent diffusion data. Proc. 5th Symp. on Turbulent Shear Flows, Cornell Univ., Ithaca, New York, 11.1-11.5.

Chatwin, P.C. and Sullivan, P.J. (1987a). Perceived statistical properties of scalars in turbulent shear flows. Proc. 6th Symp. on Turbulent Shear Flows, Toulouse, France, 9.11-9.16.

Chatwin, P.C. and Sullivan, P.J. (1987b). The probability density function for contaminant concentrations in some self-similar turbulent flows. Proc. 2nd Int. Symp. on Transport Phenomenon in Turbulent Flows, Tokyo.

Cheng, R.K. and Shepherd, I.G. (1987). A comparison of velocity and scalar spectra in premixed turbulent flames. Proc. 6th Symp. on Turbulent Shear Flows, Toulouse, France, 751-758.

Csanady, G.T. (1973). "Turbulent diffusion in the environment." D. Reidel Pub. Co..

Derksen, R.W. and Sullivan, P.J. (1988). Private communication.

Dewey, R.J. (1979). Ph.D. Thesis. Univ. Western Ontario.

Dewey, R.J. and Sullivan, P.J. (1982). Longitudinal-dispersion calculations in laminar flows by statistical analysis of molecular motion. J. Fluid Mech. 125, 203-218.

Fackrell, J.E (1978). A system for turbulent concentration measurements. J. Phys. E: Sci. Instrum. 11, 1015-1022.

Fackrell, J.E. (1980). A flame ionisation detector for measuring fluctuating concentration. J. Phys. E: Sci. Instrum. 13, 888-893.

Fackrell, J.E. and Robins, A.G. (1980). Concentration fields associated with emissions from point sources in turbulent boundary layers, Part III: Concentration fluctuations and fluxes. C.E.G.B. Report.

Fackrell, J.E. and Robins, A.G. (1982). Concentration fluctuations and fluxes in plumes from point-sources in a turbulent boundary layer. J. Fluid Mech. 117, 1-26.

Gee, J.H. and Davies, D.R. (1964). A further note on horizontal dispersion from an instantaneous ground source. Q. J. R. Met. Soc. 89, 478-480.

Gupta, M.M., Manohar, R.P. and Stephenson (1984). A single cell high order scheme for the convective-diffusion equation with variable coefficients. Int. J. Num. Methods Fluids 4, 641-651.

Hinze, J.O. (1975). "Turbulence." McGraw-Hill.

Hwang, B.C., Peskin, R.L. and So, R.M.C. (1979). Concentration distribution in a turbulent shear flow. J. Atmos. Sci. 36, 10, 1955-1966.

Lauwerier, H.A. (1954). Diffusion from a source in a skew velocity field. Appl. Sci. Res. A, 4, 153-156.

La Rue, J.C. and Libby, P.A. (1974). Temperature fluctuations in a plane turbulent wake. Physics of Fluids 17, 11, 1956-1967.

Lumley, J.L. (1978). Computational modeling of turbulent flows. Adv. Appl Mech. 18, 123-176.

Matsuoka, H. (1961). Note on two-dimensional diffusion in the atmospheric surface layer. J. Met. Soc. Japan 39, 324-330.

Mihaila, I.M. (1968). Development of the trivariate frequency function in Gram-Charlier series. Rev. Roum. Math. Pures Et. Appl. Tome xiii, 6, 803-813.

Mitchell, A.R. and Griffiths, D.F. (1980). "The finite difference method in partial differential equations." John Wiley & Sons.

Monin, A.S. and Yaglom, A.M. (1971). "Statistical Fluid Mechanics" (J.L. Lumley, ed.), Vol. 1. M.I.T Press, Cambridge, Massachusetts.

Pasquill, F. (1974). "Atmospheric diffusion." (2nd ed.), Ellis Harwood, London.

Patel, M.K., Markatos, N.C. and Cross, M. (1980). A critical evaluation of seven discretization schemes for convective-diffusion equations. Int. J. Num. Methods Fluids 5, 225-244.

Robins, A.G. and Fackrell, J.E. (1978). Continuous plumes-Their structure and prediction. Proc. IMA Conference: Mathematical Modeling of Turbulent Diffusion in the Environment, Liverpool, Academic Press, 55-113.

Raupach, M.R. and Legg, B.J. (1983). Turbulent dispersion from an elevated line source: measurements of wind-concentration moments and budgets. J. Fluid Mech. 136, 111-137.

Saetran, L.R., Honnery, S.H., Starner, S.H., and Bilger, R.W. (1987). Scalar mixing layer in grid turbulence with transport of passive and reactive species. Proc. 6th Symp. on Turbulent Shear Flows, Toulouse, France, 761-766.

Saffman, P.G. (1962). The effect of wind shear on horizontal spread from an instantaneous ground source. Q. J. R. Met. Soc. 88, 382-393.

Sansone, G. (1959). "Orthogonal functions." Vol. 9, Interscience Pub., inc., New York.

Scorer, R.S. (1968). Air pollution problems at a proposed Merseyside chemical fertilizer plant: a case study. Atmos. Environ. 2, 35-38.

Shaughnessy, E.J. and Morton, J.B. (1977). Laser light-scattering measurements of particle concentration in a turbulent jet. J. Fluid Mech. 80, 129-148.

Smith, F.B. (1957). The diffusion of smoke from a continuous elevated point-source into a turbulent atmosphere. J. Fluid Mech. 2, 49-76.

Smith, G.D. (1975). "Numerical solutions of partial differential equations: finite difference methods." (2nd ed.), Clarendon Press, Oxford.

Smith, R. (1981). The importance of discharge siting upon contaminant dispersion in narrow rivers and estuaries. J. Fluid Mech. 108, 43-53.

Smith, R. (1982a). Where to put a steady discharge in a river. J. Fluid Mech. 115, 1-11.

Smith, R. (1982b). Gaussian approximation for contaminant dispersion. Q. J. Mech. Appl. Math. XXXV part 3, 345-366.

Smith, R. (1983). Effect of boundary absorption upon longitudinal dispersion in shear flows. J. Fluid Mech. 134, 161-177.

Sreenivasan, K.R., Tavoularis, S., and Corrsin, S. (1982). A test of gradient transport and its generalization. "Turbulent Shear Flows 3," Springer-Verlag, 96-112.

Sullivan, P.J. (1983). Far-Field contaminant dispersion in environmental flows. Mathematical Modeling in Science and Technology, Proc. 4th ICMM, Zurich, Switzerland, 622-627.

Sullivan, P.J. (1984). Whence the fluctuations in measured values of mean-squared fluctuations? Proc. fourth joint conference on applications of air pollution meteorology, Portland, Oregon, 115-120.

Sullivan, P.J. and Yip, H. (1985). A solution-scheme for the Convective-diffusion equation. ZAMP 36, 596-608.

Sullivan, P.J. and Yip, H. (1987). Near-field contaminant dispersion from an elevated line-source. ZAMP 38, 409-423.

Sutton, O.G. (1947). The problem of diffusion in the lower atmosphere. Q. J. R. Met. Soc. 73 London, 257-281.

Sutton, O.G. (1953). "Micrometerology." McGraw-Hill.

Sykes, R.I., Lewellen, W.S. and Parker, S.F. (1984). A turbulent-transport model for concentration fluctuations and fluxes. J. Fluid Mech. 139, 193-218.

Tavoularis, S. and Corrsin, S. (1981). Experiments in nearly homogeneous turbulent shear flow with a uniform mean temperature gradient. Part 1. J. Fluid Mech. 104, 311-347.

Taylor, G.I. (1922). Diffusion by continuous movements. Proc. Lond. Math. Soc. Ser. 2, 20, 196-211.

Taylor, G.I. (1954). The dispersion of matter in turbulent flow through a pipe. Proc. R. Soc. A 223, 446-468.

Townsend, A. (1951). The diffusion of heat spots in isotropic turbulence. Proc. R. Soc. A 209, 418-430.

Townsend, A. (1976). "The structure of turbulent shear flow." (2nd ed.) Cambridge Univ. Press.

Warhaft, Z. and Lumley, J.L. (1978). An experimental study of the decay of temperature fluctuations in grid-generated turbulence. J. Fluid Mech. 88, 659-684.

Wilson, D.J. (1982). Predicting risk of exposure to peak concentrations in fluctuating plumes. Pollution control div., Alberta Environ. Rep.

Wilson, D.J., Robins, A.G. and Fackrell, J.E. (1982). Predicting the spatial distribution of concentration fluctuations from a ground level source. Atmos. Environ. 16, 3, 497-504.

Yip, H. (1984). M.Sc. Thesis. Univ. Western Ontario.